German Aerospace Center
Institute of Propulsion Technology

IB 225 – 2007 A 05

O. Vaschalde

Calibration of a Four-Hole Probe in Sub-, Trans- and Supersonic Flow

English version of the report:
O. Vaschalde, *Etalonnage d'une sonde de pression à quatre trous en écoulement sub, trans et supersonique,*
submitted to ENSIAME, Valenciennes, January 14th, 2008

Date:	January 2008
Client:	-
Prepared for:	practical education at DLR from September 1st, 2007 to January 31st, 2008 during 2nd year of studies at ENSIAME, Valenciennes

Head of the institute:
Prof. Dr.-Ing. R. Mönig

DLR

Keywords:

Probe calibration, transonic flow

Calibration of a Four-Hole Probe in Sub-, Trans- and Supersonic Flow

Abstract

When applying pneumatic probes within aerodynamic research there is a demand of calibrating these probes. Especially at transonic velocities there is a general lack of sensitivity resulting in big errors. To overcome this problem it is necessary to include additional information – the pressure behind the probe – into the calibration process.

In this report the wind tunnel for probe calibration and the probe of interest are described as well as the applied calibration process. Results are compared with and without considering the back pressure in the probe's wake.

German Aerospace Center e.V.
In der Helmholtz-Gemeinschaft

Site Göttingen
Institute of Propulsion Technology
Turbine Department

Content

Notations:

Wind tunnels:

RGG	Windkanal für Rotierende Gitter Göttingen (rotating cascades)
EGG	Windkanal für Ebene Gitter Göttingen (straight cascades)
NGG	Niedergeschwindigkeits-Gittermessstrecke Göttingen (straight cascades and low velocity)
SEG	Sondeneichkanal Göttingen (probe calibration)

Ma	Mach number
Re	Reynolds number

α	Incidence angle of the probe
β	Radial angle of the probe

γ	Adiabatic index (γ=1.4 for the air)
C_p	Heat capacity
T	Temperature
R	Specific gas constant
u	Flow velocity
h	Enthalpy

p_0	Total pressure
p_{0s}	Stagnation pressure of the probe (middle hole)
p_{sl}	Left tube pressure
p_{sr}	Right tube pressure
p_{bu}	Back tube pressure
p_{sm}	Mean of p_{sl} and p_{sr}

C_α	Pressure coefficient relative to α
C_{Ma}	Mach number coefficient calculated from p_{sm} and p_{0s}
C_{Mab}	Mach number calculated from p_{bu} and p_{0s}

Acknowledgment

I would first like to thank Dr. Friedrich Kost, my supervisor at DLR, for his welcome, for answering to all my questions, and for his precious help during my training course.

I also thank all the employees of the department « *Antriebstechnik – Turbine* » for their welcome and their kindness.

My acknowledgments go also to M. Bernard Desmet my supervisor in Valenciennes, to M. Alain Lecocq and the employees of the ENSIAME for giving me the chance to work in one of the most famous aerospace centers in Europe.

I. Introduction

I.1. Presentation of DLR

DLR (Deutsches Zentrum für Luft- und Raumfahrt) is the German center for research in aeronautics and aerospace. It is involved in many research projects national as well as international.

It was created in 1969 from the merge of three German centers of research:

- **AVA** (Aerodynamische Versuchsansalt Göttingen), experimental laboratory of aerodynamics at Göttingen, founded in 1907 by Ludwig Prandtl;
- **DVL** (Deutsche Versuchsanstalt für Luftfahrt), German experimental laboratory of aeronautics, created in 1912 ;
- **DFL** (Deutsche Forschungsanstalt für Luftfahrt), German laboratory of research in aeronautics, founded in 1936.

Today, DLR employs nearly 5000 people at several sites in Germany and in the World: Köln-Porz, Berlin-Adlershof, Bonn-Oberkassel, Braunschweig, Göttingen, Lampoldshausen, Oberpfaffenhoffen, Stuttgart, Bruxelles, Paris and Washington.
DLR also established partnerships with other research centers like EREA (Etablissements de Recherche Européens en Aéronautique), NASA, NASDA (Japan) and the Russian research.
The different programs studied at the DLR cover a large spectrum of disciplines, such as:

- fluid mechanics
- flight mechanics
- energetics
- materials
- mechatronics and robotics
- telecommunications and high-level electronics
- optics
- biophysics

The site of Göttingen is one of the most famous aerospace research centers in Germany. Research here is focused on aerodynamics, aeroelasticity, turbines and acoustics.

Figure 1: DLR site of Göttingen

I completed my training course in the turbine department, specialized in the study of turbine blades. This department owns four wind tunnels to study different kinds of flows:

* SEG (Sondeneichkanal Göttingen) to calibrate probes.
* RGG (Windkanal für Rotierende Gitter Göttingen), for the study of turbine stages.
* EGG (Windkanal für Ebene Gitter Göttingen) for the study of straight cascades.
* NGG (Niedergeschwindigkeits-Gittermessstrecke Göttingen) has the same function as EGG but allows for larger models at lower flow velocities.

I.2. Subject of the training course

In order to study turbine cascades, the department *« Antriebstechnik-Turbine »* needs pressure probes. However, before using these probes, they have to be calibrated. That's why DLR designed a wind tunnel specifically intended for probe calibration.

The main task of my training course was to calibrate a four-hole probe at the SEG for use in other wind tunnels, like the RGG.

This task can be divided into three steps: firstly, we will determine the coefficients which will be used along our study. Secondly, we will proceed to several measurements with our probe in the SEG by changing independently the Mach number and the Reynolds number. Thirdly, we will study all the data acquired and we will try to set up equations describing the behaviour of our probe.

II. SEG wind tunnel

Figure 2: SEG wind tunnel

II.1. Description of the wind tunnel

The wind tunnel is a closed circuit where dried air is blown. In order to reduce operating expenses, SEG shares with RGG two compressors of 90kW. Used independently or in parallel, their compression ratio is 3 and they provide an air flow of 43 m^3/s.
Cooling units are located downstream of the compressors, allowing to maintain the fluid at a desired temperature between 22°C and 42°C.

A compressed air reserve as well as a vacuum pump respectively located upstream and downstream of the test section allows obtaining a total pressure between 30 kPa and 290 kPa.

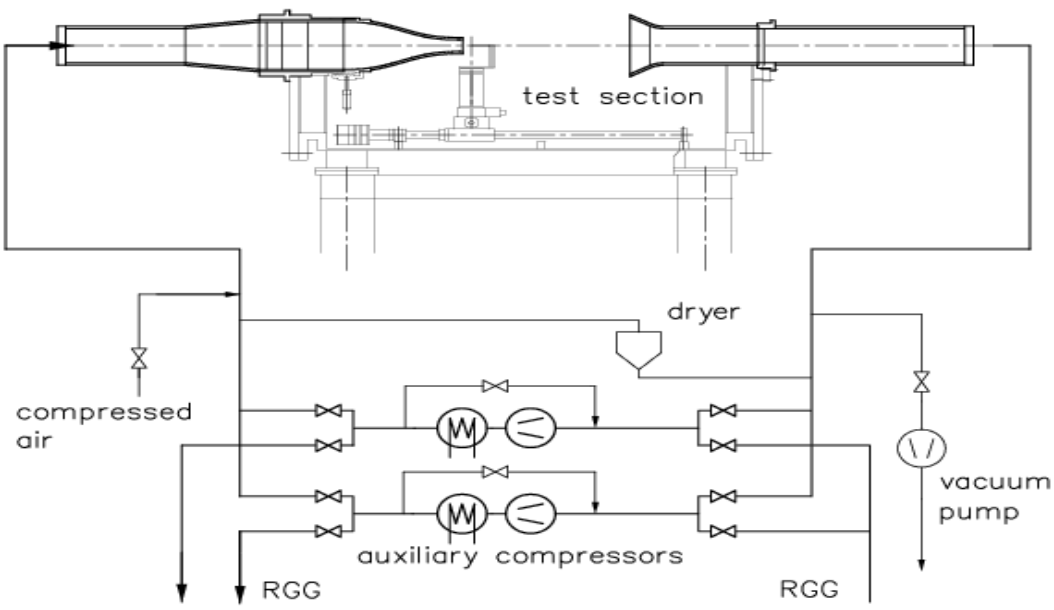

Figure 3: Diagram of the SEG circuit

The test section is located in a large chamber where probes up to 700 mm long can be installed. Motorized systems controlled by a computer allow setting the probe at different positions. The air passes first filters and a grid to be homogenized, then an exchangeable nozzle before arriving at the probe. This system of exchangeable nozzles provides a good flexibility to the SEG and allows choosing precisely the desired Mach number.

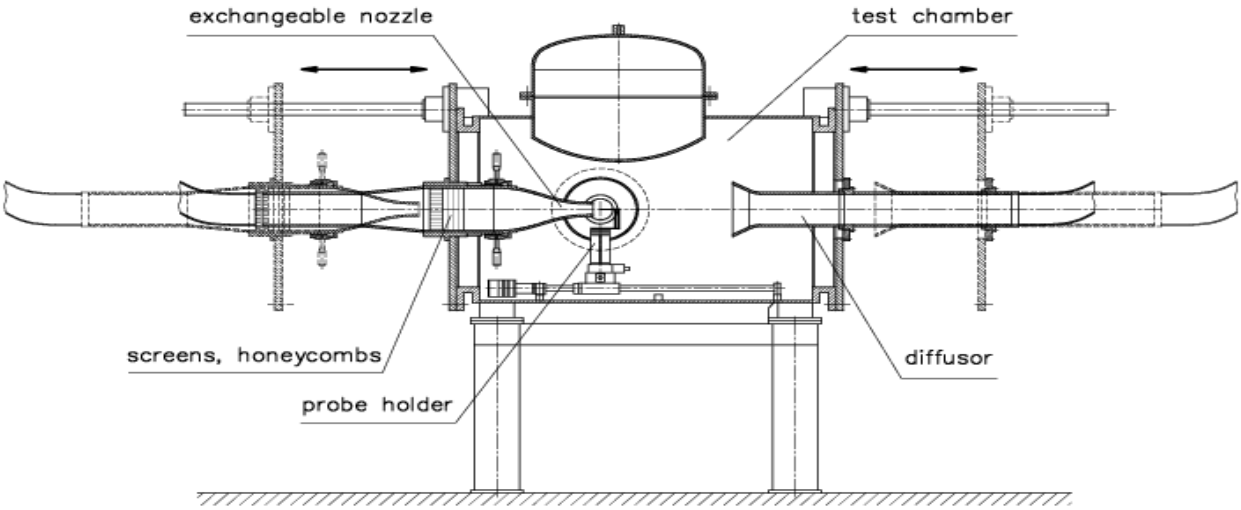

Figure 4: Test chamber of SEG

By choosing the right pressure and the right nozzle, this wind tunnel, gives us the ability to set a Mach number independently from the Reynolds number. Indeed, the Mach number is a function of the ratio between the total pressure, $p_{0,}$ and the pressure in the test chamber, p, according to the following equation:

$$Ma = \sqrt{\frac{2}{\gamma - 1}\left[\left(\frac{p_0}{p}\right)^{\frac{\gamma-1}{\gamma}} - 1\right]}$$

for an adiabatic flow and a perfect diatomic gas. We will develop this formula later in this report.

SEG operates at Mach numbers between 0.2 and 1.8 and Reynolds number from 10^5 to $2.1*10^6$.

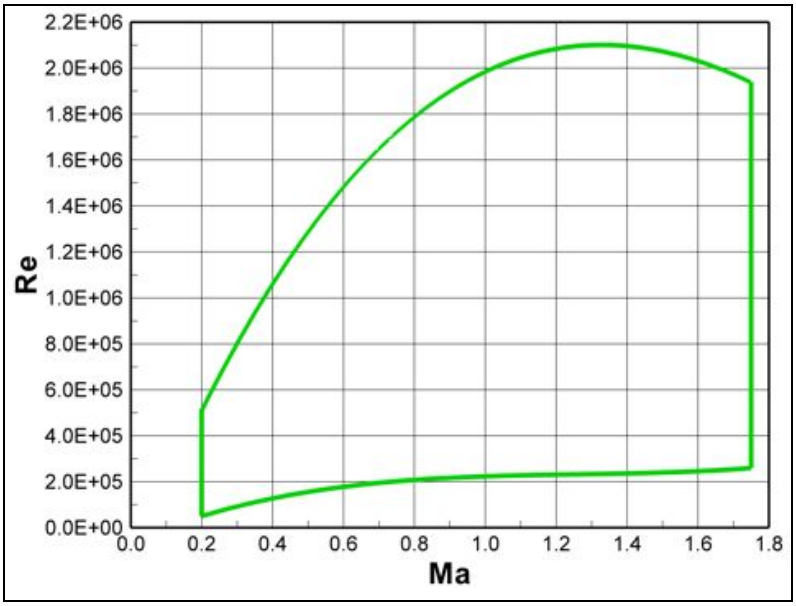

Figure 5: Range of operation

II.2. Operation of the wind tunnel

Two computers allow the control of the SEG.

The first one runs the SIMATIC software (Siemens) which controls in real time the Mach number, the temperature and the desired pressures.

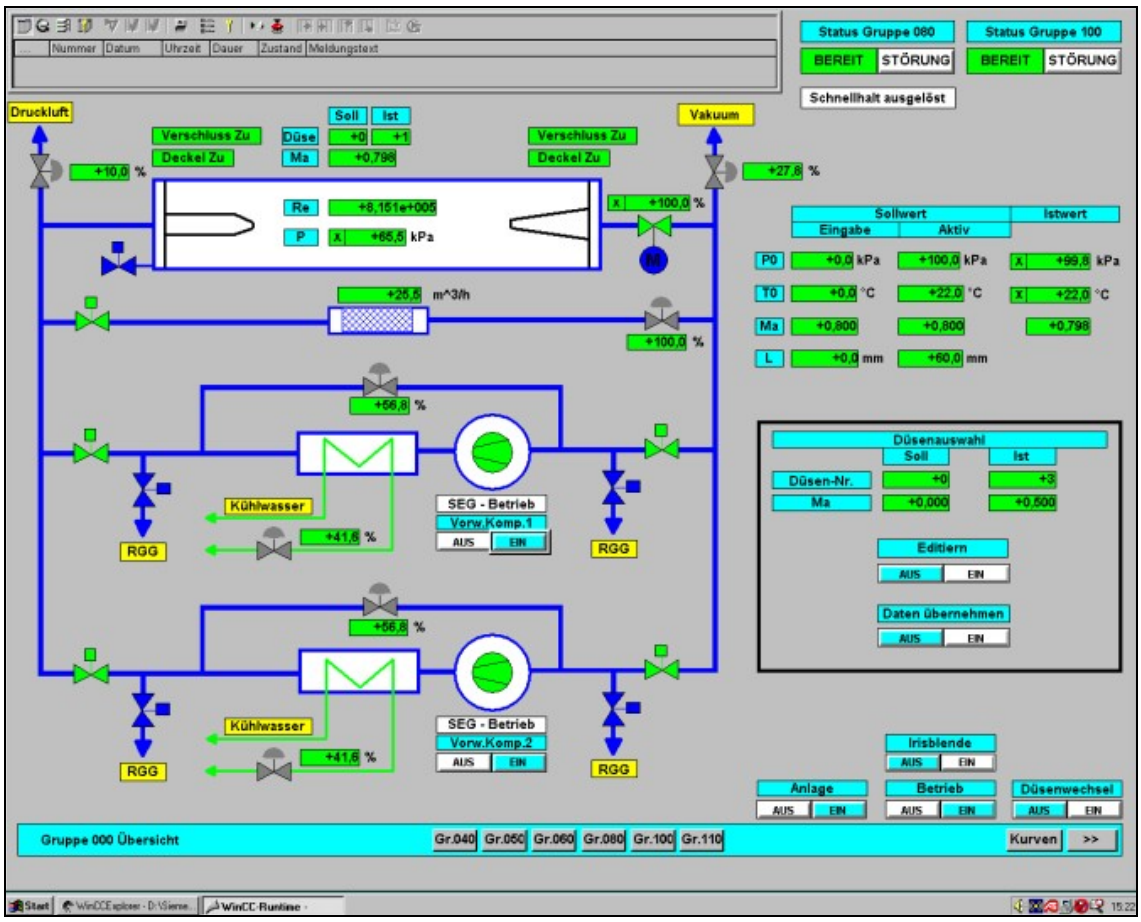

Figure 6: Screenshot of the wind tunnel control software (SIMATIC main window)

The second one runs the LabVIEW software which collects all the data from the measurements applying the DatSEG program. It enables also to control the positioning of the probe during the calibration process.

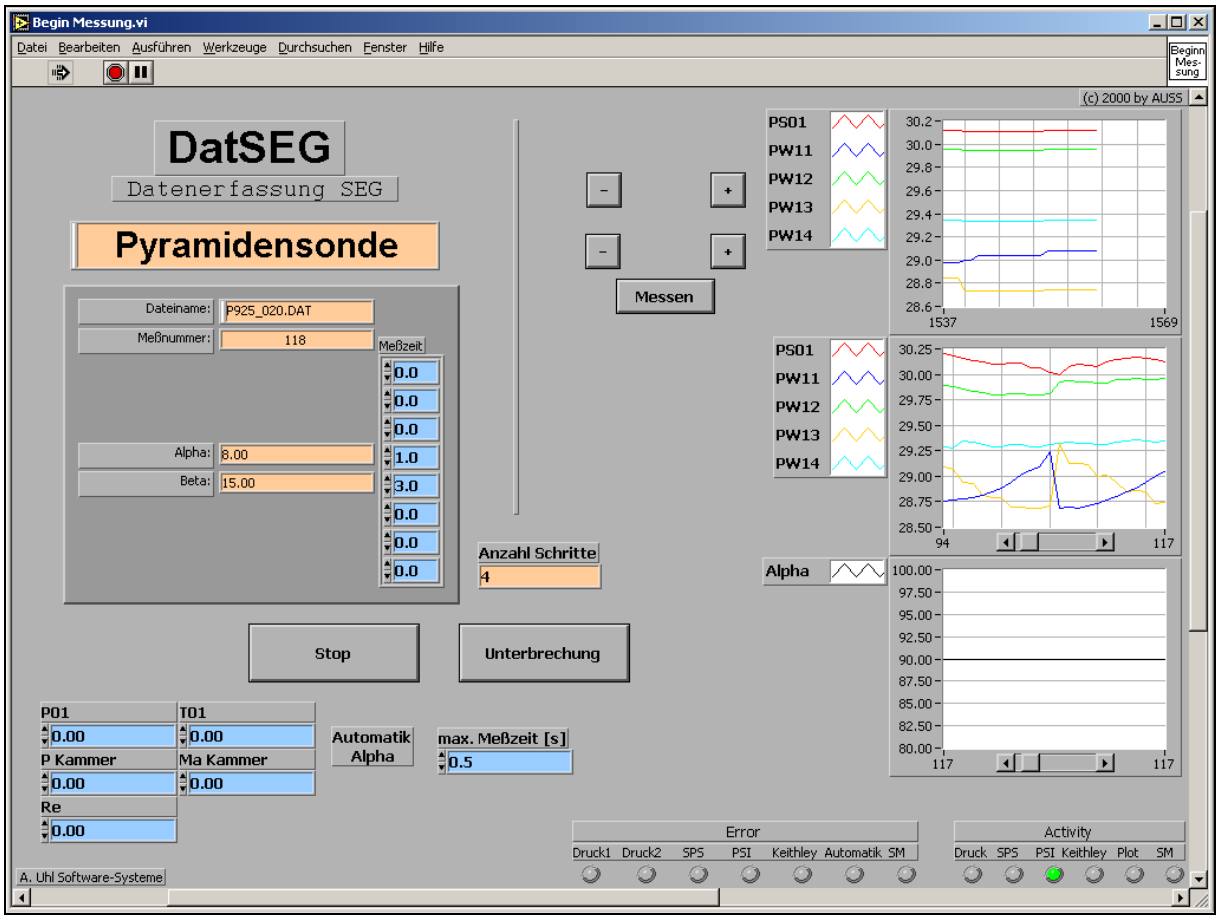

Figure 7: Screenshot of the probe control software (LabVIEW)

III. The probe

III.1. General information about pressure probes

The design of a probe must obey several criteria. Indeed, due to the intrusive nature of this type of measurements the influence of the probe on the flow characteristics has to be limited as well as the accuracy of the measurements kept. As a result we have to take in account these following criteria:

⇨ 1- **Mechanical criterion:** the probe has to resist its conditions of use from the mechanical point of view.

⇨ 2- **Criterion of adaptability:** the probe should be applicable for different test campaigns.

⇨ 3- **Aerodynamic criterion:** the probe inevitably modifies the behaviour of the flow around it. It will thus be necessary to reduce the disturbances to the minimum and, accordingly, to optimize the shape.

⇨ 4- **Criterion of manufacture:** the probe has to be machined, in spite of, generally, its small dimensions.

Moreover, the user of the probe has to limit the measurement errors, which are static or dynamic. This can be carried out during a trial run:

⇨ by minimizing the number of measurements with the probe;

⇨ by choosing the coefficients of calibration adequately.

III.2. Description of the probe

The probe, which was built here at DLR Göttingen, will be called RRT6 probe. It is made of three tubes one-millimetre in diameter welded side by side and folded at 90° at their end. This particular shape (« cobra » probe) allows introducing the probe in very narrow spaces, such as between a stator and a rotor of a turbine. Although this configuration isn't perfect (the stem of the probe affects the flow), this kind of probe is very easy to manufacture at low cost. The left and right tubes are bevelled to 45° at their end. There is also a thermocouple in the front of the probe and a fourth tube at the back of the probe, which is not folded like the others one, but bevelled backwards 45° at its end.

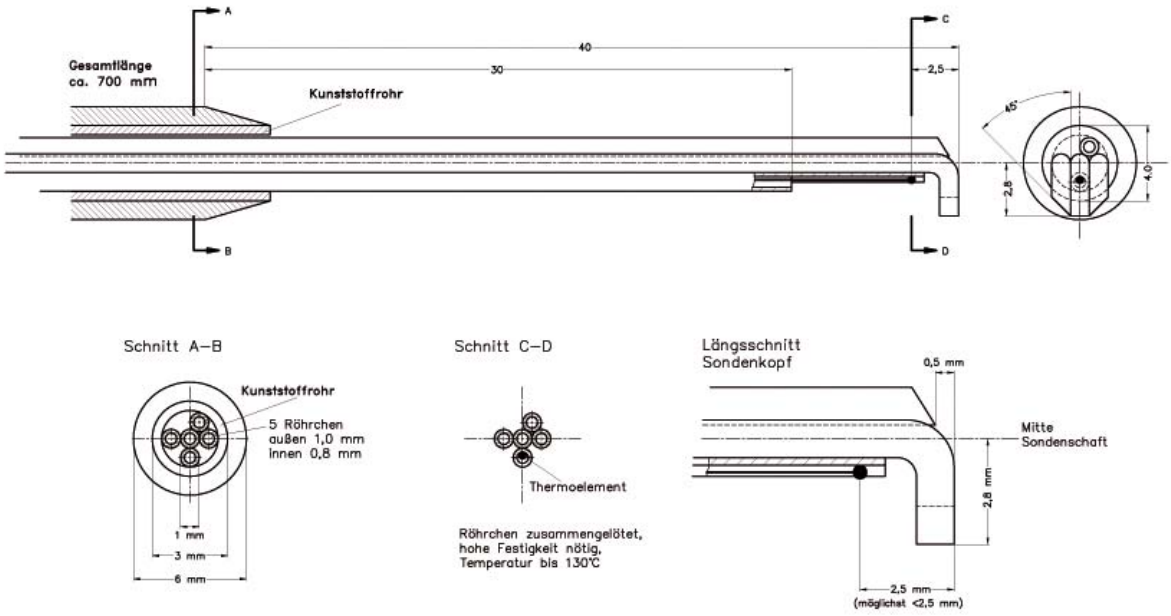

Figure 8: Sketch of the RRT6 probe

Therefore, we have 4 pressure tappings that were named as follows:

➔ psl: left tube (when we look directly face to the probe))
➔ psr: right tube
➔ p0s: center tube (Pitot pressure)
➔ pbu: back tube

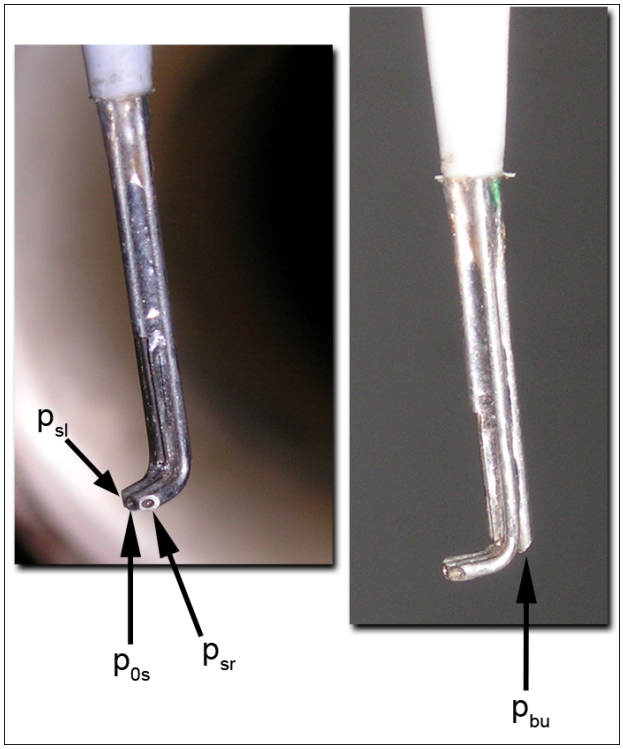

Figure 9: Photograph of the probe

IV. Theoretical study

IV. 1. Basic equations

Calibrating a probe means to study how the probe reacts to a flow the characteristics of which are known. Then we are going to establish the equations of the behaviour of the probe in order to use it for its initial purpose: find the characteristics of the flow from the pressures given by the probe.
Nevertheless, before doing this we have to define dimensionless coefficients from the raw data acquired by the probe.

If we have:
$$psm = \frac{psl + psr}{2}$$

We define:
$$C_\alpha = \frac{psl - psr}{p0s - psm} \quad (1)$$

$$C_{Ma} = Ma(psm, p0s) \quad (2)$$

$$C_{Mab} = Ma(pbu, p0s) \quad (3)$$

where the Mach number is obtained from the following formula:

$$Ma(p,p_0) = \sqrt{\frac{2}{\gamma - 1}\left[\left(\frac{p}{p_0}\right)^{\frac{1-\gamma}{\gamma}} - 1\right]} \quad (4)$$

with γ = 1.4 for air.

IV. 2. Calculation of Mach number in SEG

Let's derive the formula which gives the Mach number from the total pressure p_0 and from the pressure in the test chamber p. We will consider air as a perfect gas and the flow in the SEG as steady and adiabatic.

$$\boxed{h + \frac{u^2}{2} = const.}$$

which can also be written: $$C_p T + \frac{u^2}{2} = C_p T_0 = const.$$

$$\frac{T_0}{T} = 1 + \frac{u^2}{2 C_p T}$$

applying: $$C_p = \frac{\gamma R}{\gamma - 1}$$ (Mayer formula)

We find: $$\frac{T_0}{T} = 1 + \frac{(\gamma - 1) u^2}{2 \gamma R T}$$

and as we know that the Mach number is given by the following formula:

$$Ma = \frac{u}{c} = \frac{u}{\sqrt{\gamma R T}}$$

$$\boxed{\frac{T_0}{T} = 1 + \frac{(\gamma - 1) Ma^2}{2}}$$

Finally, if we consider the flow as isentropic, we can use the Laplace law:

$$\frac{p_0}{p} = \left(\frac{T_0}{T}\right)^{\frac{\gamma}{\gamma-1}}$$

so:

$$\frac{p_0}{p} = \left(1 + \frac{\gamma-1}{2} Ma^2\right)^{\frac{\gamma}{\gamma-1}}$$

And we get the Mach number according to the following formula:

$$Ma(p,p_0) = \sqrt{\frac{2}{\gamma-1}\left[\left(\frac{p}{p_0}\right)^{\frac{1-\gamma}{\gamma}} - 1\right]}$$

V. Probe calibration

V.1. General procedure

We are going to do several measurements with our probe in the SEG, at different Mach numbers and different Reynolds numbers. We then plot the results applying the software TECPLOT. We have to find the best interpolation of our plots in order to be able to get the flow values from the pressure coefficients.

V.2. Measurement program and positioning of the probe

To calibrate the probe, we have to record the pressures given by the four tapping points of the probe at different angle values. The probe can be rotated according to two angles:

- ⇨ the incidence angle α (from -30° to 30°)
- ⇨ the radial angle β (from -10° to 10°)

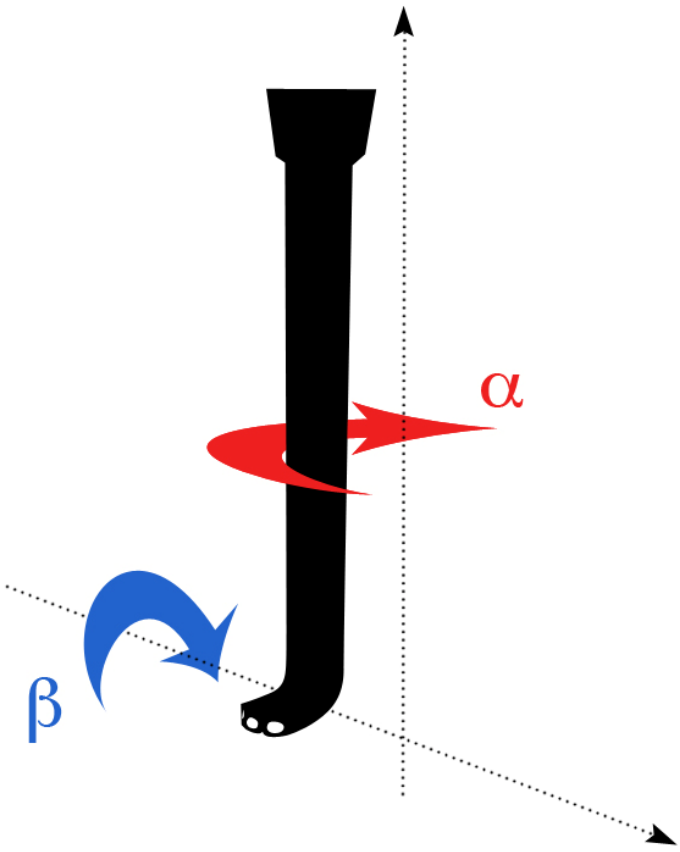

Figure 10: Angles of rotation of the probe

For each measurement point, the probe stops moving for half a second, which is sufficient for the flow to become steady again around the probe. The total pressure in the inlet will be set either to 100kPa or 30kPa in order to have different Reynolds numbers for the future use of the probe in the RGG. The temperature will be around 22°C.

The calibration of the probe covers a wide range of Mach numbers, beginning at Ma=0.2 and ending at Ma=1.8. We thus obtain measurements for 18 different Mach numbers. To achieve these velocities, we utilize in the SEG a subsonic nozzle (Ma = 0.2 - 0.9), a transonic nozzle (Ma = 0.95 - 1.3) and three supersonic (Laval) nozzles (Ma = 1.4, 1.6, 1.8).

Before staring the probe needs to be aerodynamically centered, because its « geometrical zero » according to α can differ from its « aerodynamic zero ». Therefore the probe is positioned in the SEG face to the flow, and then when the air runs at a fixed Mach number, the probe rotates according to α from -30° to +30°. Finally, the LabVIEW software acquires and saves all the pressure data, we only have to check the incidence angle which is associated with psl = psr. This angle will be the « aerodynamic zero » of our probe and all the further measurements will be referred to this angle.

The raw data from the LabVIEW software aren't easily processable, so an existing program written in FORTRAN will rearrange the data in order to be able to use them directly in TECPLOT.

s237_080.dat

```
#    Makm   pkmean  Tomean  ;  RRT6-Sonde 2007
#    0.802  0.6548  22.50
# alpha   beta    Mar     Mad    p01      p0s     psl    psr      pbu    calfa     cma    T01   qT0s[%] T01-T0s rT0s   cmab
ZONE T="Ma0.80", I=23, J= 5
  -30.0   -10.0 0.8020  0.808 100.0075  0.8986  0.6167  0.9795  0.5540 -3.6097  0.4151  22.48  1.1225   3.32  0.9015  0.8609
  -25.0   -10.0 0.7984  0.807  99.8413  0.9245  0.6461  0.9703  0.5546 -2.7890  0.4424  22.48  1.0997   3.25  0.9027  0.8866
  -20.0   -10.0 0.7999  0.808  99.8738  0.9459  0.7000  0.9550  0.5515 -2.1545  0.4412  22.48  1.0883   3.22  0.9041  0.9128
  -16.0   -10.0 0.8007  0.808  99.8491  0.9593  0.7355  0.9390  0.5514 -1.6666  0.4453  22.48  1.0851   3.21  0.9045  0.9258
  -14.0   -10.0 0.8004  0.808  99.8144  0.9650  0.7497  0.9290  0.5501 -1.4264  0.4509  22.49  1.0799   3.19  0.9049  0.9334
  -12.0   -10.0 0.7995  0.807  99.7787  0.9696  0.7638  0.9187  0.5501 -1.2067  0.4550  22.48  1.0720   3.17  0.9054  0.9376
  -10.0   -10.0 0.8002  0.809  99.7498  0.9736  0.7796  0.9085  0.5508 -0.9951  0.4563  22.48  1.0723   3.17  0.9055  0.9401
   -8.0   -10.0 0.8006  0.809  99.7374  0.9769  0.7931  0.8974  0.5509 -0.7923  0.4595  22.48  1.0622   3.14  0.9065  0.9429
   -6.0   -10.0 0.8018  0.810  99.7365  0.9792  0.8064  0.8852  0.5500 -0.5910  0.4622  22.48  1.0565   3.12  0.9073  0.9464
   -4.0   -10.0 0.7902  0.798  99.5423  0.9812  0.8231  0.8740  0.5600 -0.3838  0.4602  22.47  1.0572   3.13  0.9048  0.9322
   -2.0   -10.0 0.7961  0.805  99.6773  0.9816  0.8353  0.8600  0.5567 -0.1842  0.4625  22.48  1.0585   3.13  0.9059  0.9378
    0.0   -10.0 0.7960  0.804  99.7263  0.9814  0.8486  0.8467  0.5586  0.0139  0.4623  22.48  1.0594   3.13  0.9058  0.9346
    2.0   -10.0 0.8012  0.809  99.7990  0.9807  0.8602  0.8307  0.5559  0.2182  0.4654  22.49  1.0652   3.15  0.9064  0.9383
    4.0   -10.0 0.7994  0.808  99.7655  0.9796  0.8729  0.8156  0.5569  0.4238  0.4658  22.48  1.0704   3.16  0.9055  0.9357
    6.0   -10.0 0.8005  0.809  99.8009  0.9775  0.8843  0.7991  0.5571  0.6271  0.4673  22.48  1.0763   3.18  0.9052  0.9335
    8.0   -10.0 0.8029  0.812  99.8457  0.9745  0.8951  0.7812  0.5561  0.8356  0.4691  22.48  1.0810   3.20  0.9054  0.9323
   10.0   -10.0 0.8013  0.810  99.8044  0.9708  0.9054  0.7637  0.5573  1.0396  0.4699  22.48  1.0805   3.19  0.9051  0.9270
   12.0   -10.0 0.8019  0.810  99.7197  0.9667  0.9148  0.7453  0.5579  1.2403  0.4717  22.47  1.0821   3.20  0.9050  0.9221
   14.0   -10.0 0.8054  0.815  99.7231  0.9614  0.9229  0.7232  0.5529  1.4427  0.4765  22.47  1.0851   3.21  0.9055  0.9254
   16.0   -10.0 0.7996  0.799  99.6938  0.9565  0.9330  0.7087  0.5657  1.6528  0.4726  22.47  1.0951   3.24  0.9034  0.8997
   20.0   -10.0 0.7996  0.808  99.6973  0.9421  0.9480  0.6613  0.5575  2.0860  0.4800  22.47  1.1042   3.26  0.9026  0.8993
   25.0   -10.0 0.8027  0.812  99.7944  0.9184  0.9620  0.6097  0.5528  2.6595  0.4771  22.47  1.1266   3.33  0.9013  0.8833
   30.0   -10.0 0.8082  0.817  99.9171  0.8895  0.9715  0.5669  0.5477  3.3641  0.4604  22.48  1.1416   3.38  0.9012  0.8621
  -30.0    -5.0 0.8059  0.813  99.7296  0.9051  0.6017  0.9875  0.5477 -3.4914  0.4354  22.48  1.1231   3.32  0.9023  0.8785
  -25.0    -5.0 0.8003  0.809  99.6059  0.9324  0.6495  0.9775  0.5440 -2.7591  0.4458  22.47  1.1067   3.27  0.9025  0.9121
  -20.0    -5.0 0.8001  0.807  99.6695  0.9552  0.6987  0.9623  0.5364 -2.1152  0.4514  22.47  1.0896   3.22  0.9040  0.9466
  -16.0    -5.0 0.8008  0.807  99.7319  0.9695  0.7342  0.9460  0.5337 -1.6368  0.4571  22.48  1.0879   3.22  0.9043  0.9643
```

Figure 11: Example of a data file for use with TECPLOT

During the calibration, we encountered a problem: we could not come down to 30kPa total pressure with supersonic flows. The inlet pressure of the compressor 2 was below 15 kPa which prompted the automatic control system of the SEG to stop the compressor. We had to choose the lowest total pressures that we could reach, which were:

- p_0 = 35 kPa at Ma= 1.4
- p_0 = 40 kPa at Ma= 1.6
- p_0 = 51 kPa at Ma= 1.8

Nevertheless, it will not be a problem for the future use of the probe. Indeed, once positioned between a stator and a rotor of a turbine, where the flow is supersonic, the total pressure is about 100 kPa.

V.3. Characteristics of the probe in a three-dimensional flow field

As we obtained numerous data (almost 150 plots with TECPLOT) it will be impossible to detail all the results. That's why we will study results for only specific Mach numbers, other results will be shown in the annex.

After importing raw data in TECPLOT, we plotted the evolution of C_α and p_{0s} against α and β in order to study the three-dimensional behaviour of the probe. Here are the results:

➔ Subsonic flow:

p_0= 30 kPa:

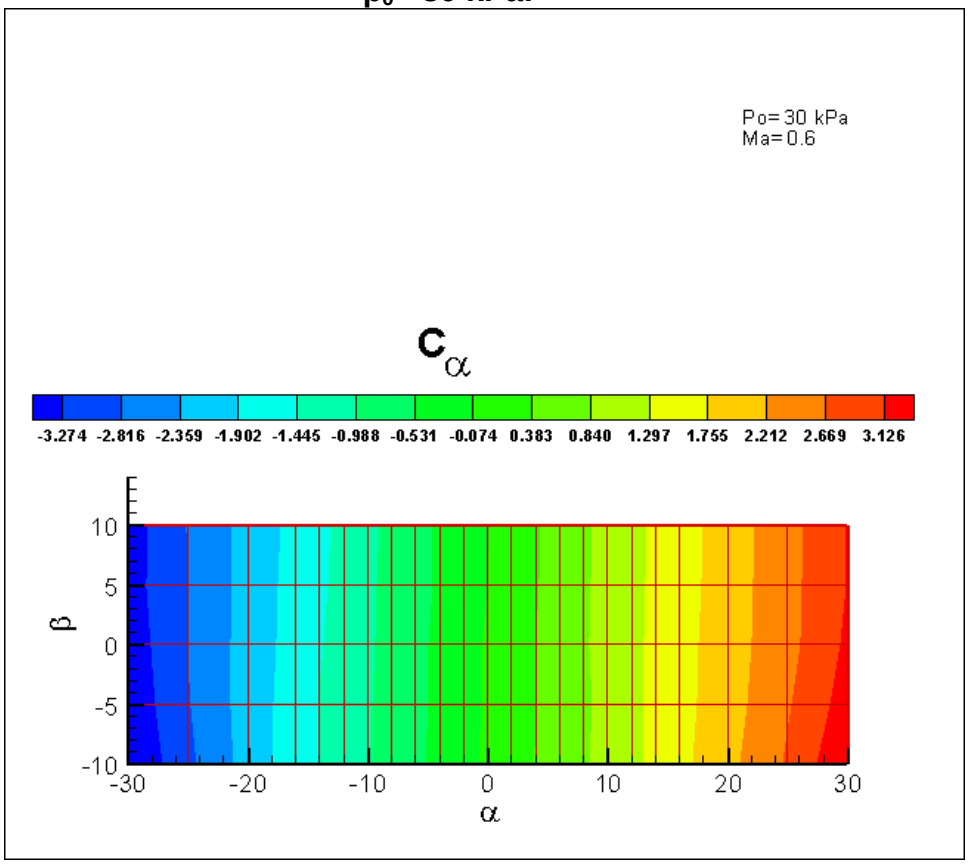

Figure 12: Evolution of C_α against α and β at Ma=0.6 and p_0=30kPa

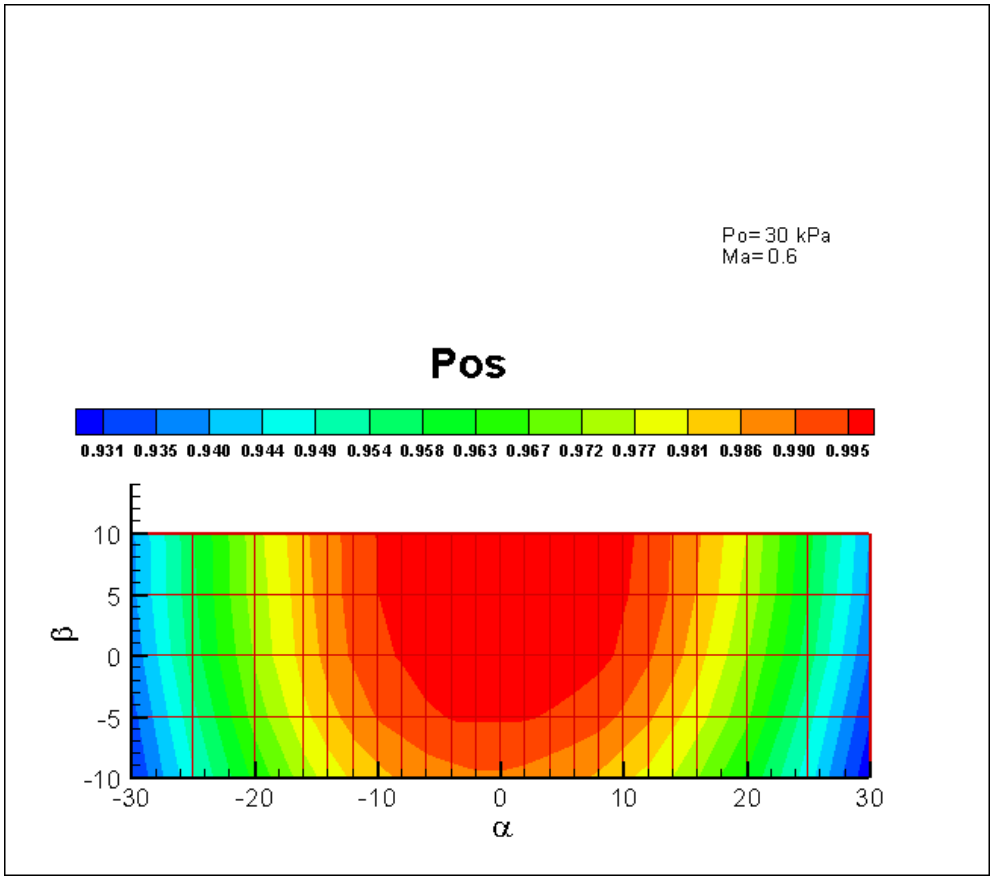

Figure 13: Evolution of p_{0s} against α and β at Ma=0.6 and p_0=30kPa

p_0= 100 kPa:

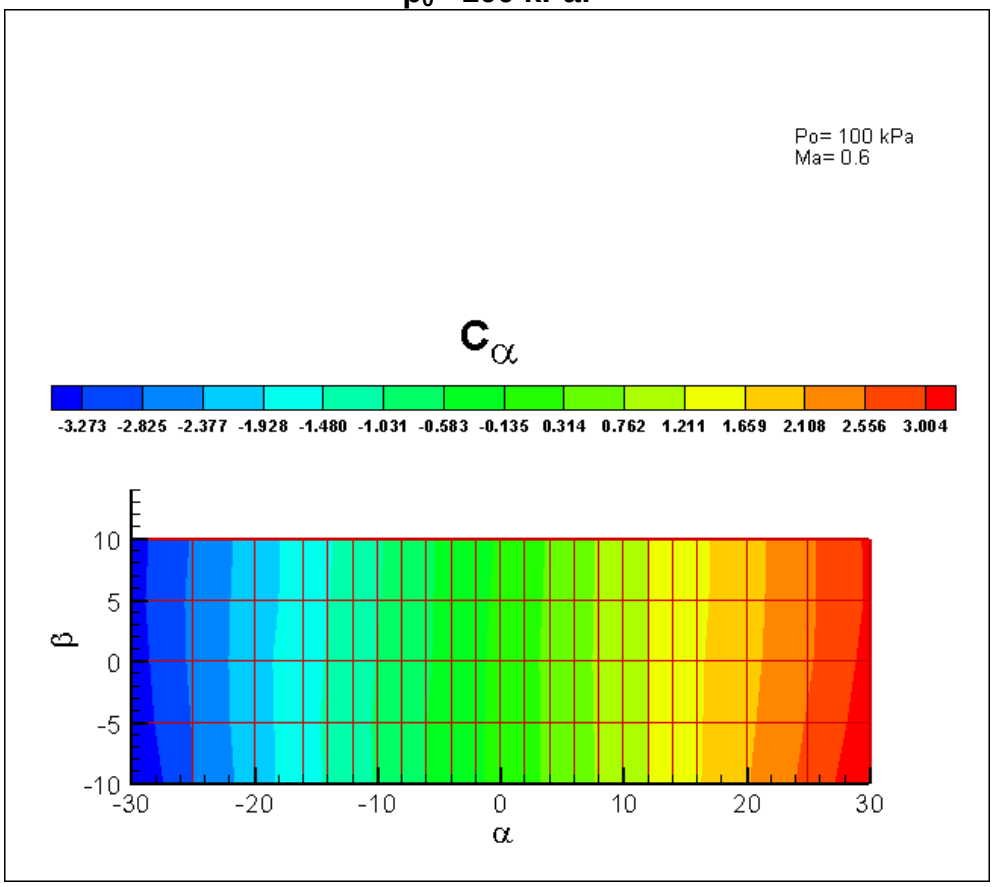

Figure 14: Evolution of C_α against α and β at Ma=0.6 and p_0=100kPa

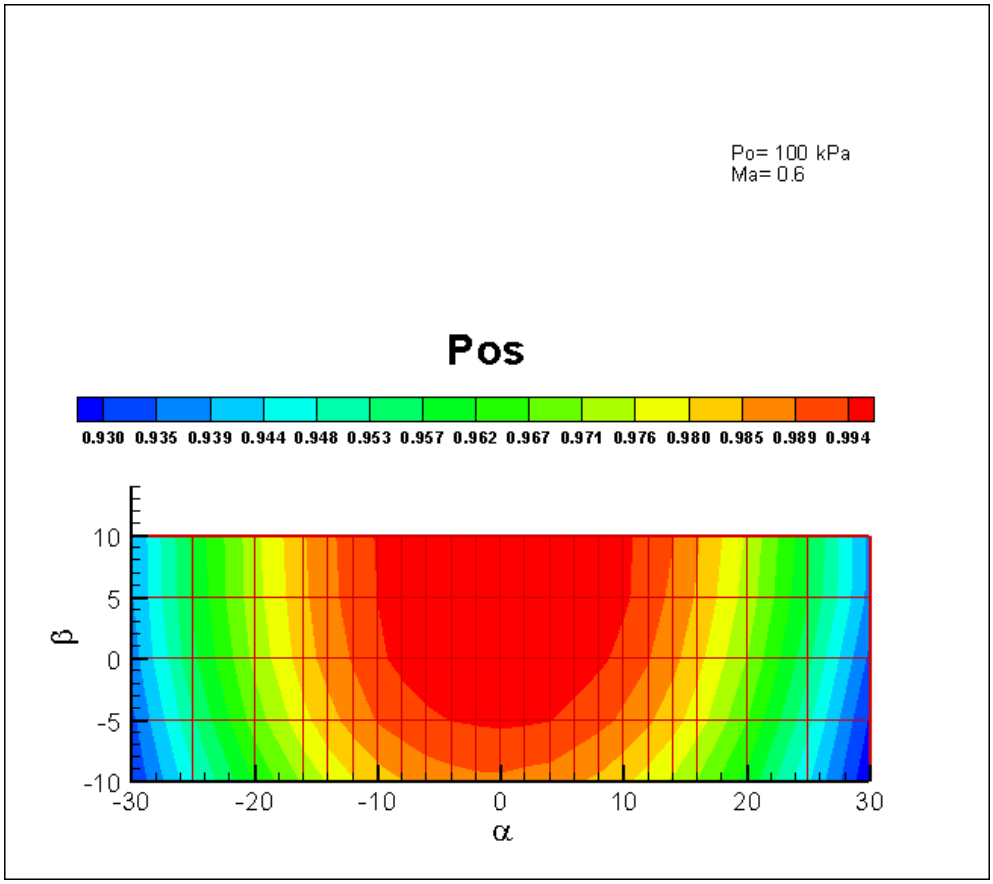

Figure 15: Evolution of p_{0s} against α and β at Ma=0.6 and p_0=100kPa

➔ Transonic flow:

p_0= 30 kPa:

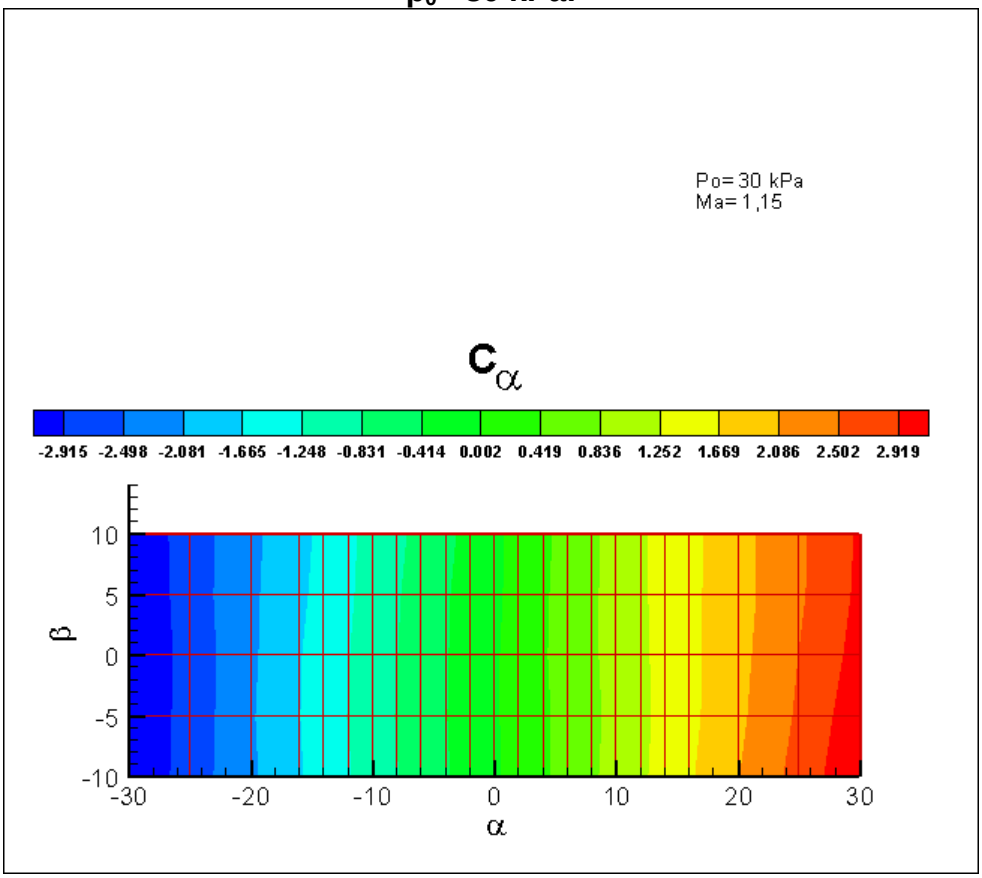

Figure 16: Evolution of C_α against α and β at Ma=1.15 and p_0=30kPa

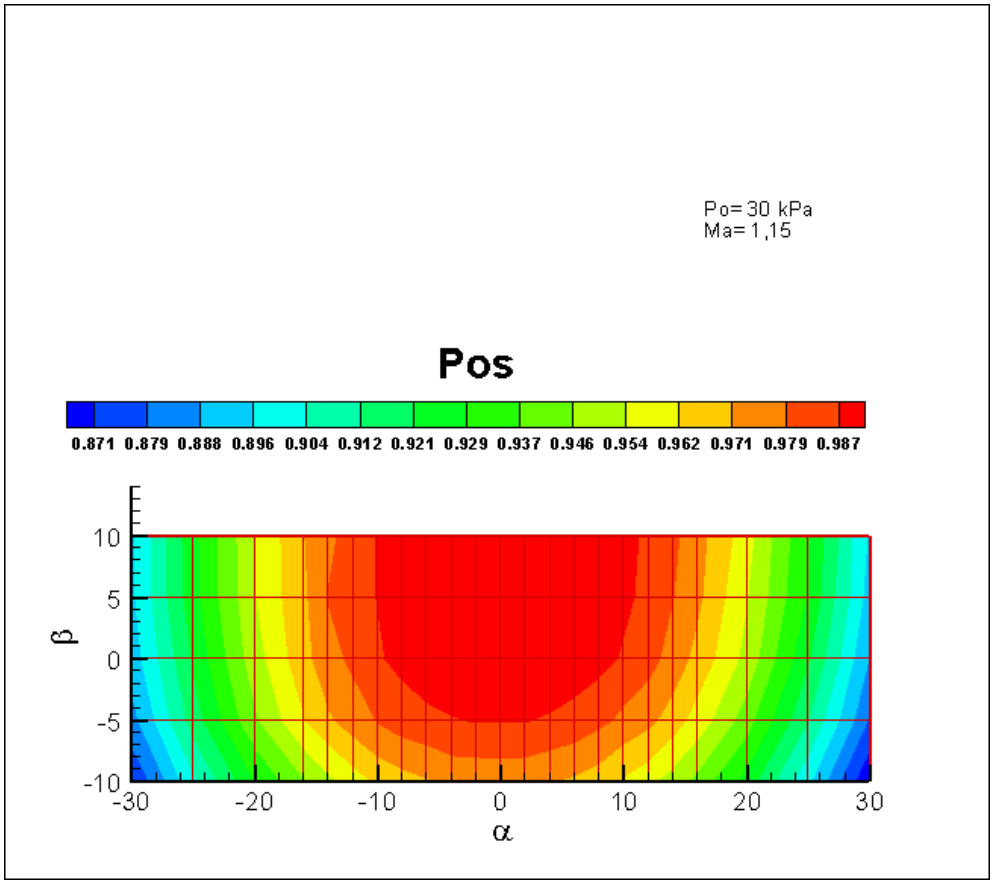

Figure 17: Evolution of p_{0s} against α and β at Ma=1.15 and p_0=30kPa

p_0= 100 kPa:

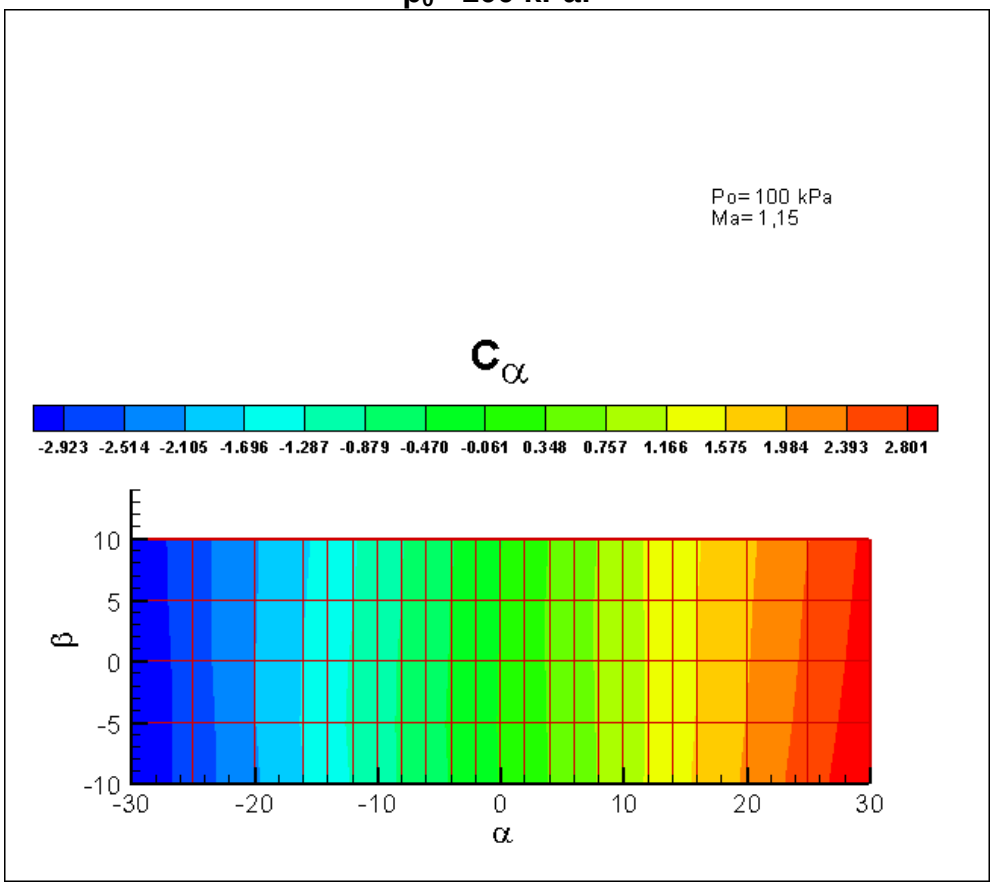

Figure 18: Evolution of C_α against α and β at Ma=1.15 and p_0=100kPa

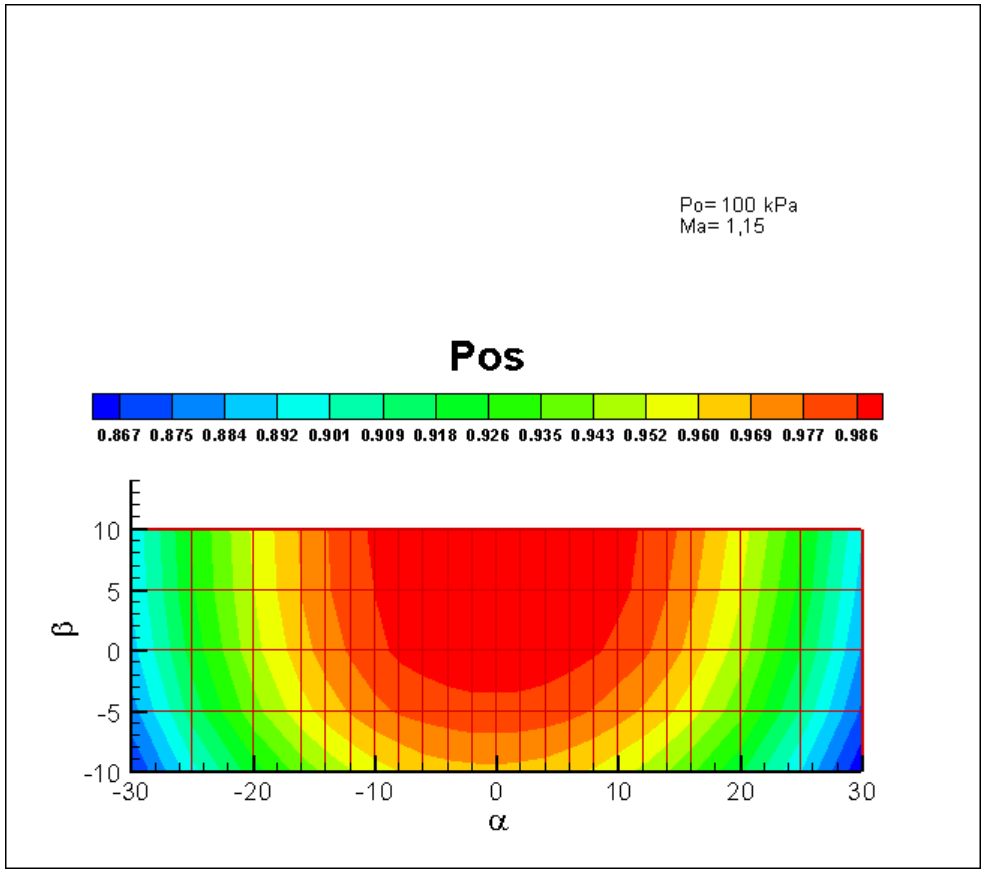

Figure 19: Evolution of p_{0s} against α and β at Ma=1.15 and p_0=100kPa

➔ Supersonic flow:

p_0= 40 kPa:

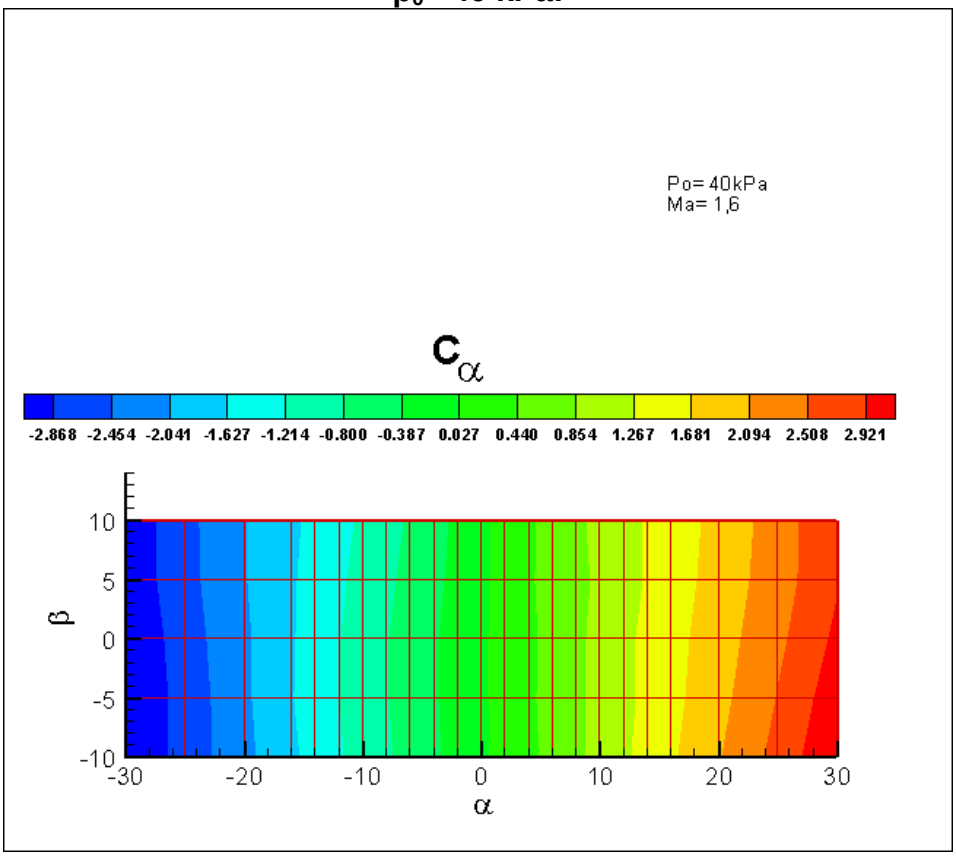

Figure 20: Evolution of C_α against α and β at Ma=1.6 and p_0=40kPa

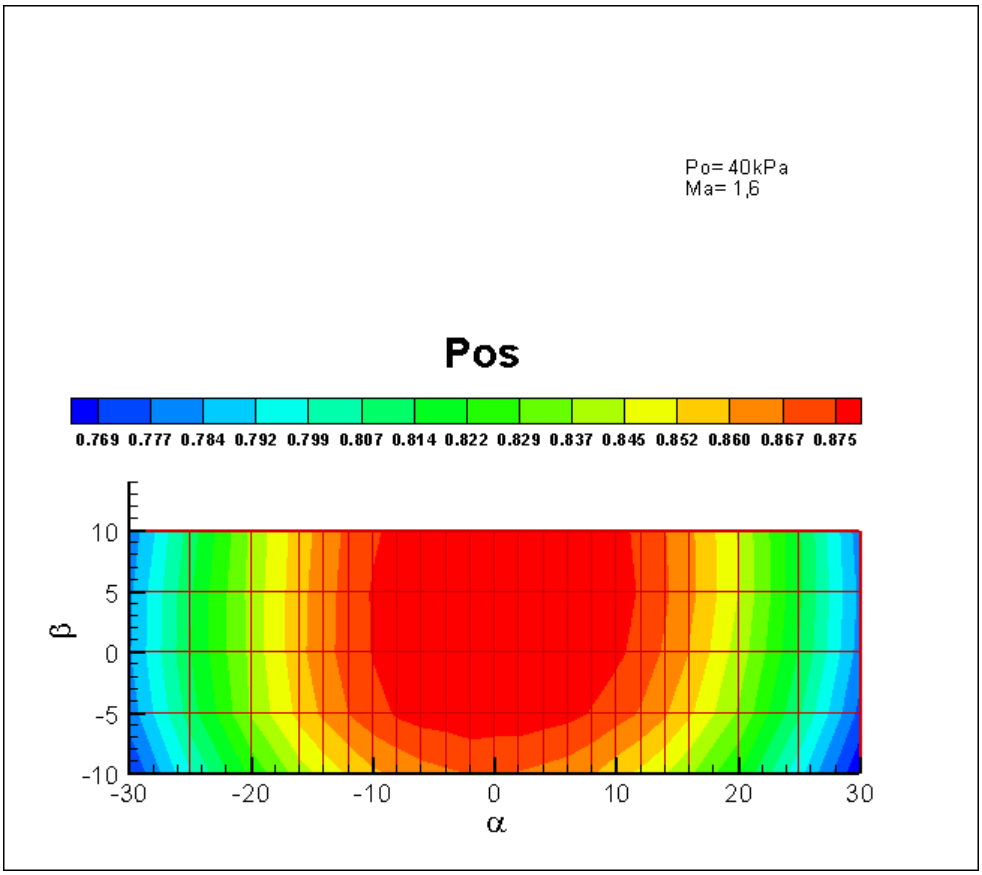

Figure 21: Evolution of p_{0s} against α and β at Ma=1.6 and p_0=40kPa

p_0= 100 kPa:

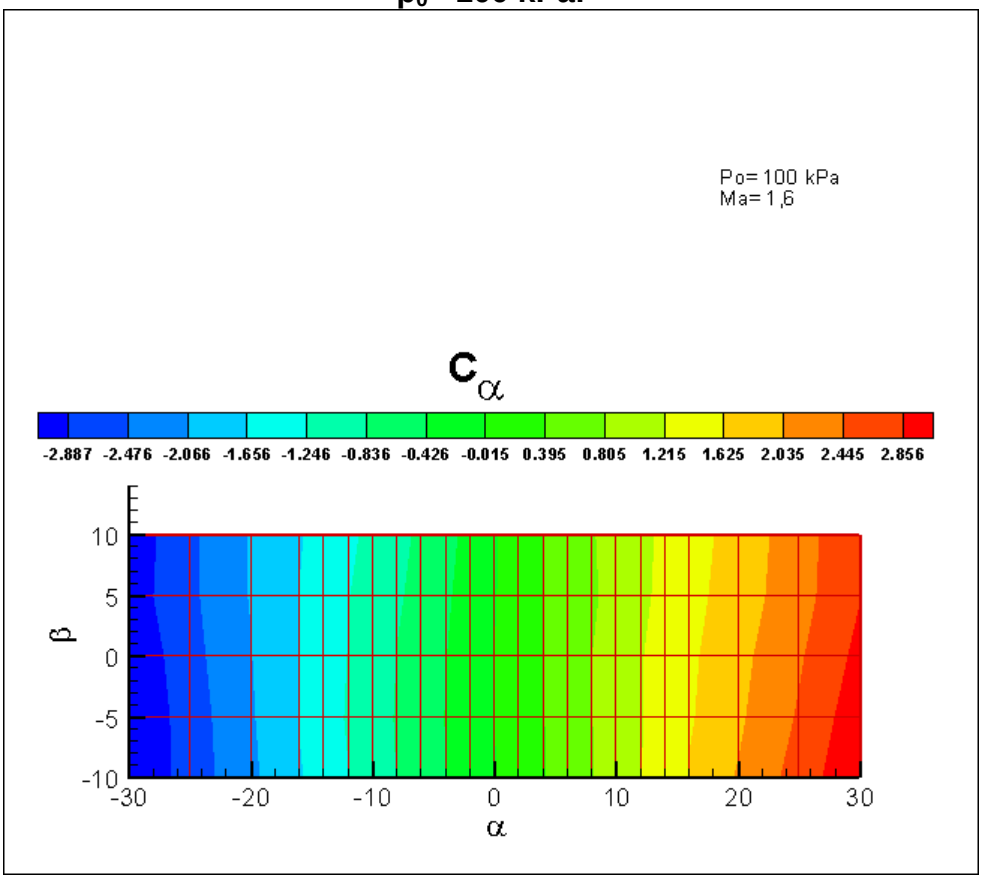

Figure 22: Evolution of C_α against α and β at Ma=1.6 and p_0=100kPa

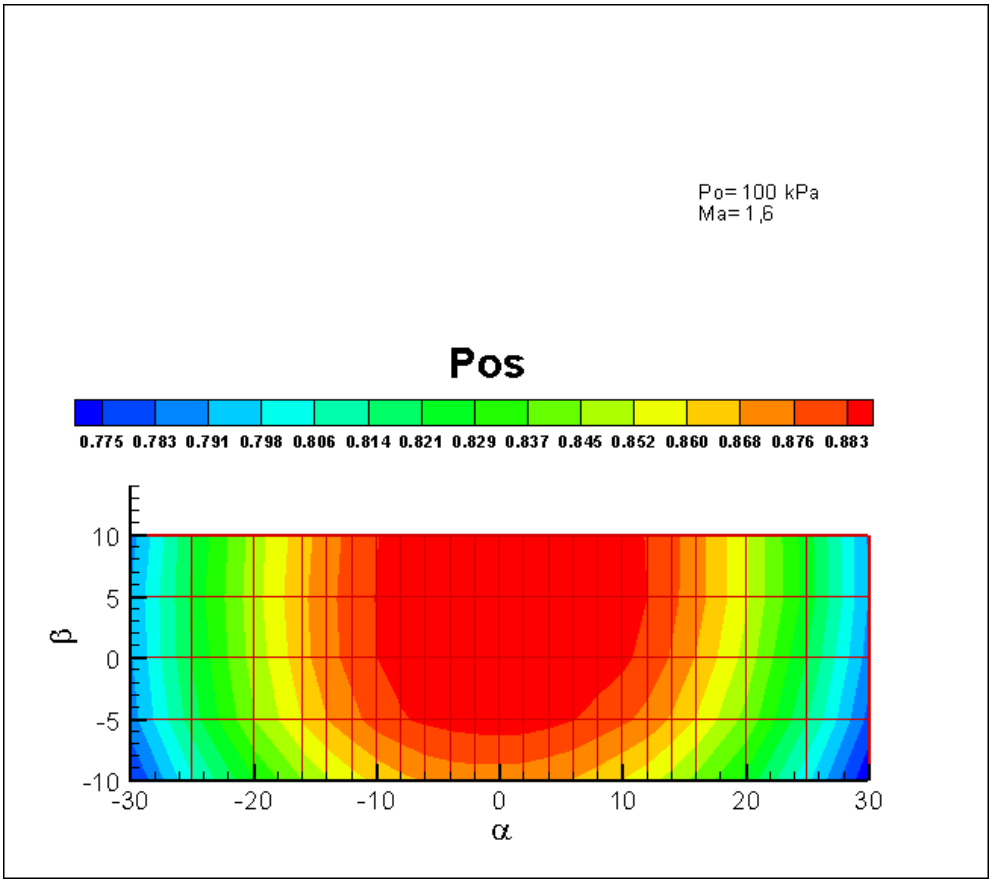

Figure 23: Evolution of p_{0s} against α and β at Ma=1.6 and p_0=100kPa

We can notice that for all Mach numbers and all total pressures, the pressure coefficient C_α is independent of the radial angle β with the exception of high incidence angles ($|\alpha| > 20°$). This will be useful to determine the incidence angle α.

On the other hand, the stagnation pressure, $p_{0s,}$ measured by the probe is dependent on both, incidence angle and radial angle.

This behaviour is similar for all Mach numbers and all the Reynolds numbers of the calibration.

V.4. Incidence angle effects

V.4.a. Determination of α from C_α

If we plot the evolution of the pressure coefficient, $C_{\alpha,}$ against the incidence angle α, we notice that, for all Mach numbers, we obtain a linear relation. This relation is visualized by a linear fit for incidence angles between -16° and +16°.

➔ Subsonic flow:

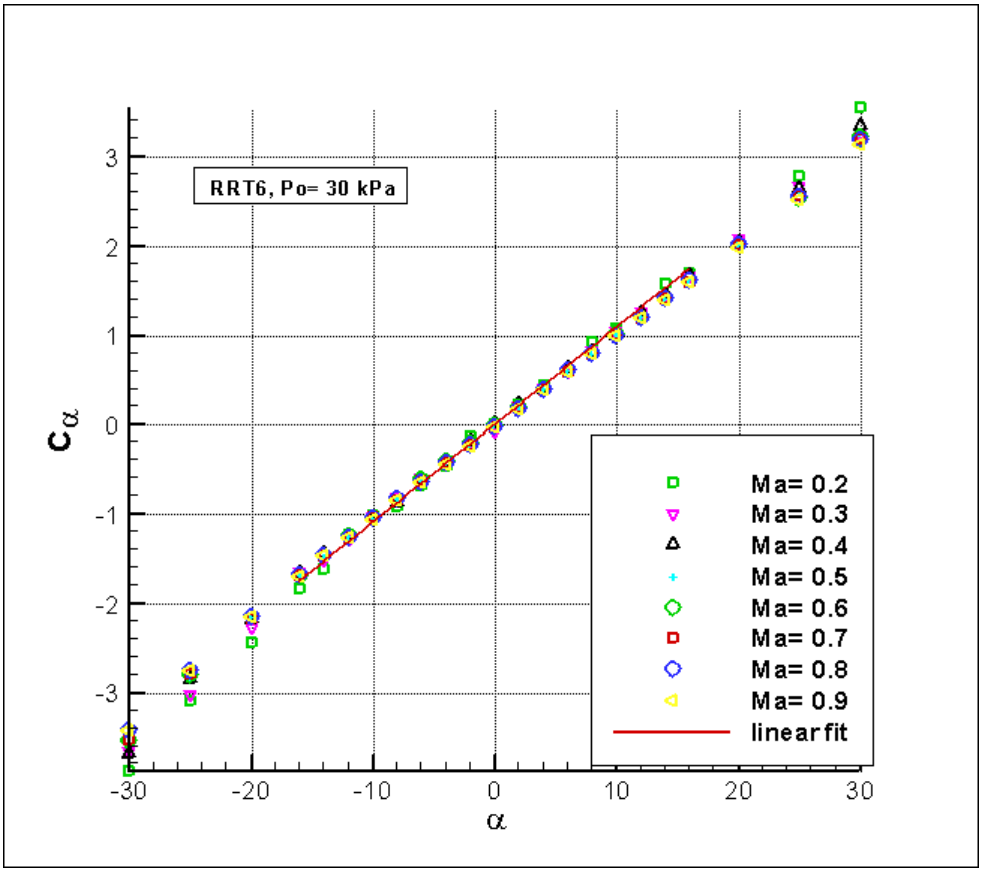

Figure 24: Evolution of C_α against α for subsonic flow and p0=30kPa

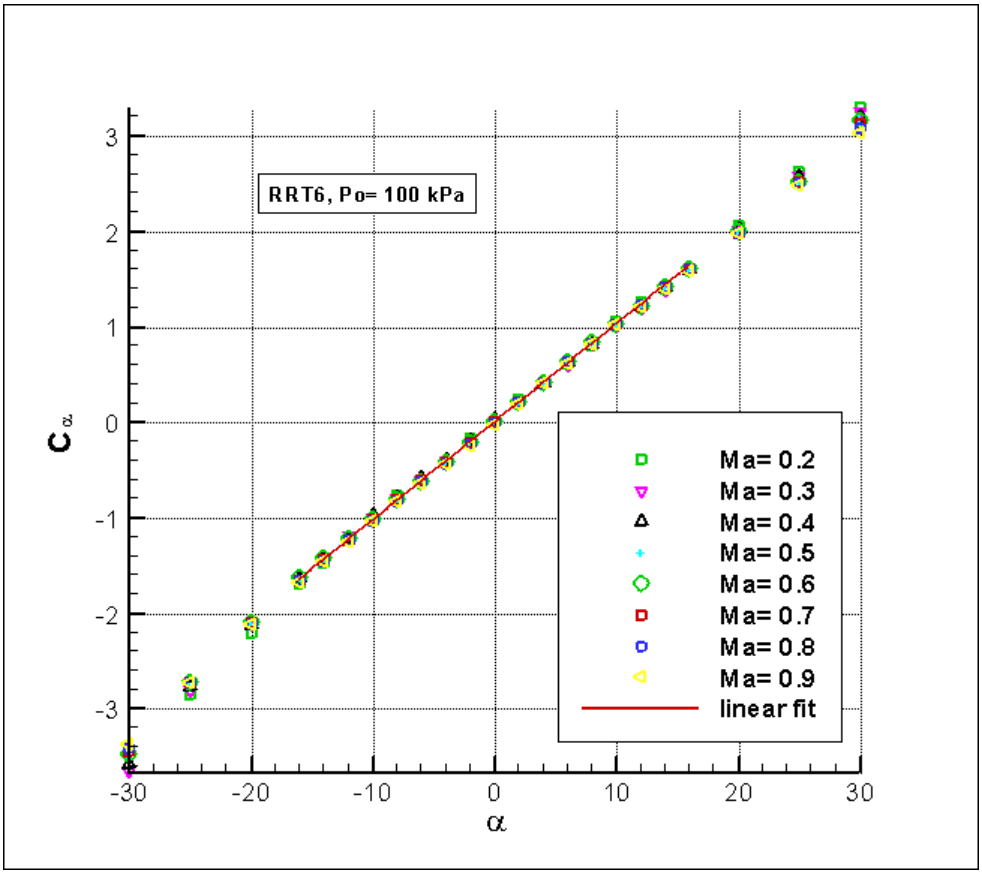

Figure 25: Evolution of C_α against α for subsonic flow and p_0=100kPa

➔ Transonic flow:

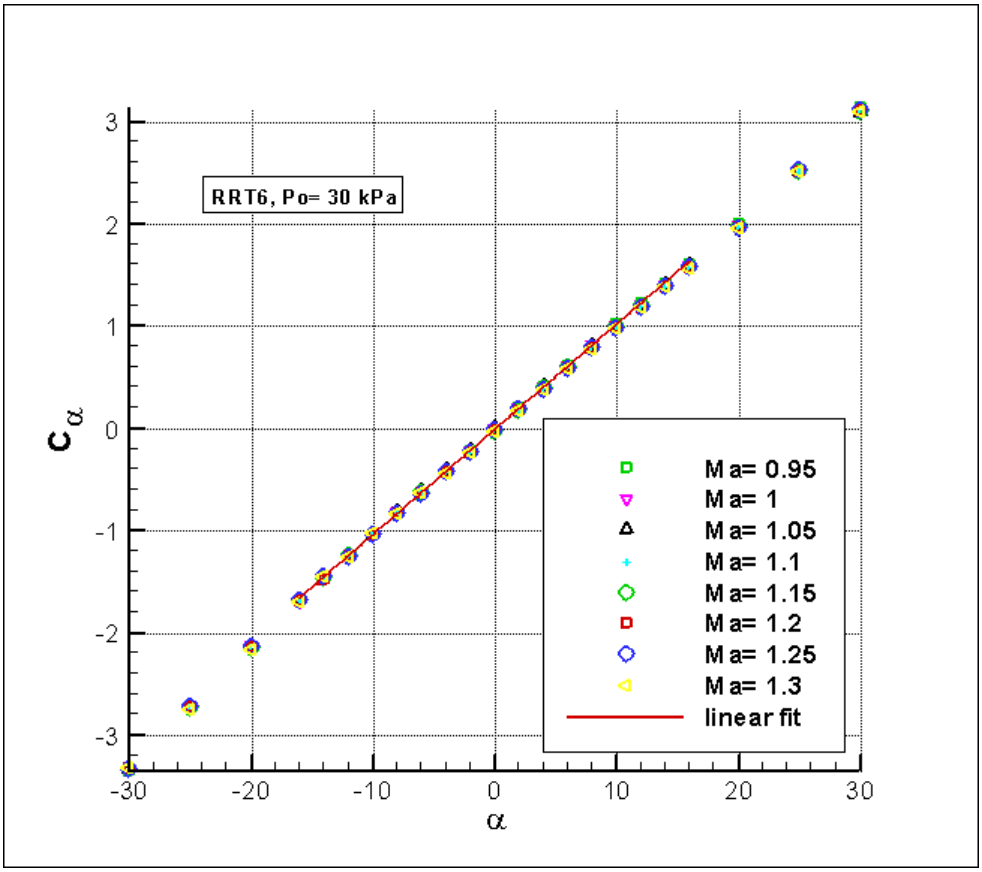

Figure 26: Evolution of C_α against α for transonic flow and p_0=30kPa

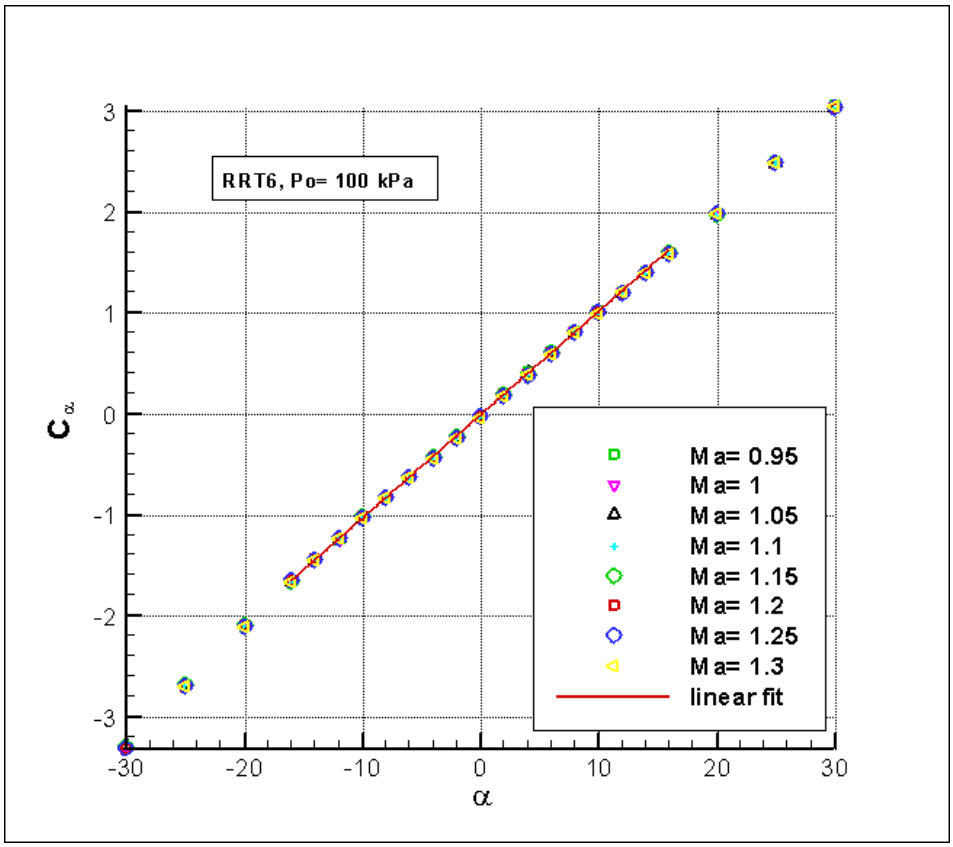

Figure 27: Evolution of C_α against α for transonic flow and p_0=100kPa

➔ Supersonic flow (only for p_0 = 100kPa):

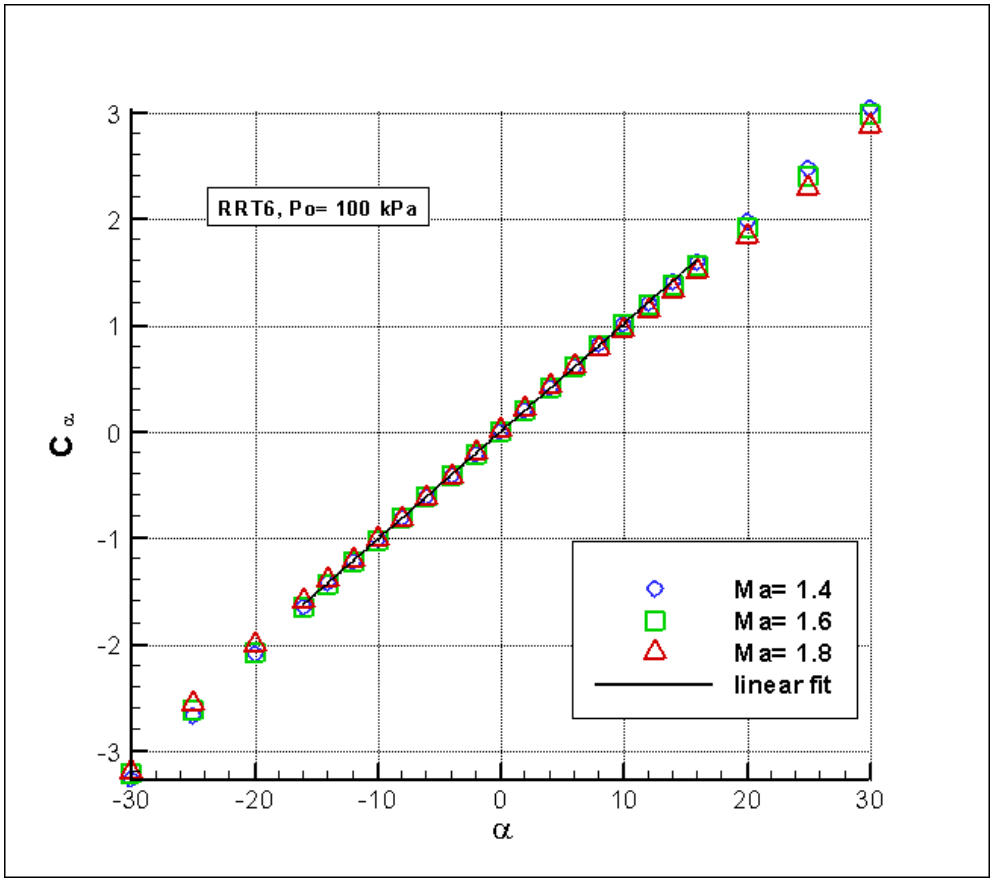

Figure 28: Evolution of C_α against α for supersonic flow and p_0 =100kPa

Once again, these results remain valid for all Mach numbers and all Reynolds numbers.
The linear behaviour of the pressure coefficient allows to write:

$$C_\alpha = a_1 \cdot \alpha + a_0$$

We observed that a_0 could be neglected (values around 10^{-2} and 10^{-3}), so the final equation is:

$$C_\alpha = a_1 \cdot \alpha \quad (5)$$

The different a_1 coefficients for $-16° < \alpha < +16°$ are listed below:

➔ Subsonic flow:

p_0= 30kPa

Ma	a_1
0.2	0.1092
0.3	0.1040
0.4	0.1039
0.5	0.1030
0.6	0.1026
0.7	0.1026
0.8	0.1026
0.9	0.1027

p_0= 100kPa

Ma	a_1
0.2	0.1027
0.3	0.1010
0.4	0.1001
0.5	0.1015
0.6	0.1019
0.7	0.1023
0.8	0.1025
0.9	0.1024

➔ Transonic flow:

p_0= 30kPa

Ma	a_1
0.95	0.1029
1.00	0.1026
1.05	0.1021
1.10	0.1017
1.15	0.1017
1.20	0.1017
1.25	0.1015
1.30	0.1014

p_0= 100kPa

Ma	a_1
0.95	0.1023
1.00	0.1021
1.05	0.1019
1.10	0.1019
1.15	0.1016
1.20	0.1015
1.25	0.1015
1.30	0.1016

➔ Supersonic flow:

Only for p_0 = 100kPa because of the limitations of the compressor.

Ma	a_1
1.4	0.1013
1.6	0.1010
1.8	0.09812

Thus, we get a mean value of the coefficient $a_1 = 0.10215 \pm 0.54$ E-3

We can now easily determine the incidence of the air flow on the probe by calculating the pressure coefficient C_α thanks to equation (1) and to obtain α from the equation (5). Besides, this method will allows us to find the « aerodynamic zero » very quickly.

V.4.b. Study of the probe at zero incidence

The figures *29*, *30* and *31* show the evolution of the coefficient C_{Ma} against Mach number for the total pressure p_0 = 100 kPa with α= 0 and β = 0.

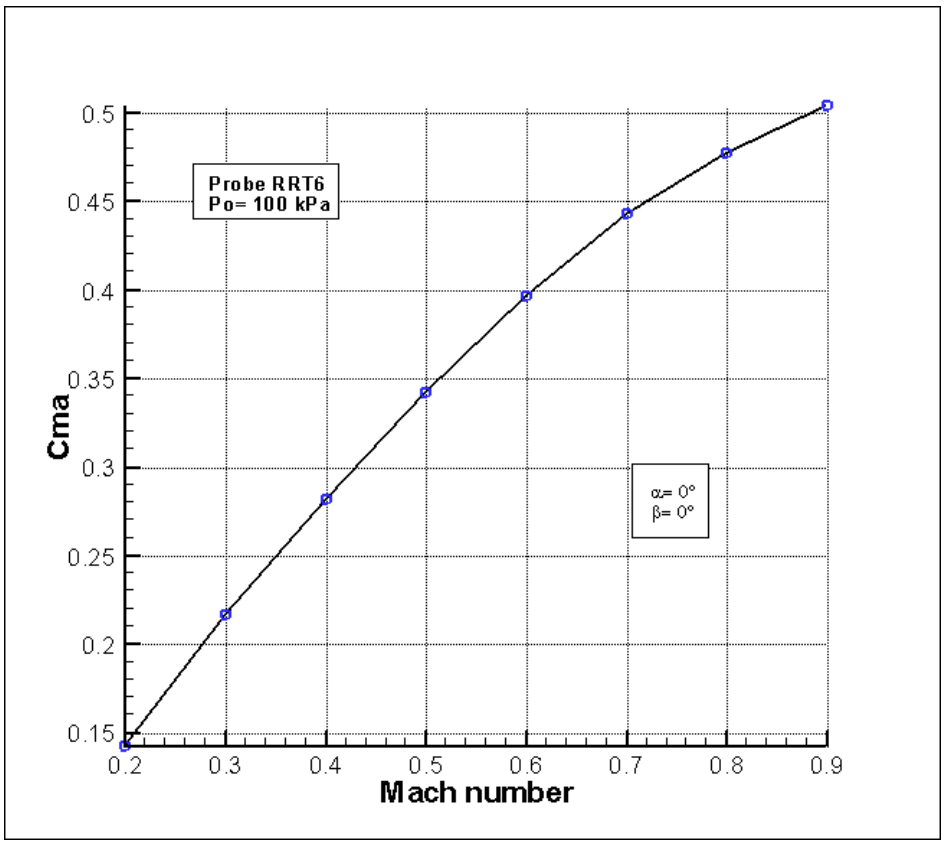

Figure 29: Evolution of C_{Ma} against Ma for subsonic flow and p_0 = 100 kPa

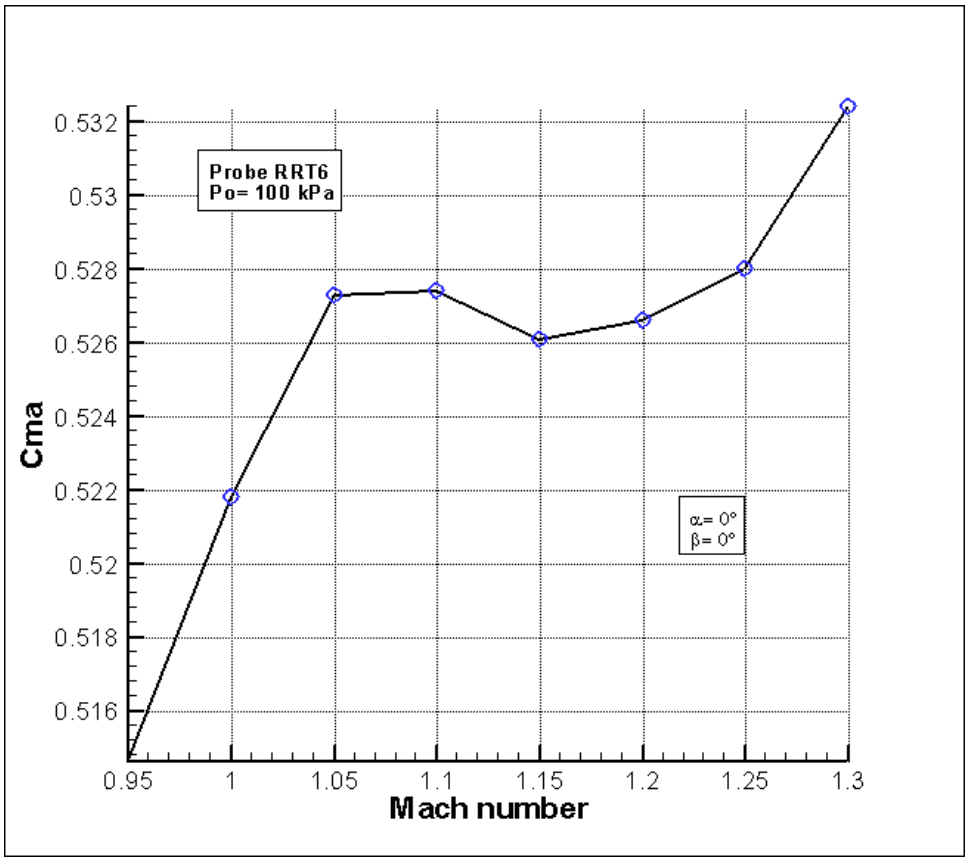

Figure 30: Evolution of C_{Ma} against Ma for transonic flow and p_0 = 100 kPa

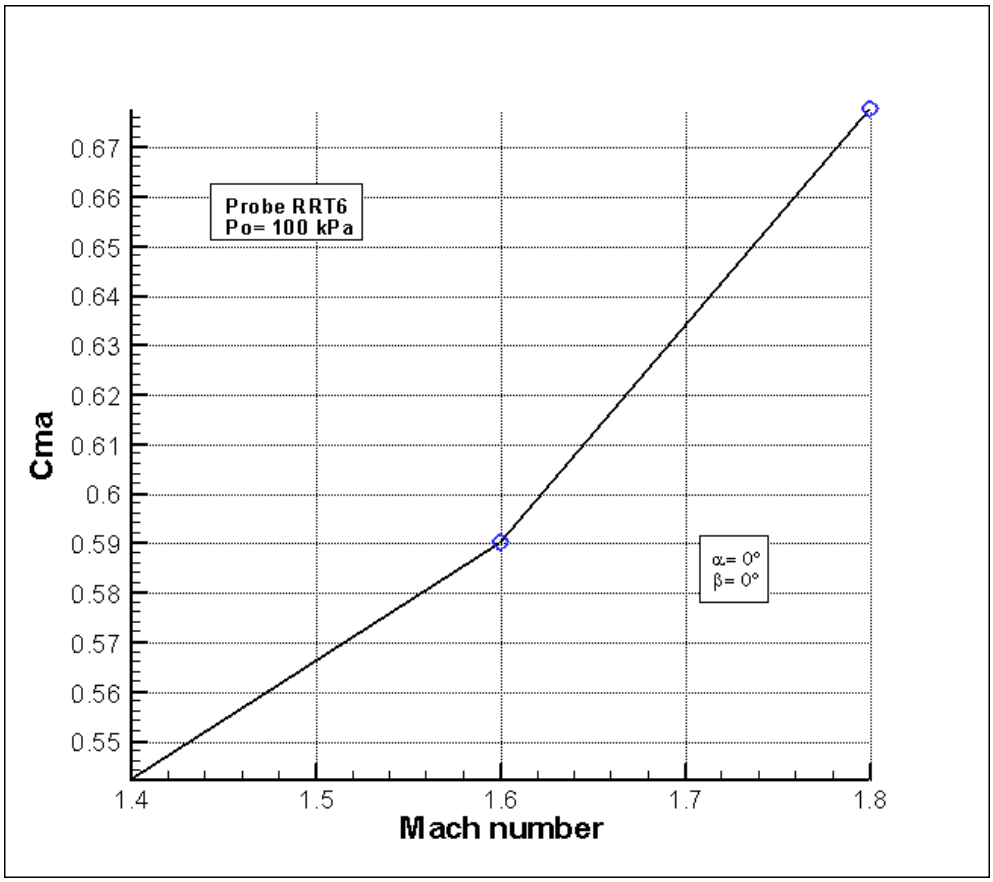

Figure 31: Evolution of C_{Ma} against Ma for supersonic flow and p_0 = 100 kPa

Once the probe is calibrated, we are able, thanks to these plots, to find the velocity of the flow from the coefficient C_{Ma}. Subsonic and supersonic speeds allow finding Ma from C_{Ma} easily. But for the transonic speeds, we can see on the *Figure 30* that the curve has locally a negative gradient. This phenomenon is due to a shock wave in front of the probe which causes subsonic conditions at the pressure tappings; this wave is getting closer to the probe when the Mach number increases, but the conditions at the pressure tappings remain subsonic. As a result, there is a lack of information at transonic speeds.

This transonic « zero gradient » phenomenon affects the determination of the Mach number and creates errors because a small variation of C_{Ma} covers a wide range of Mach numbers.

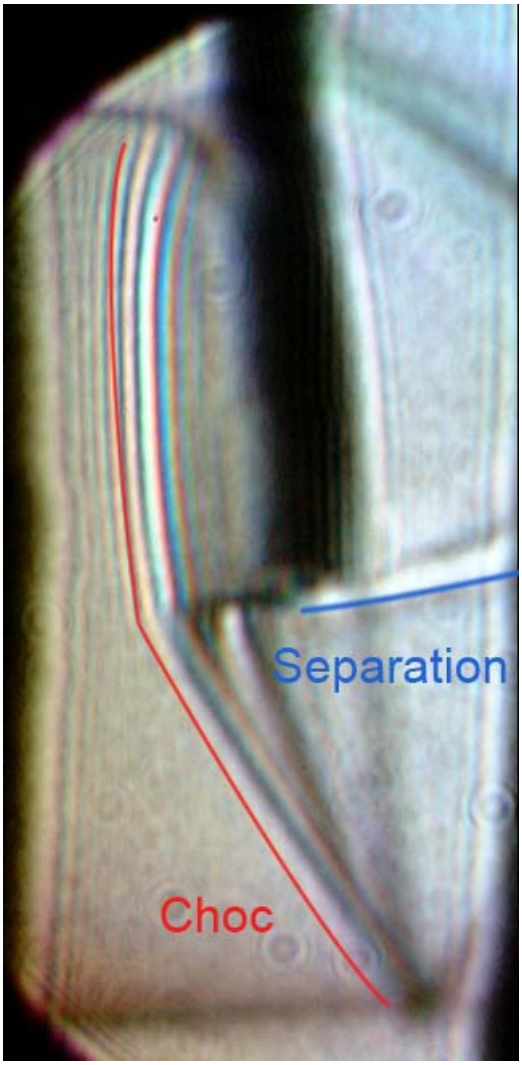

Here is a schlieren picture of the probe during the calibration process at Mach 1.4. Schlieren pictures allow highlighting areas where the gas density suddenly changes thanks to the deviation of the light. The larger the density gradient, the more the light is deviated. On this picture we can see the shock wave in front of the probe and the separation of the flow at the back of the probe.

Figure 32: Schlieren picture of the probe

We can observe this problem on the *figures 33* and *34* which represent now the evolution of the Mach number against C_{Ma}.

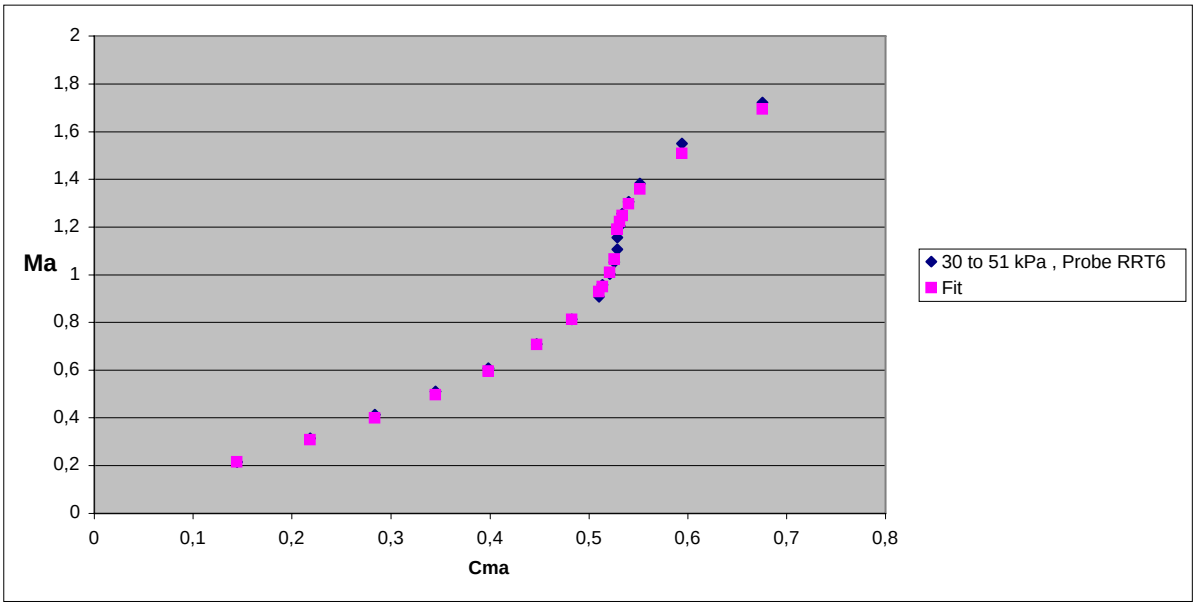

Figure 33: Evolution of Ma against C_{Ma} for p_0=30 to 51kPa

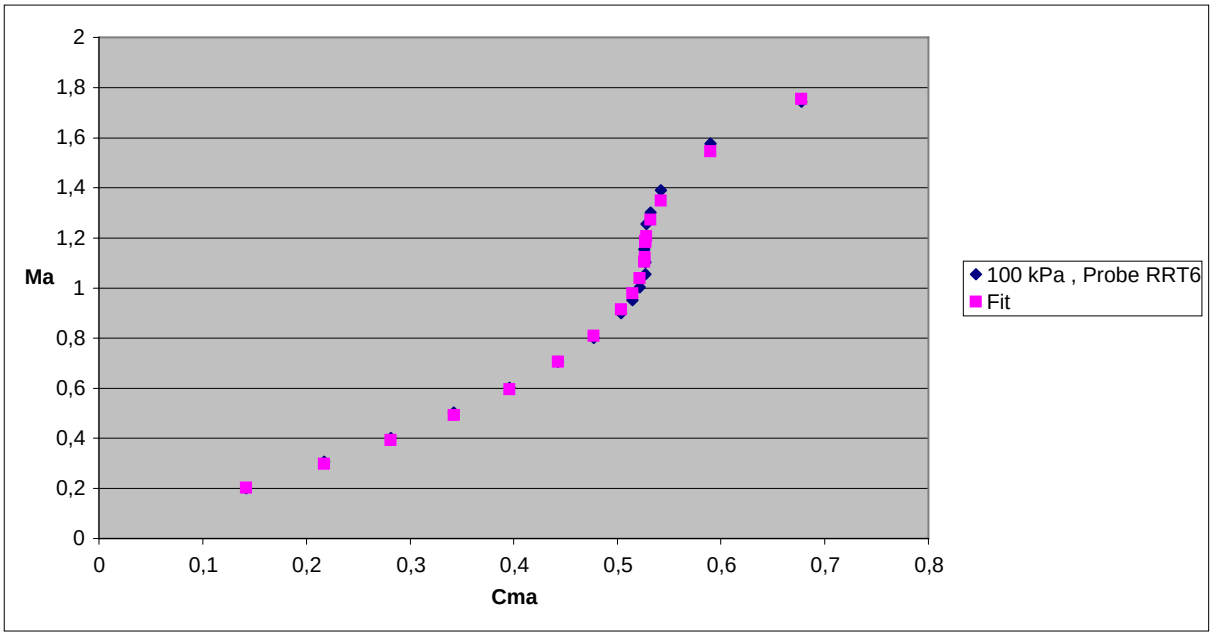

Figure 34: Evolution of Ma against C_{Ma} for p_0 = 100 kPa

We will talk about these fits further in this report.

V.4.c. The transonic problem for the determination of the Mach number

To get rid of this problem, we will take advantage of the fourth pressure tapping at the back of the probe measuring the pressure p_{bu}. This tube is located in an area where the flow velocity is still subsonic (downstream of the shock wave and in the wake of the probe), so the probe will be far more sensitive to a pressure variation. If we consider equation (3), and if we plot the evolution of the Mach number against C_{Mab}, the « zero gradient » disappears for transonic flows, and the determination of the Mach number is more precise.

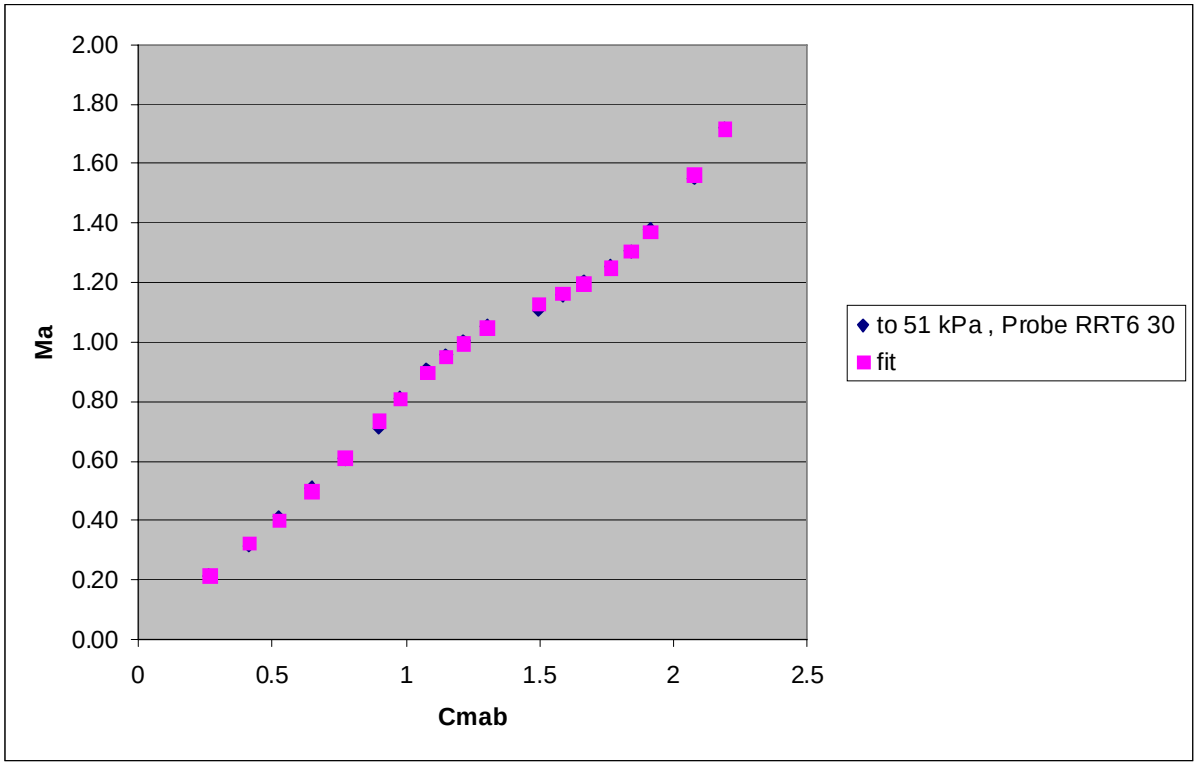

Figure 35: Evolution of Ma against C_{Mab} for p_0 = 30 to 51 kPa

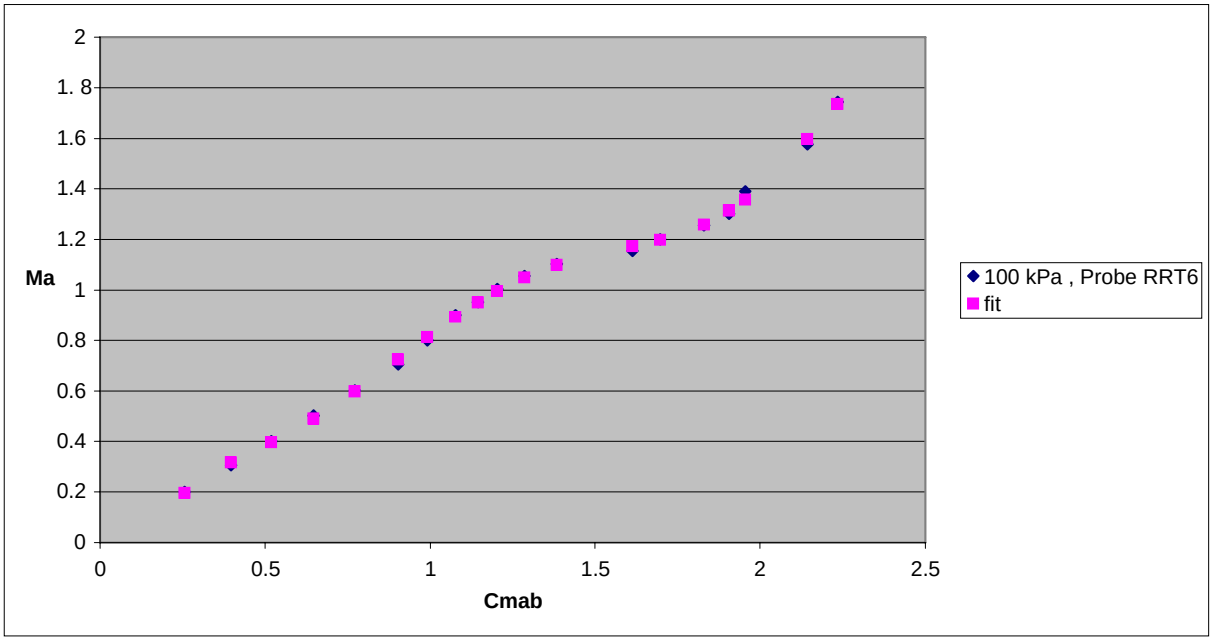

Figure 36: Evolution of Ma against C_{Mab} for p_0 = 100 kPa

These curves were fitted by the following functions:

$$Ma = b_0 + b_1 \times \frac{(C_{Ma} - 0.527)}{|C_{Ma} - 0.527|^{0,5}} + b_2 \times \frac{(C_{Ma} - 0.527)}{|C_{Ma} - 0.527|^{0,7}}$$

Where:

Probe RRT6	30 à 51 kPa	100 kPa
Coefficient b_0	1.124711223017	1.15510659458
Coefficient b_1	1.443185445788	1.4861884779
Coefficient b_2	0.0222934922878	0.040941033949

Polynomial function of C_{Mab}:

$$Ma = g_0 + g_1 \times (C_{Mab}) + g_2 \times (C_{Mab})^2 + g_3 \times (C_{Mab})^3 + g_4 \times (C_{Mab})^4 + g_5 \times (C_{Mab})^5 + g_6 \times (C_{Mab})^6 + g_7 \times (C_{Mab})^7$$

where:

Probe RRT6	30 à 51 kPa	100 kPa
Coefficient g_0	-0.3225466461649	-0.373381399514
Coefficient g_1	3.869297067202	3.940303837422
Coefficient g_2	-10.47696194858	-9.37331497695
Coefficient g_3	16.27384862194	12.08893627133
Coefficient g_4	-12.33385166483	-6.504600173734
Coefficient g_5	4.418654255879	0.5919247647549
Coefficient g_6	-0.5982357629218	0.5915794349819
Coefficient g_7	----------	-0.1410152394165

Thanks to these coefficients and these fit functions, we are now able to get with a quite good precision the flow velocity from the pressures given by the probe.

V.5. Error sensitivity

We wanted to know how an error on the stagnation pressure p_{0s} could affect our calculation of the Mach number. So we added to our values of p_{0s} an error of 0.1%, which spread in our calculations: new p_{0s}, new C_{Ma} coefficient which, once injected in our fit function, gives a new Mach number.
The final error is described as:

$$error = old\ Mach\ number - new\ Mach\ number$$

Results obtained for p_0 = 30 to 51 kPa:

Ma	Error computed from C_{Ma}	Error computed from C_{Mab}
0.2	0.006279612	0.004475113
0.3	0.01260087	0.009600603
0.4	0.018604019	0.010916716
0.5	0.019198992	0.011753944
0.6	0.016031805	0.003648256
0.7	0.006758402	0.02462669
0.8	0.004710999	0.002833135
0.9	0.012600779	0.012657851
0.95	0.016711748	0.006116905
1	0.007109954	0.007990864
1.05	0.013231746	0.005839854
1.1	0.048200076	0.021081748
1.15	0.004920327	0.006969407
1.2	0.000413756	0.008051434
1.25	0.021793126	0.005304657
1.3	0.018508777	0.000219402
1.4	0.029352356	0.011559107
1.6	0.045011247	0.01304997
1.8	0.030635246	0.006049075

This was plotted against the Mach number:

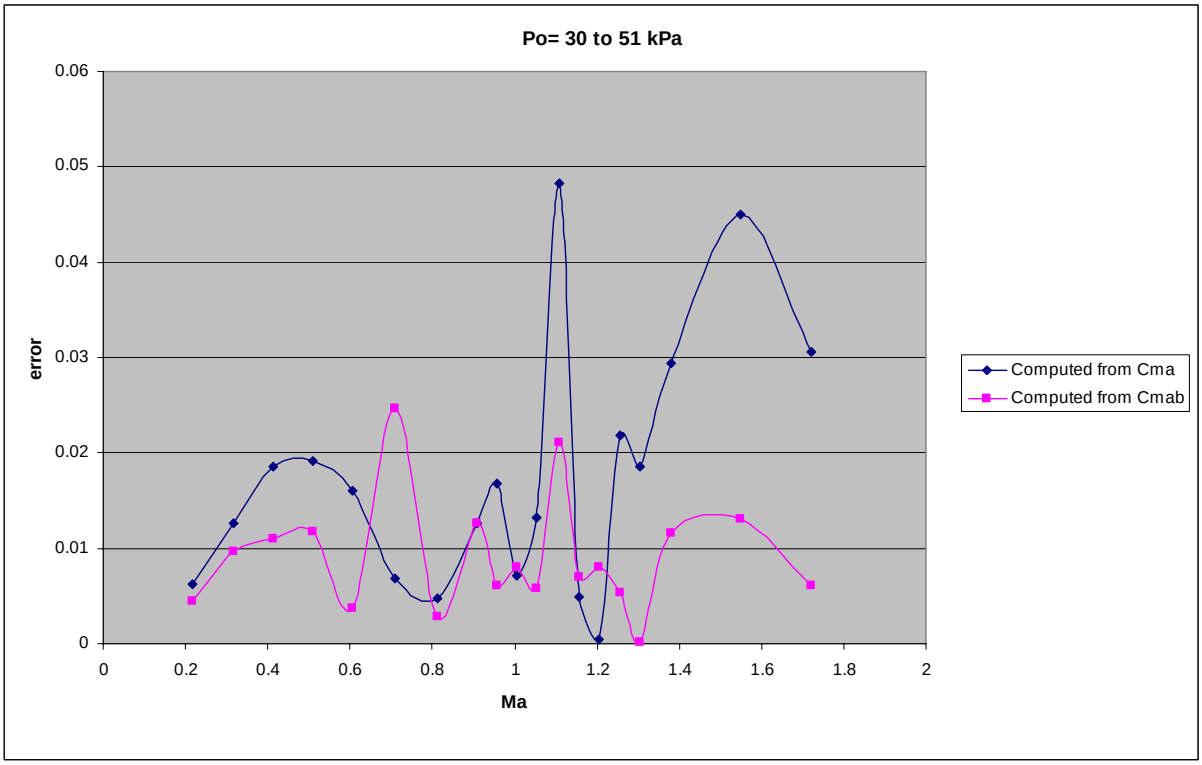

Figure 37: Evolution of the error against Ma for p_0 = 30 to 51 kPa

When the Mach number is computed from C_{Ma} (blue curve), we can see that the error on p_{0s} begins to have a significant impact on the calculation of the Mach number for transonic and supersonic flows. On the other hand, when the Mach number is computed from C_{Mab} (pink curve), an error is still present but less important (between 0.0002 and 0.025).

Same procedure, for p_0 = 100 kPa:

Ma	Error computed from C_{Ma}	Error computed from C_{Mab}
0.2	0.003455555	0.006042992
0.3	0.011615299	0.009367573
0.4	0.014035767	0.005198751
0.5	0.01483303	0.013579558
0.6	0.010583185	0.004838935
0.7	0.003831044	0.018673784
0.8	0.001984011	0.010519003
0.9	0.007903073	0.00845876
0.95	0.016304456	0.003397662
1	0.020683636	0.008141015
1.05	0.041661297	0.006994561
1.1	0.002013759	0.003790201
1.15	0.07850483	0.018174007
1.2	0.115074279	0.002895968
1.25	0.138908574	0.002683272
1.3	0.046023817	0.011165046
1.4	0.05066408	0.033129569
1.6	0.034662282	0.019333817
1.8	0.008390101	0.008844278

The results were plotted:

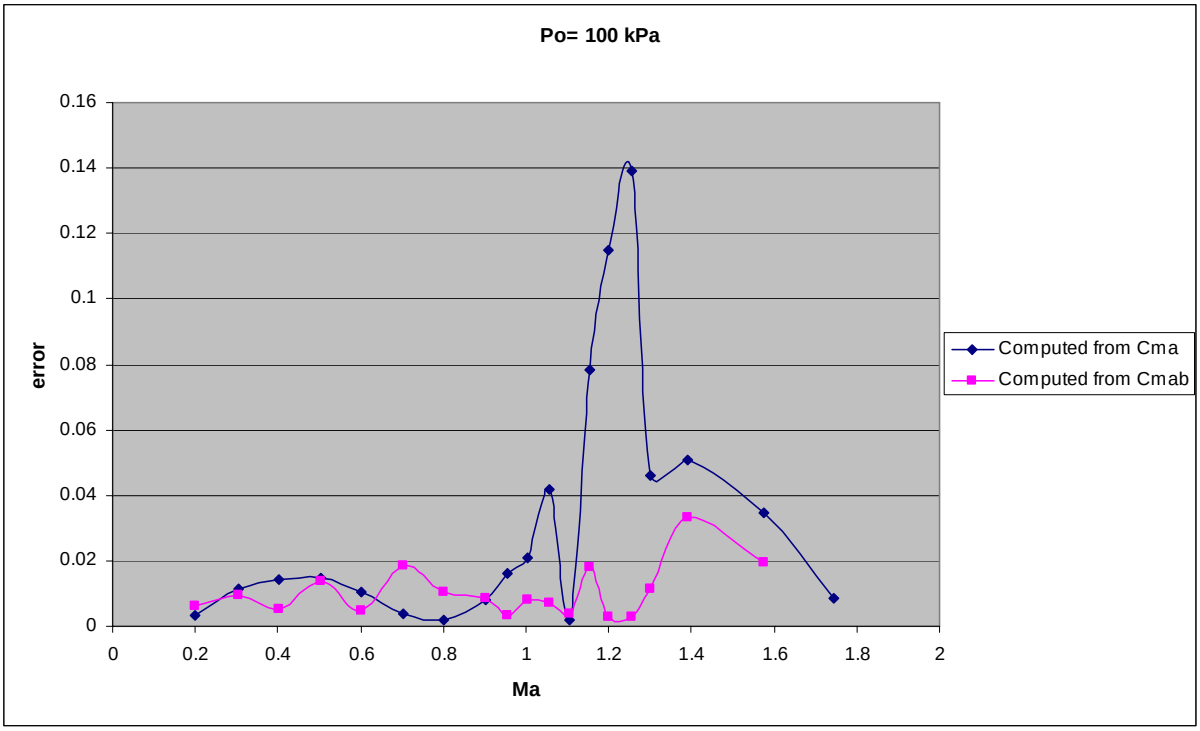

Figure 38: Evolution of the error against Ma for p_0=100kPa

We can see as before that for transonic and supersonic flows the error on p_{0s} seriously affects the determination of the Mach number when it is computed from C_{Ma}, whereas the calculation from C_{Mab} remains relatively stable.

Once more the shock wave ahead of the probe is responsible for this error sensitivity in transonic and supersonic flows. The fourth pressure tapping works very effective in such cases to reduce the error.

VI. Conclusion

All the data acquired thanks to the SEG allowed us to understand the behaviour of our probe. We have defined coefficients useful for the calibration of the probe and fit functions which will give us the Mach number of the flow. We encountered a technical problem which prevented us to maintain a 30kPa total pressure for supersonic flows during the calibration process. Nevertheless, in the future and for supersonic flows, the probe will be used with a 100 kPa total pressure only, a domain which was successfully calibrated.

What this training course highlighted, is the good effectiveness of the fourth tube located at the back of the probe. On one hand this pressure tapping is less sensitive to an error due to a shock, and on the other hand it avoids the transonic « zero gradient » problem and provides a more precise Mach number for transonic speeds. But, as every intrusive measurement system, this probe will always have an impact on the flow and will always modify it, which will bring errors. But the use of non-intrusive optical measurement systems (thanks to lasers) is still too expensive and too complicated compared with the use of this probe. DLR has now a calibrated probe at low cost, which is relatively effective and which can be used for a wide range of flow speeds.

Bibliography:

[1] Gieβ P.-A., Rehder H.-J., Kost F.
A New Test Facility for Probe Calibration Offering Independent Variation of Mach number and Reynolds Number.
Proceedings of the 15th Symposium on «*Measuring Techniques in Transonic and Supersonic Flow in Cascades and Turbomachines*»,
Firenze, Italy. September 21-22, 2000

[2] Kost F.
Calibration of Combined Pressure, Temperature Probes for Application in the Rotating Cascade Tunnel (RGG).
DLR Internal Report IB 225 – 2006 A 04, November 2006

[3] Steinville R.
Calibration of a three-hole cylindrical pressure probe in sub- and supersonic flow
DLR Internal Report IB 225 – 2005 A 01, January 2005

[4] Leost Y.
Eichung einer zylindrischen 4-Lochsonde in Unter- und Überschallströmung
DLR Internal Report IB 225 – 2006 A 08, December 2006

[5] Délery J.
Méthodes de mesures en aérodynamique
ONERA

[6] Amtec Engineering Inc.
Tecplot 9.0 User's Manual
2001

List of figures:

➘ *Supersonic Ma=1.8 p_0=51kPa*

➘ *Supersonic Ma=1.4-1.6-1.8 p_0=100kPa*

Appendix

Subsonic, p_0= 30kPa

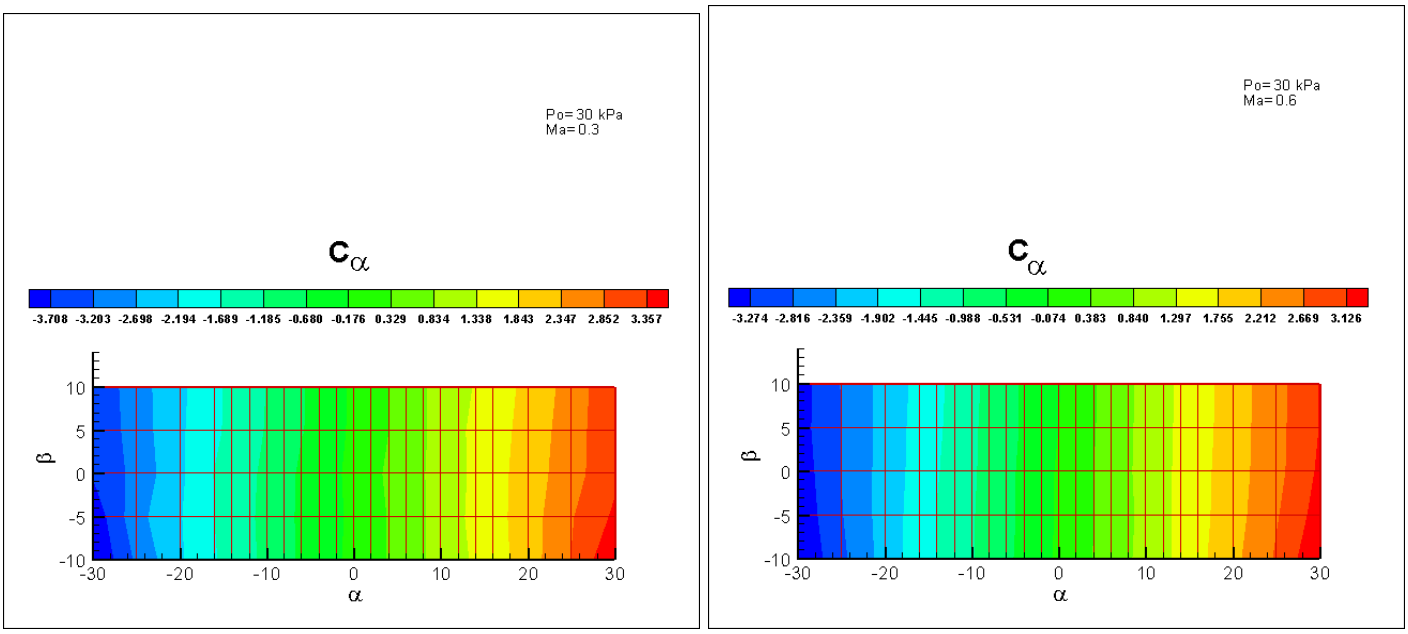

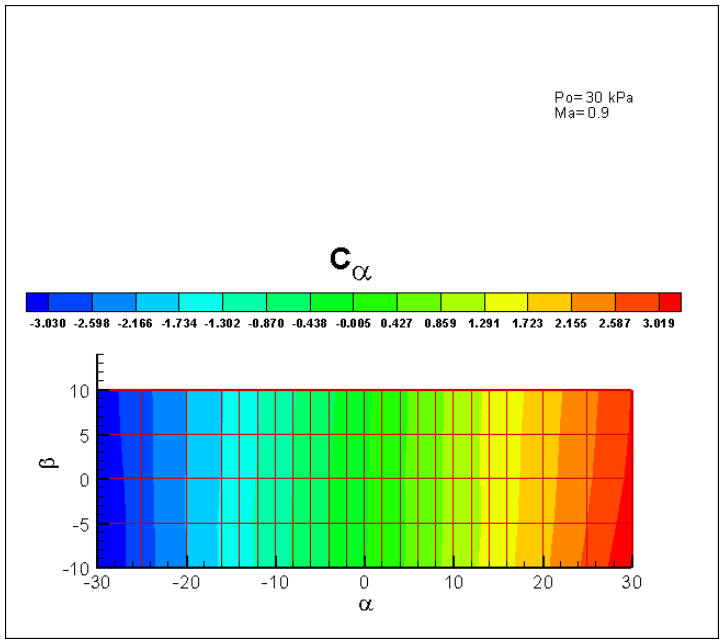

Figure 39: Evolution of C_α against α and β at Ma=0.3
0.6
0.9

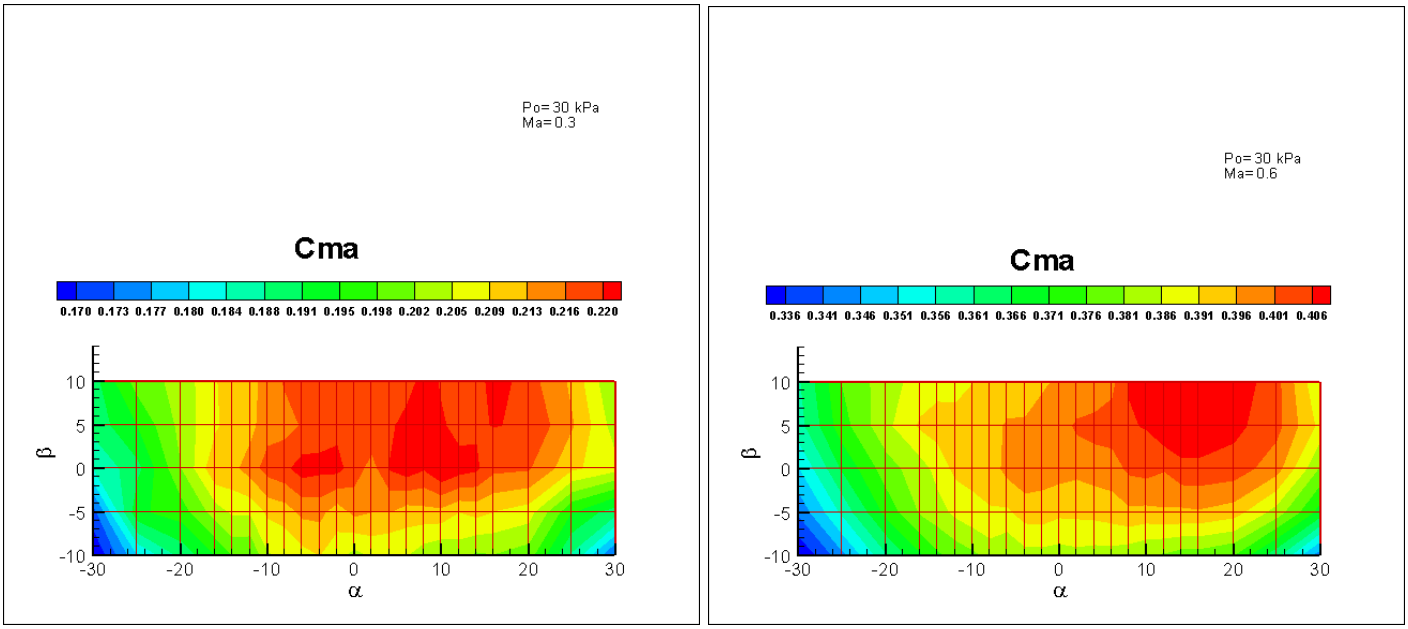

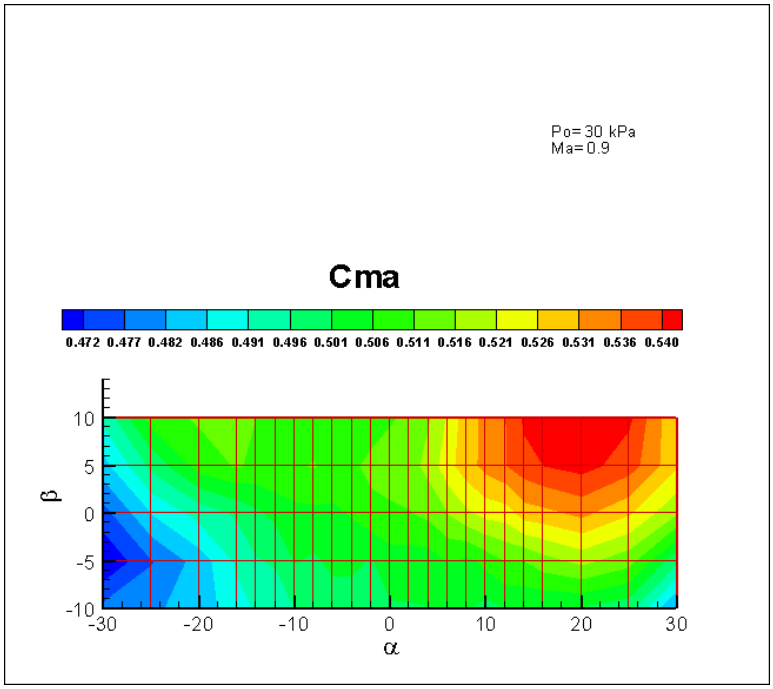

Figure 40: Evolution of C_{Ma} against α and β at Ma=0.3
0.6
0.9

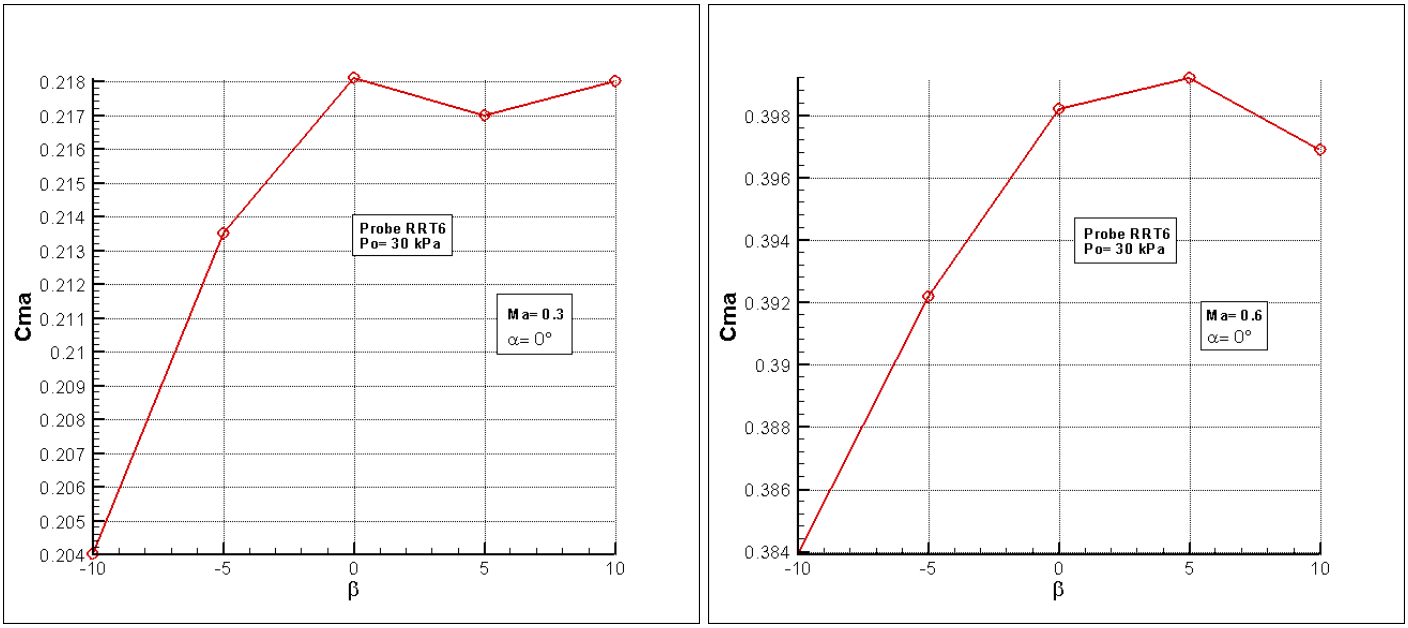

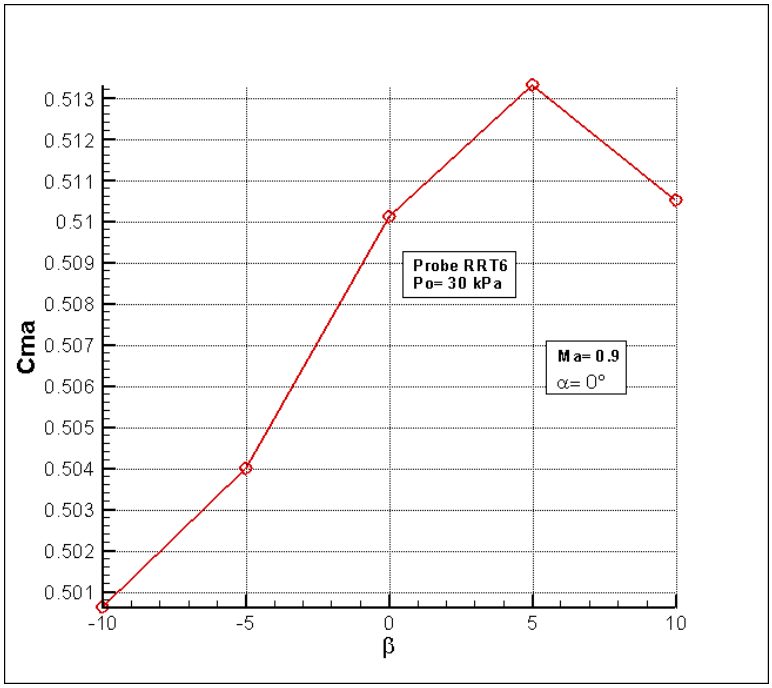

Figure 41: Evolution of C_{Ma} against β at Ma=0.3
0.6
0.9

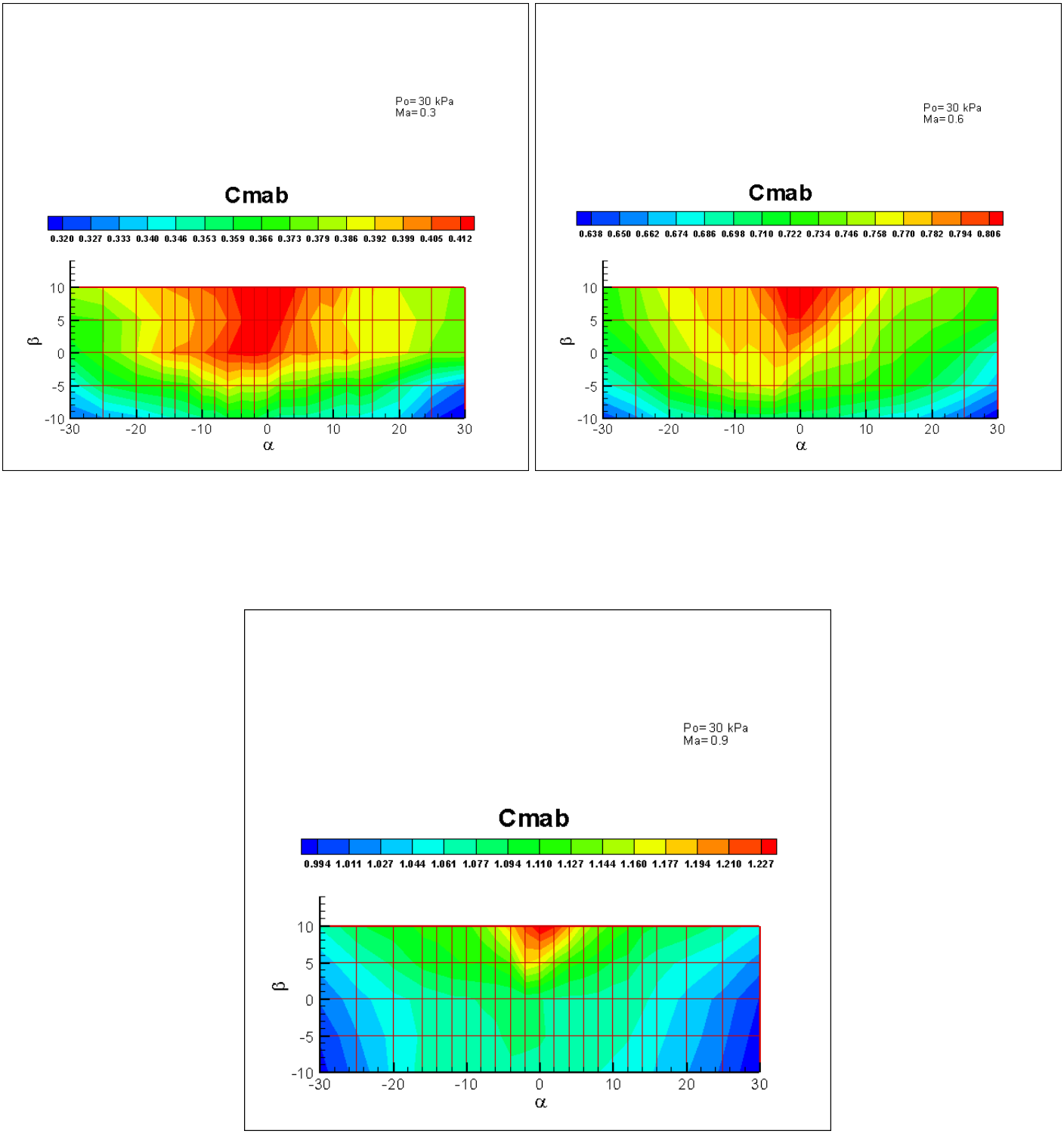

Figure 42: Evolution of C_{Mab} against α and β at Ma=0.3
0.6
0.9

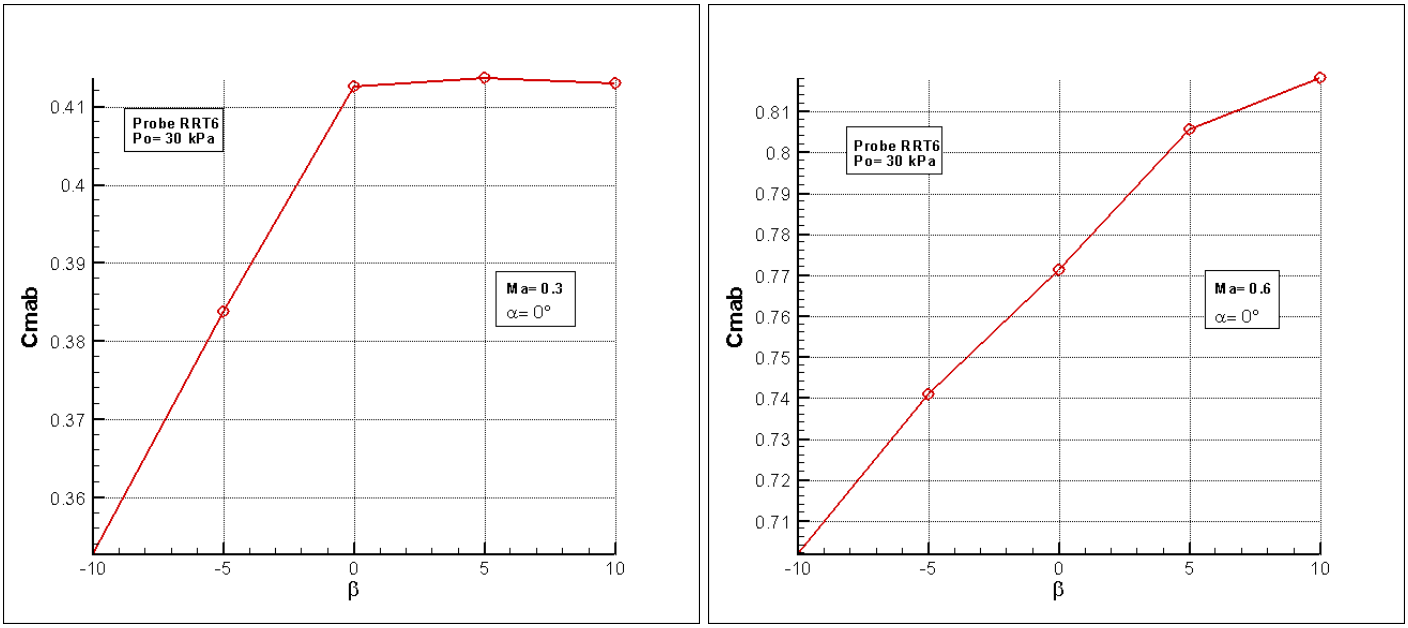

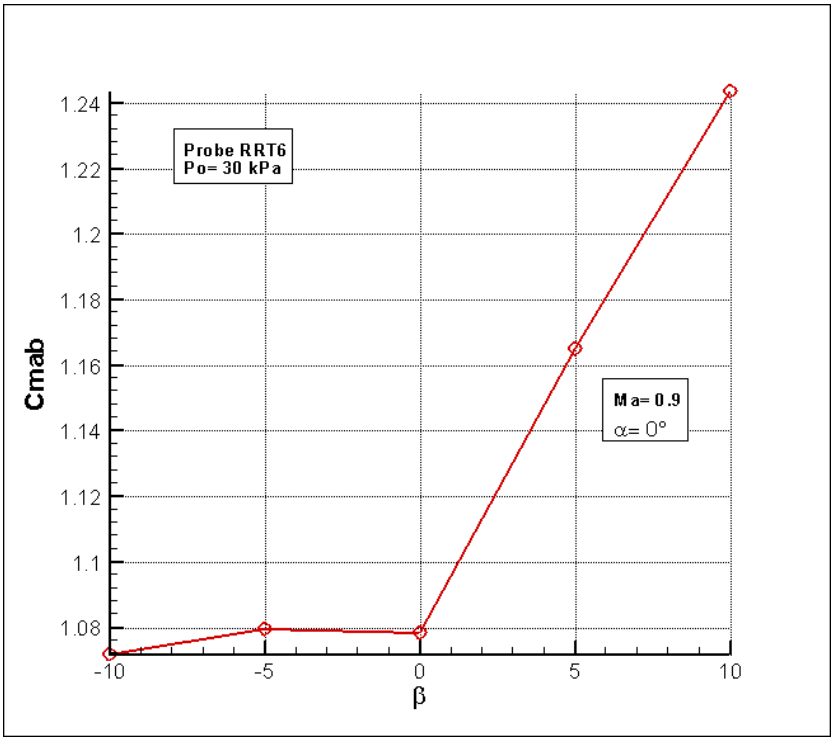

Figure 43: Evolution of C_{Mab} against β at Ma=0.3
0.6
0.9

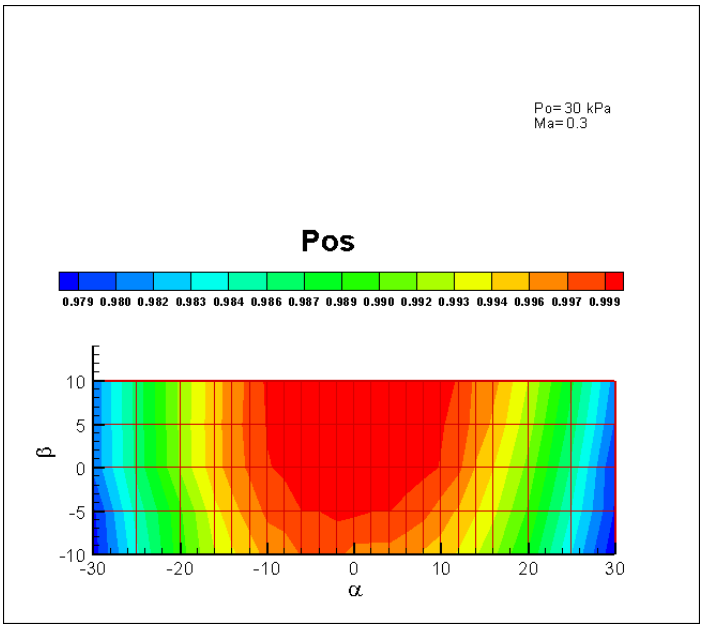

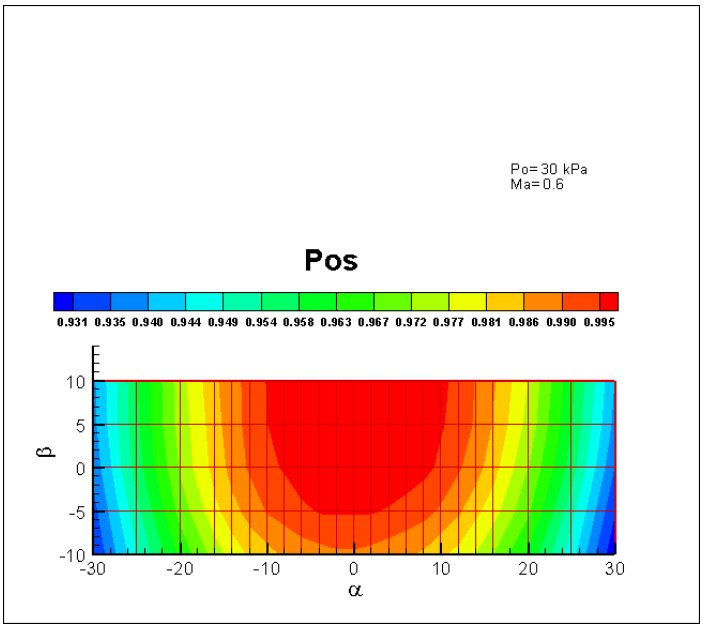

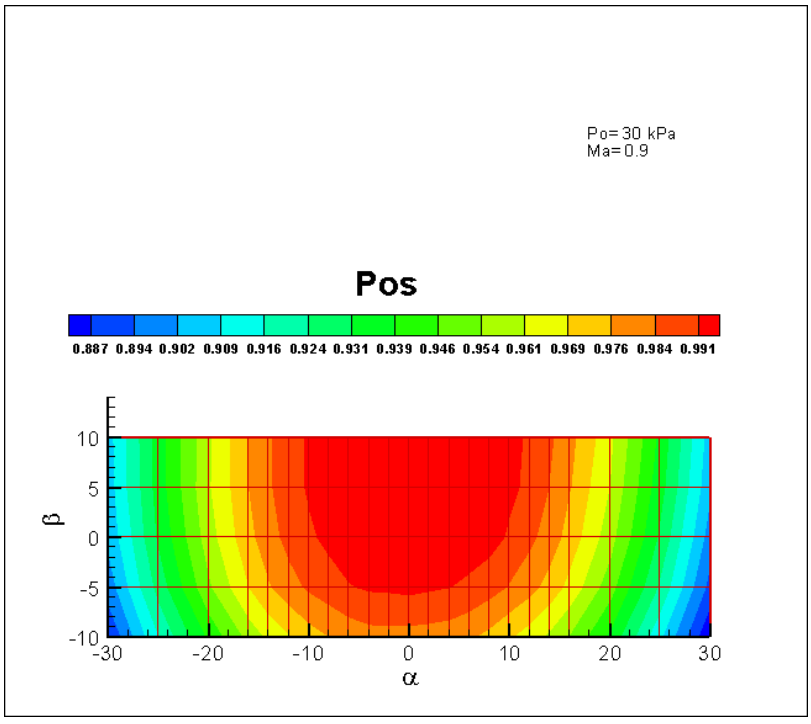

Figure 44: Evolution of p_{0s} against α and β at Ma=0.3
0.6
0.9

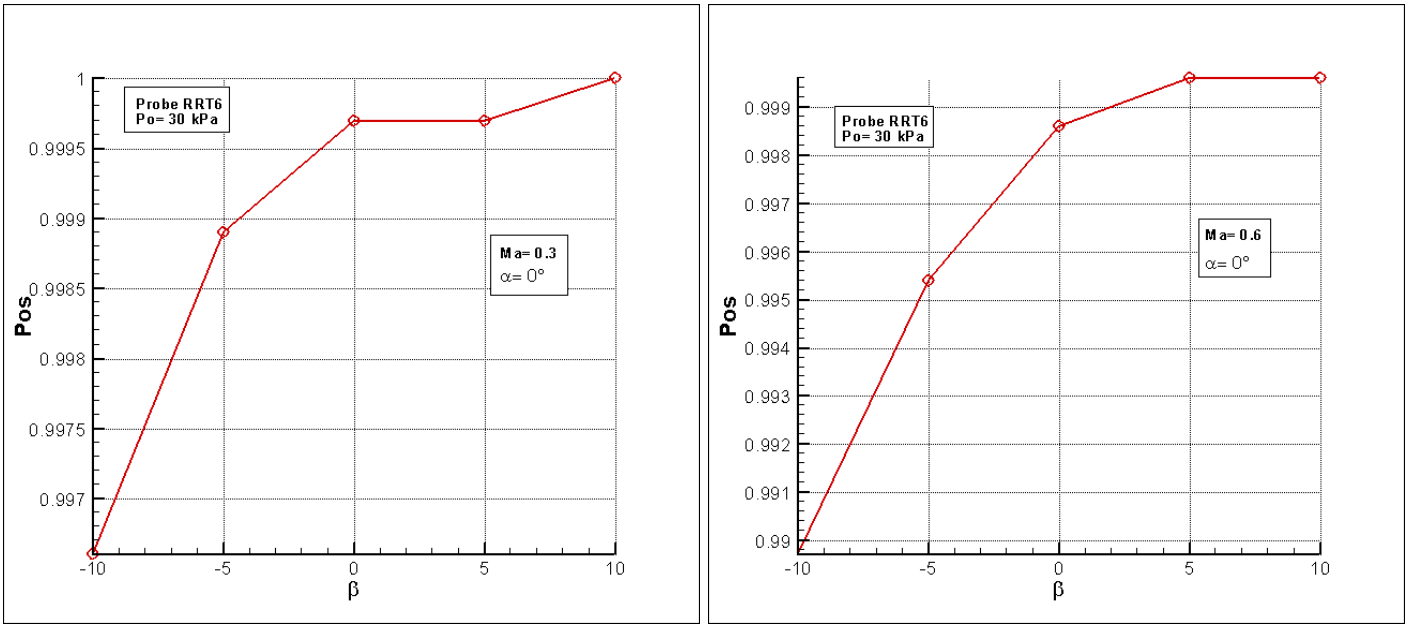

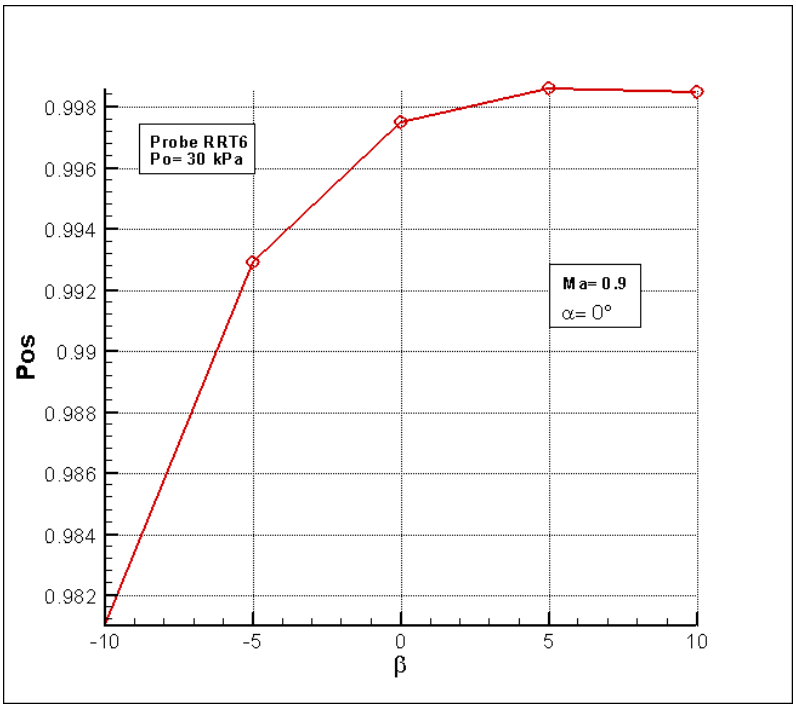

Figure 45: Evolution of p_{0s} against β at Ma=0.3
0.6
0.9

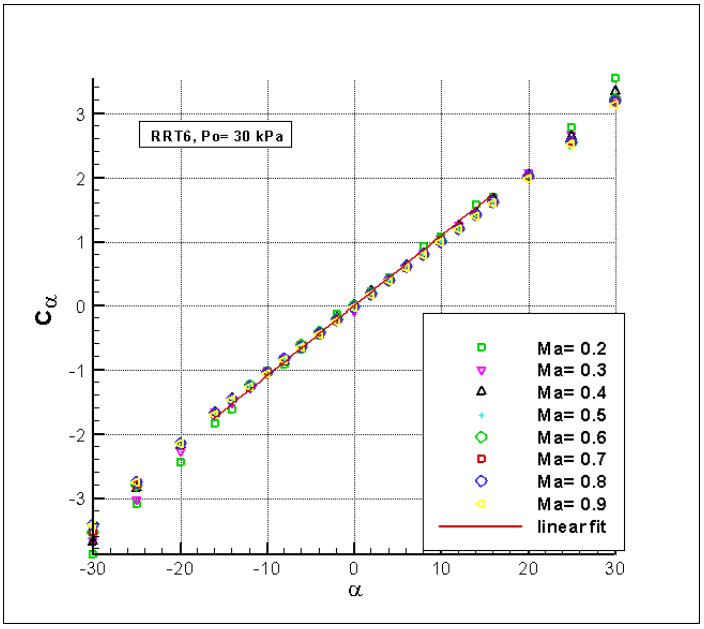

Figure 46: Evolution of C_α against α

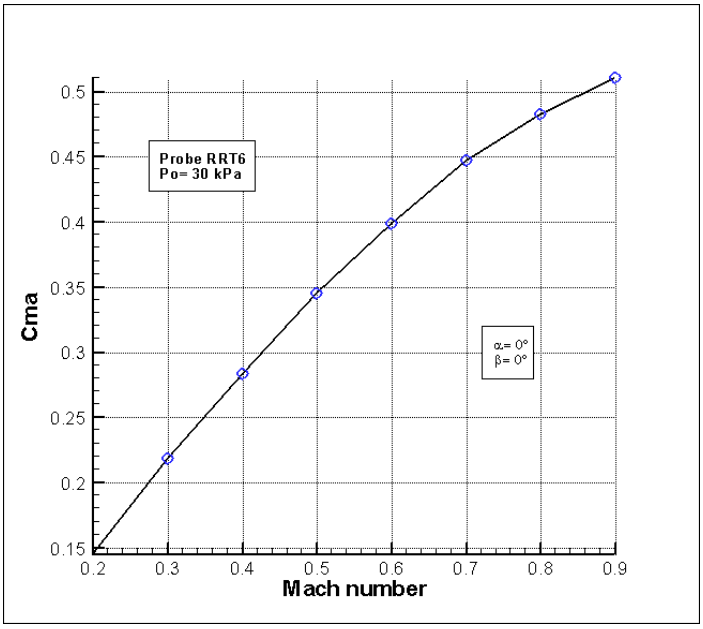

Figure 47: Evolution of C_{Ma} against Ma

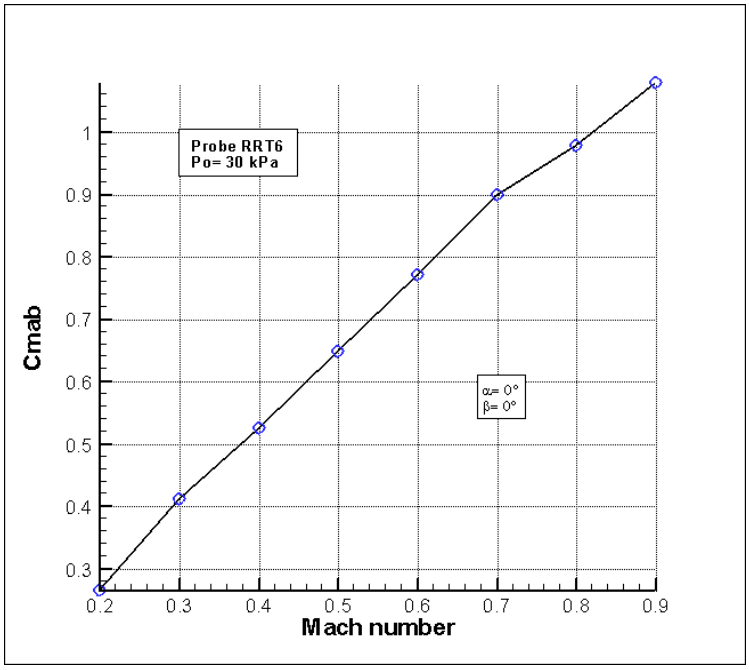

Figure 48: Evolution of C_{Mab} against Ma

Subsonic, p_0= 100kPa

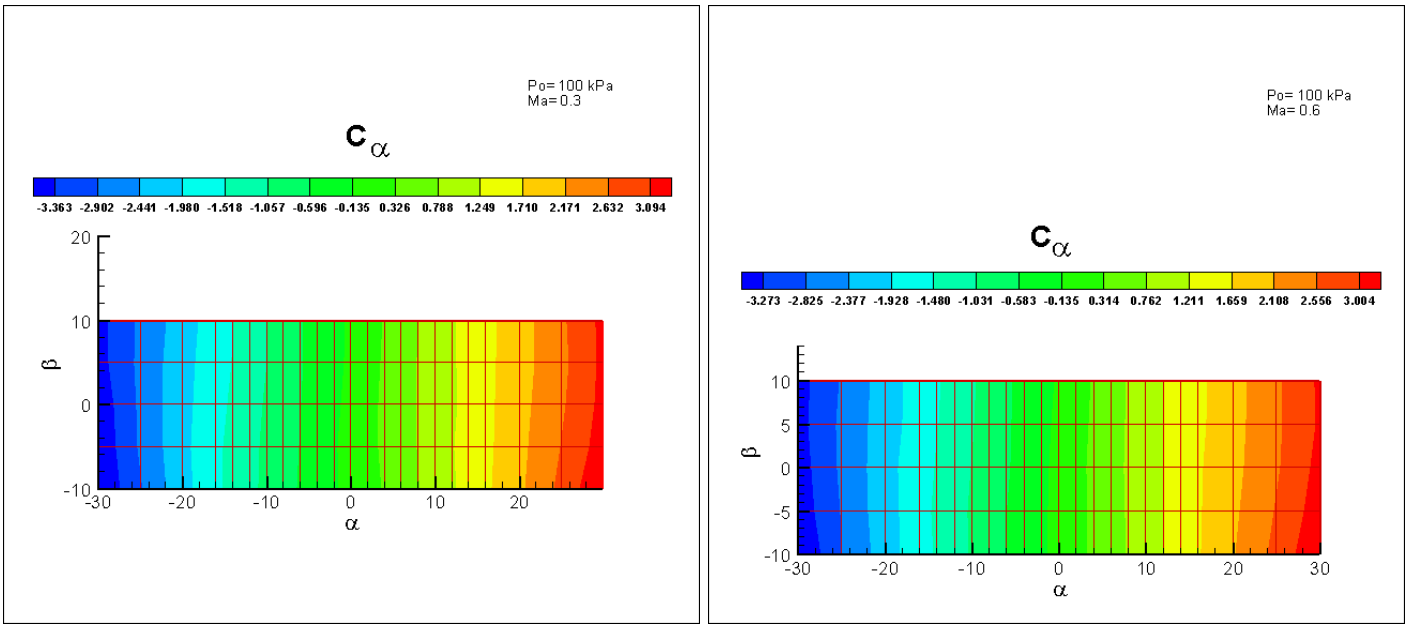

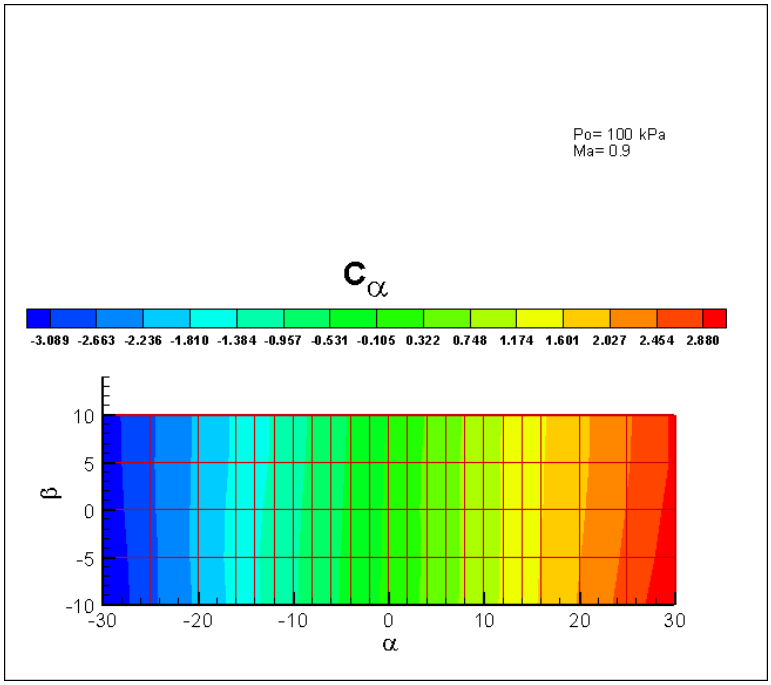

Figure 49: Evolution of C_α against α and β at Ma=0.3
0.6
0.9

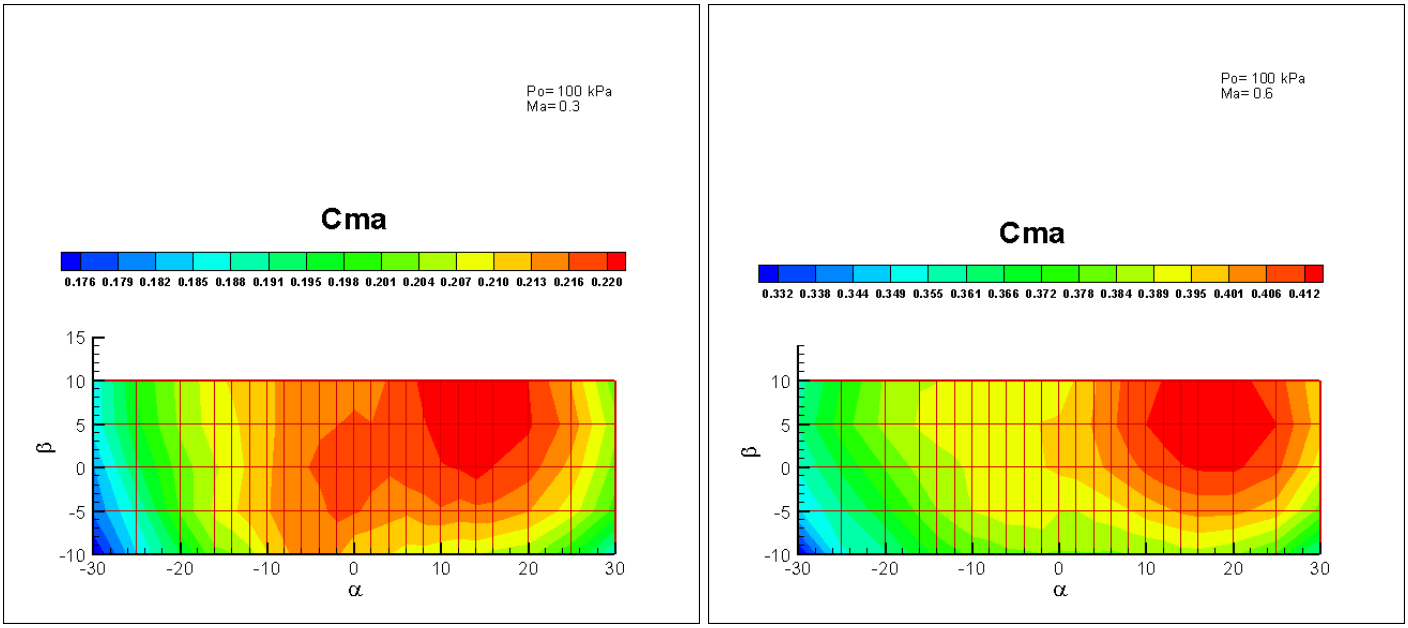

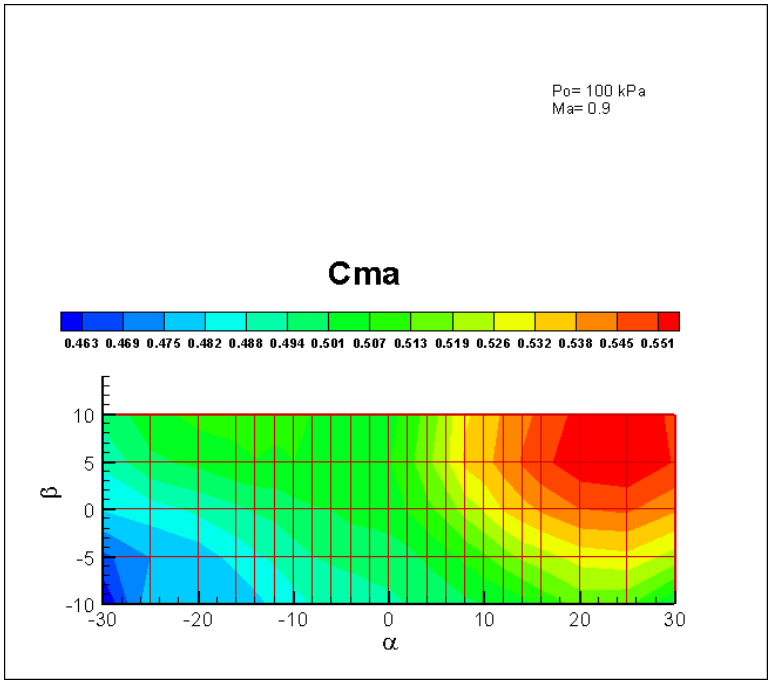

Figure 50: Evolution of C_{Ma} against α and β at Ma=0.3
0.6
0.9

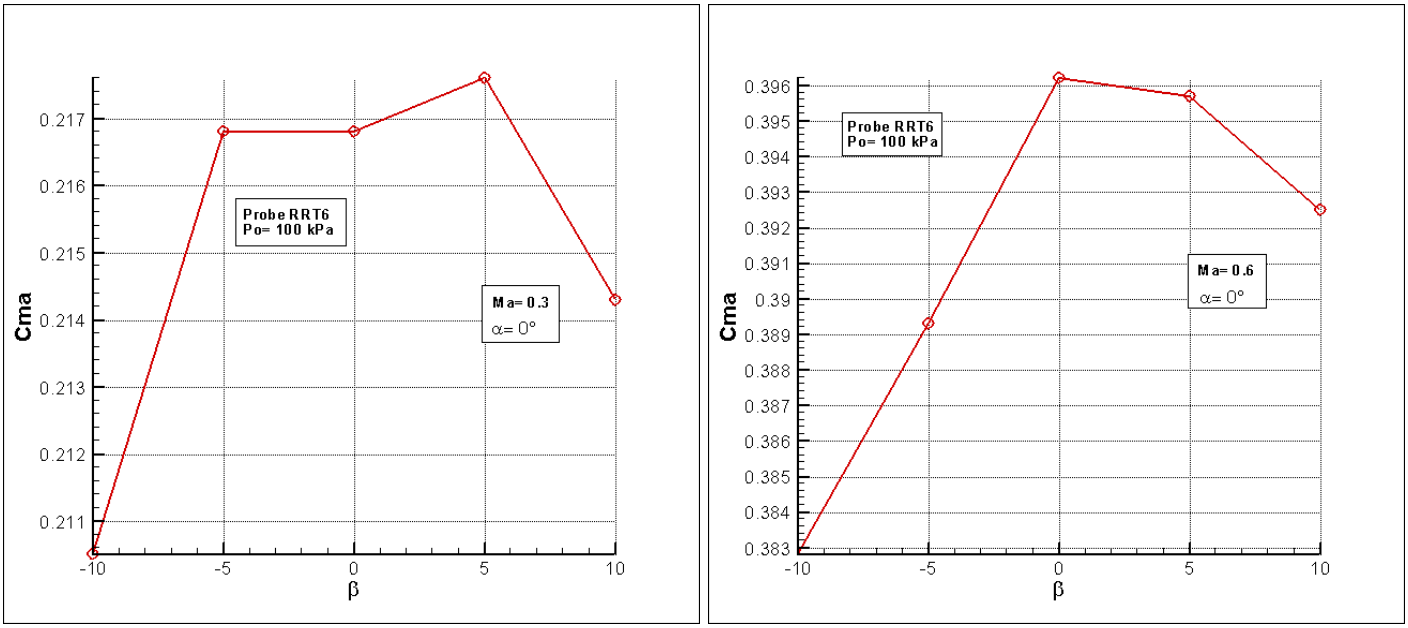

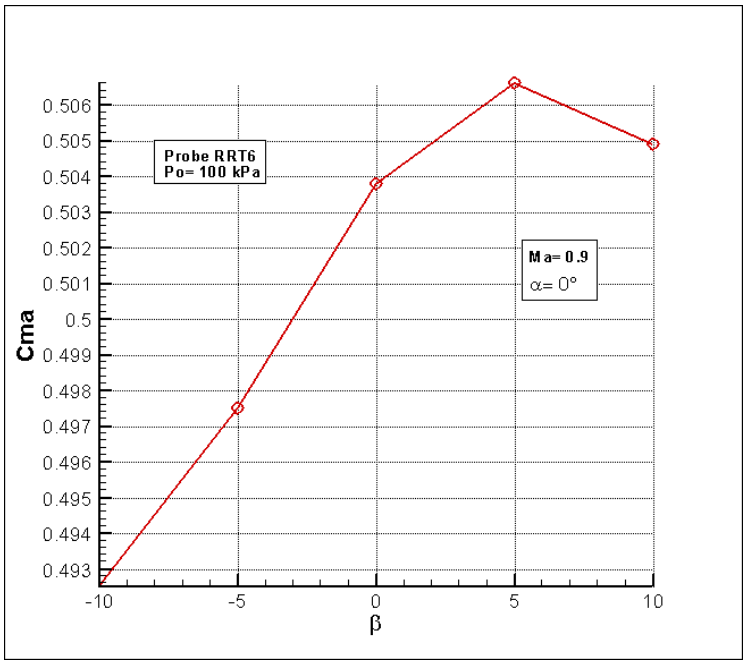

Figure 51: Evolution of C_{Ma} against β at Ma=0.3
0.6
0.9

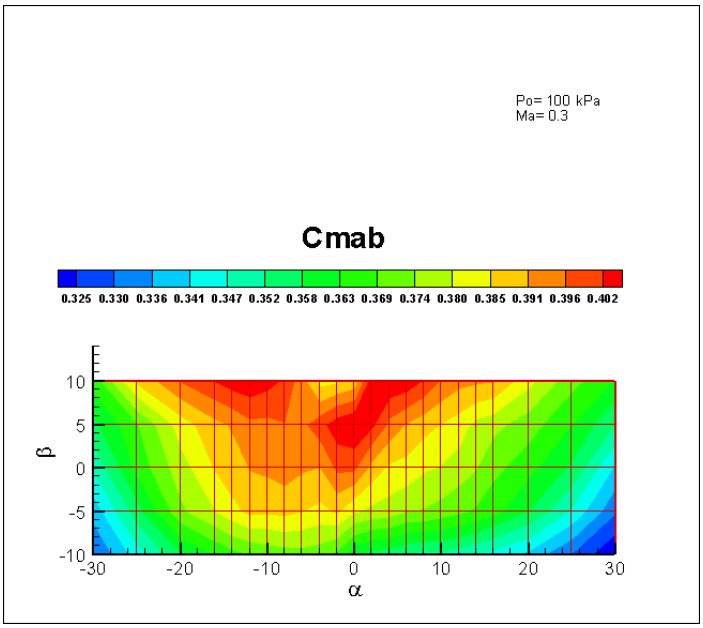

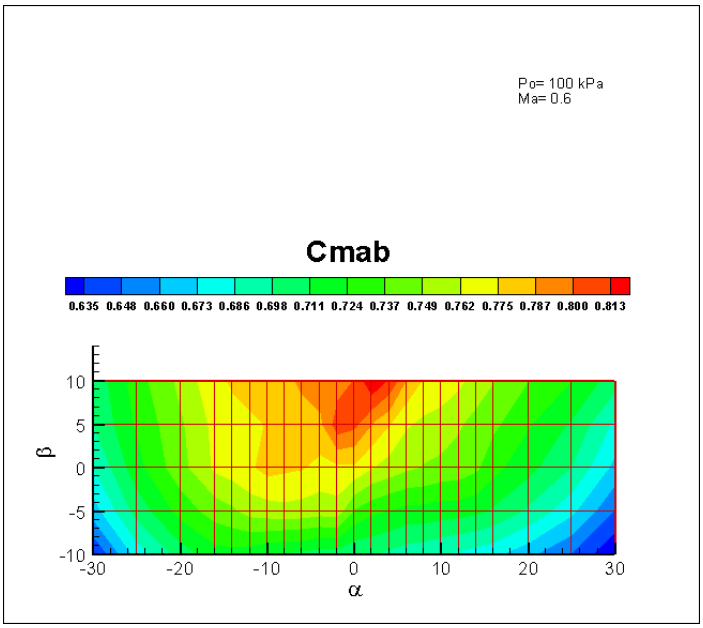

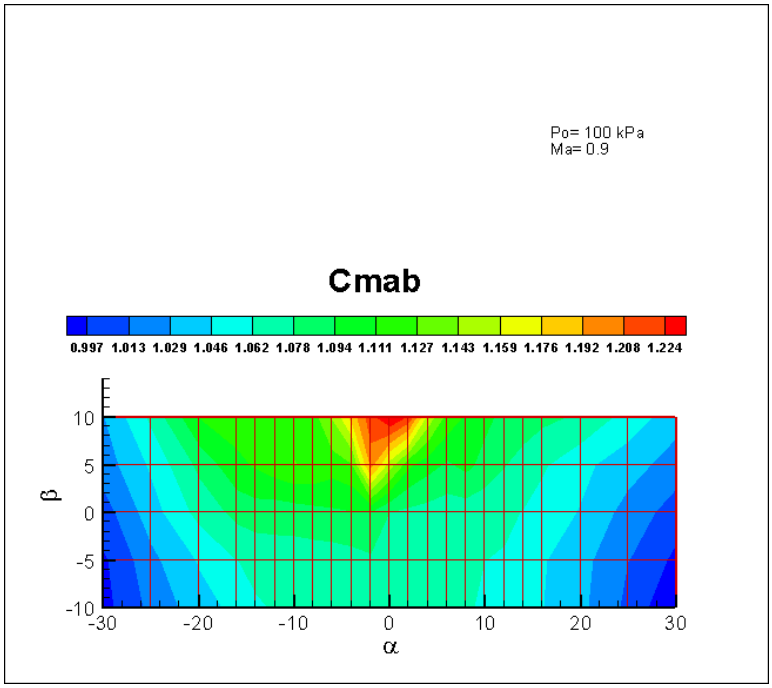

Figure 52: Evolution of C_{Mab} against α and β at Ma=0.3
0.6
0.9

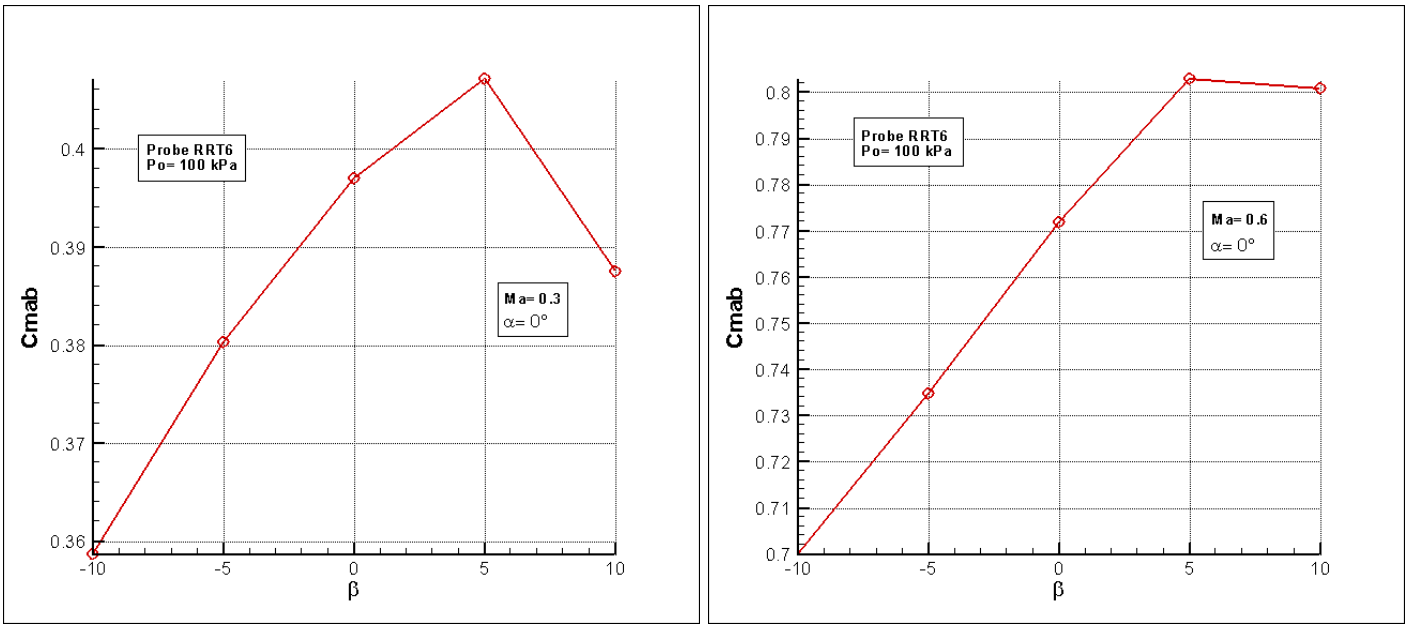

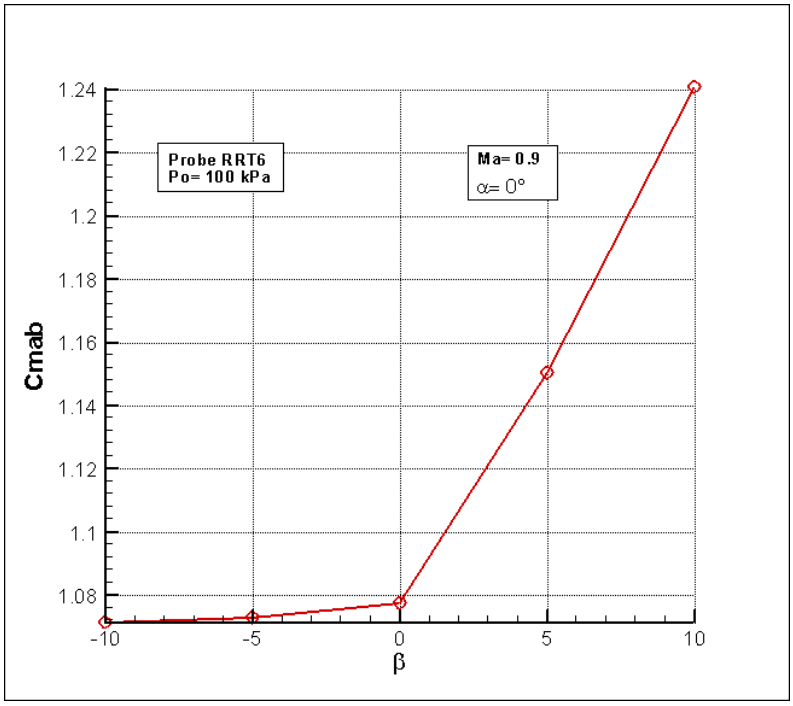

Figure 53: Evolution of C_{Mab} against β at Ma=0.3
0.6
0.9

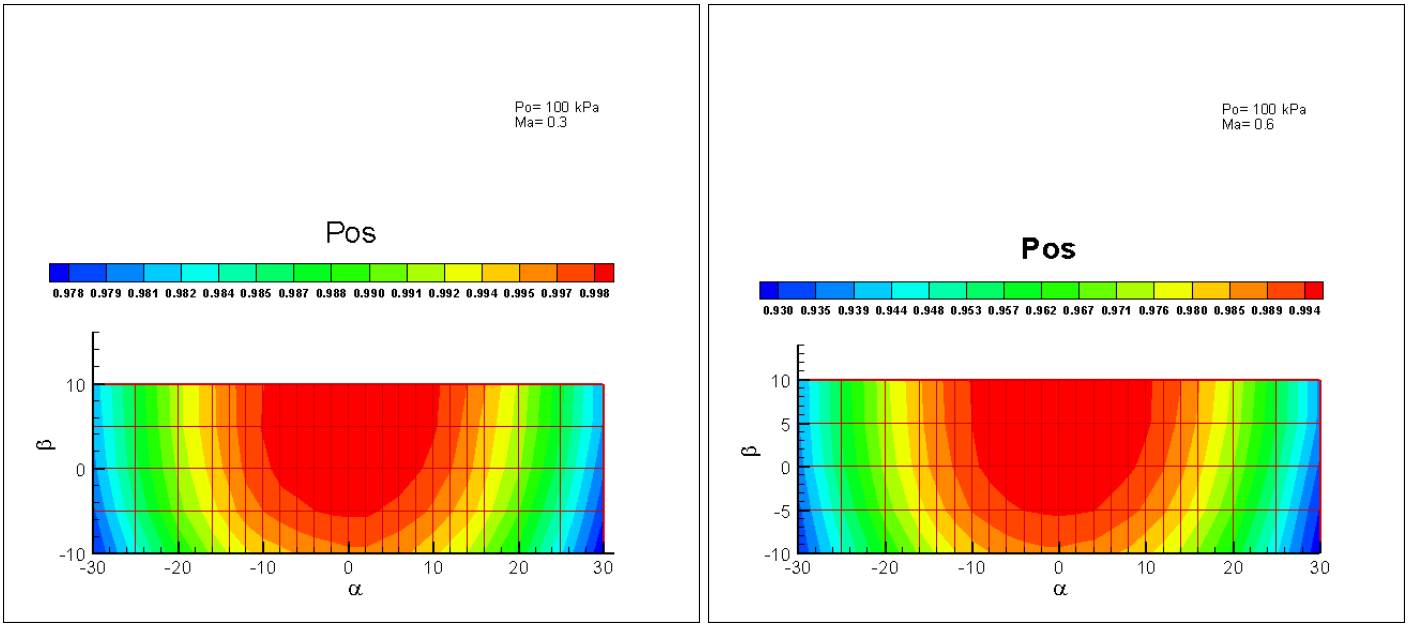

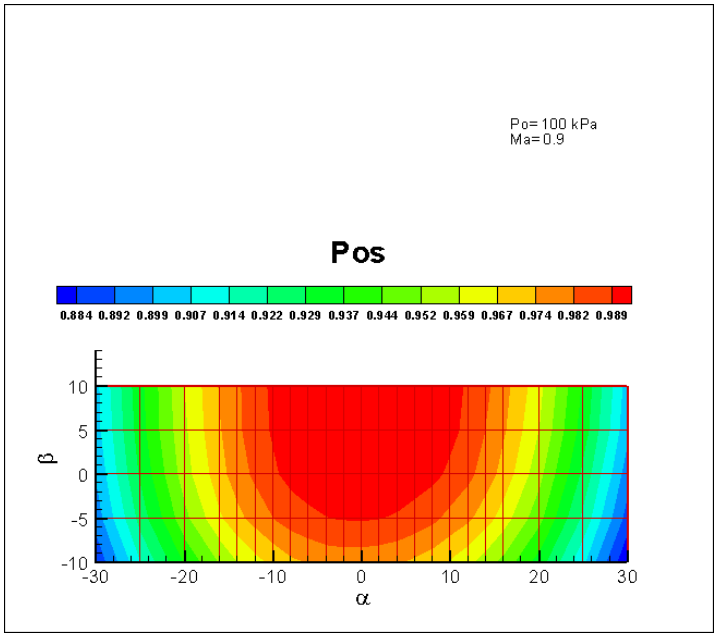

Figure 54: Evolution of p_{0s} against α and β at Ma=0.3
0.6
0.9

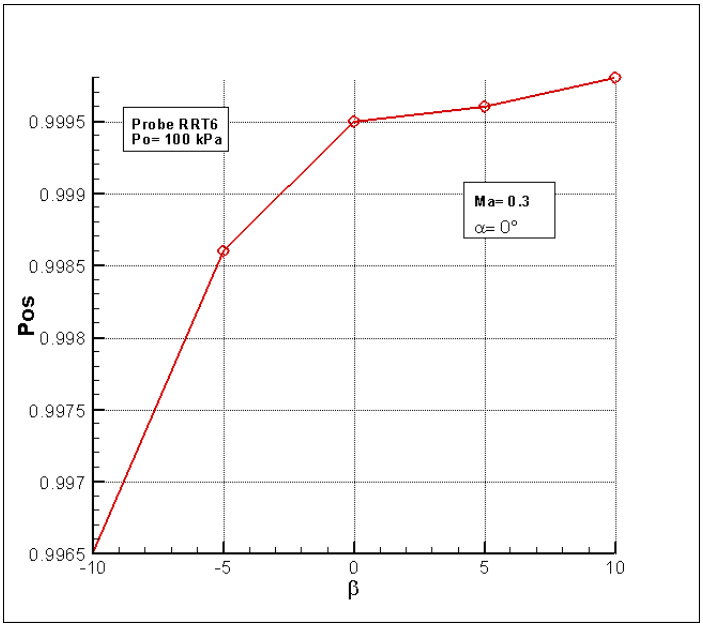

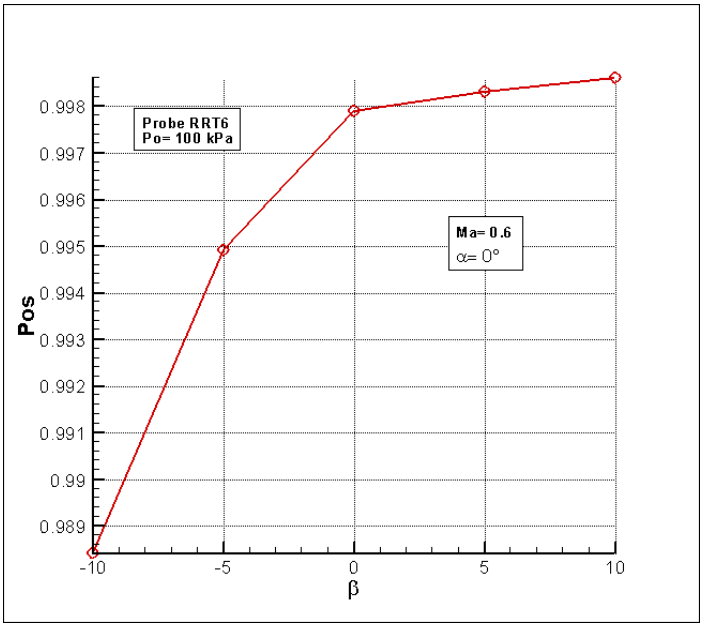

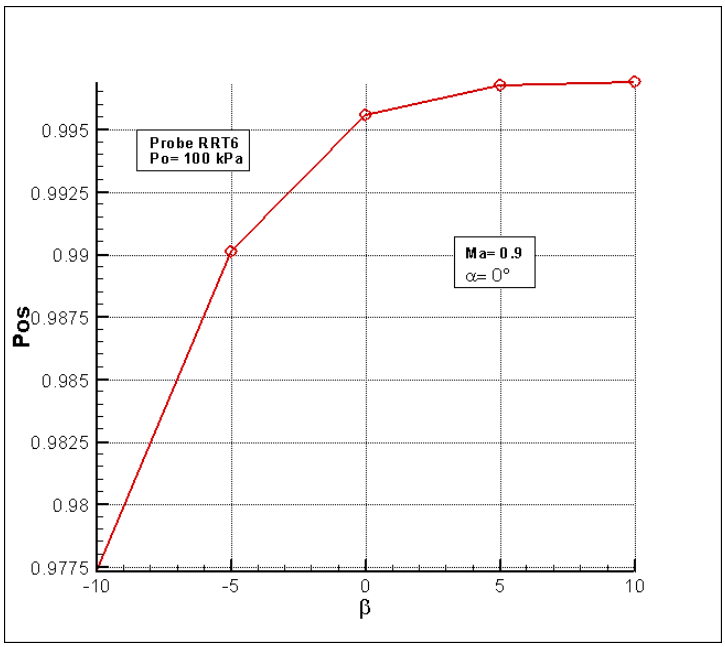

Figure 55: Evolution of p_{0s} against β at Ma=0.3
0.6
0.9

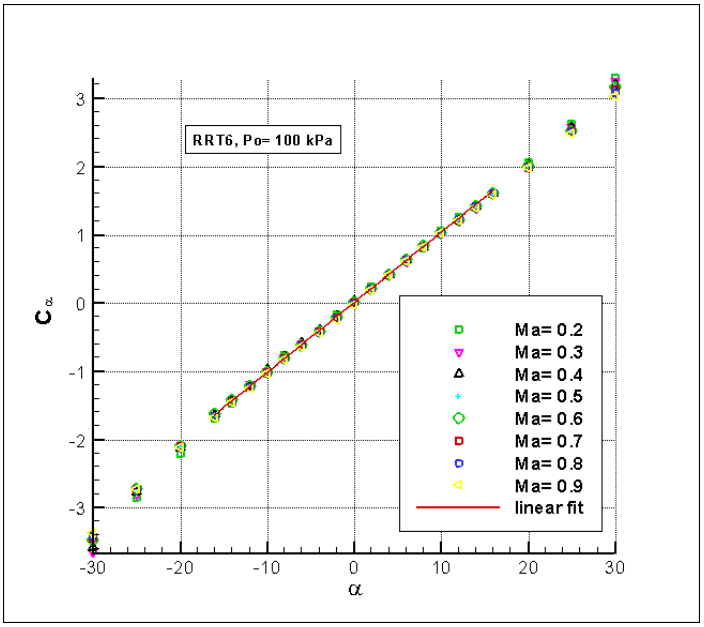

Figure 56: Evolution of C_α against α

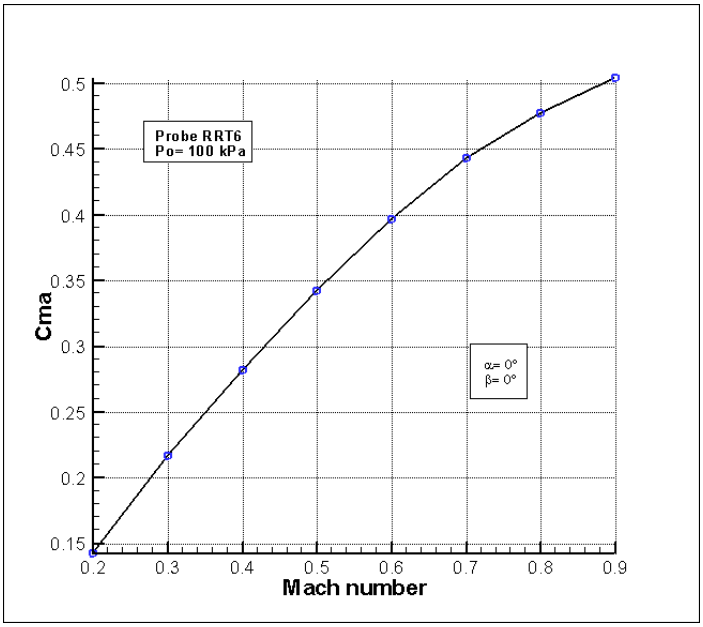

Figure 57: Evolution of C_{Ma} against Ma

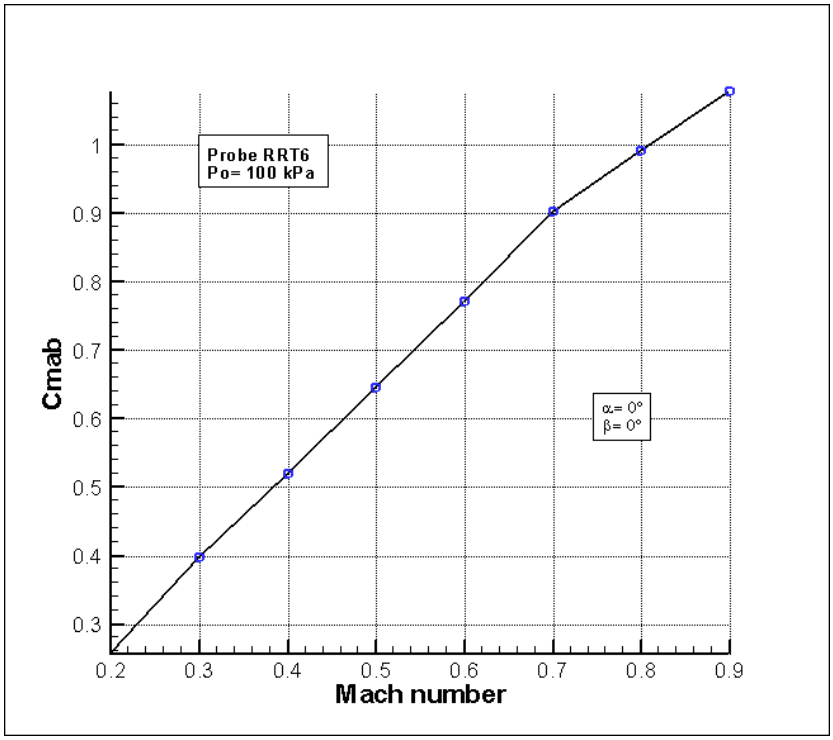

Figure 58: Evolution of C_{Mab} against Ma

Transonic, p_0= 30kPa

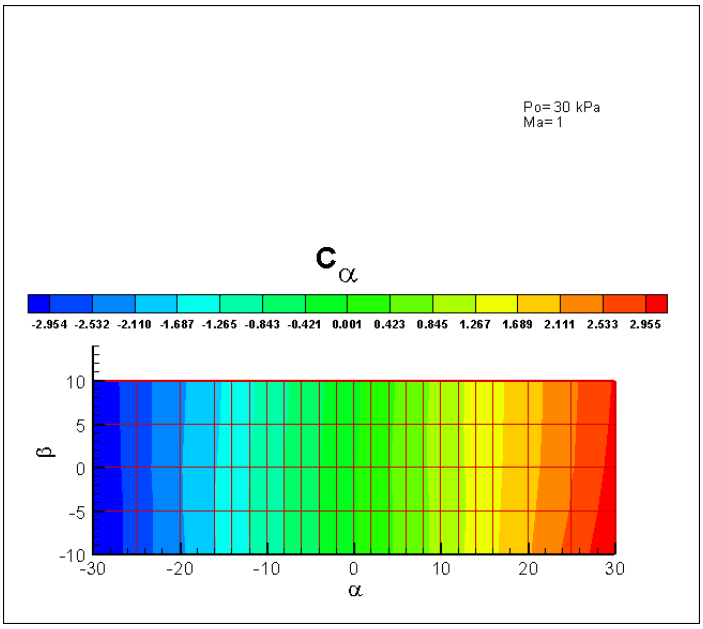

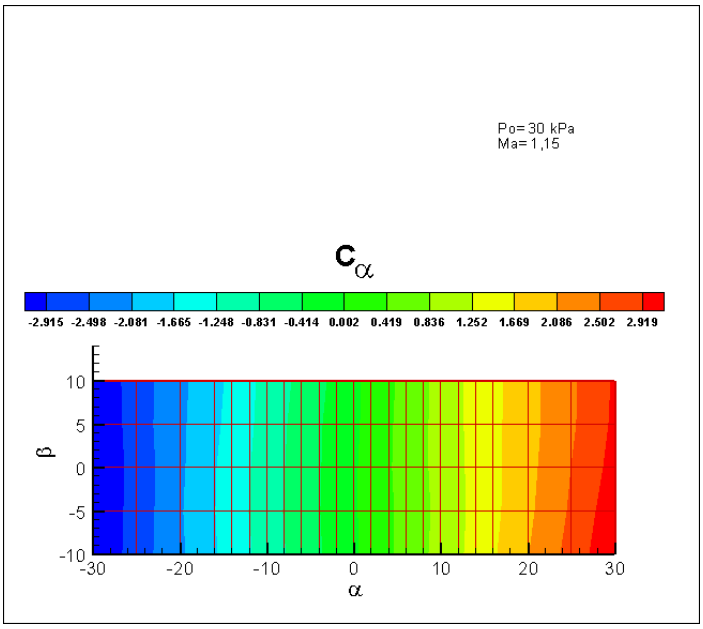

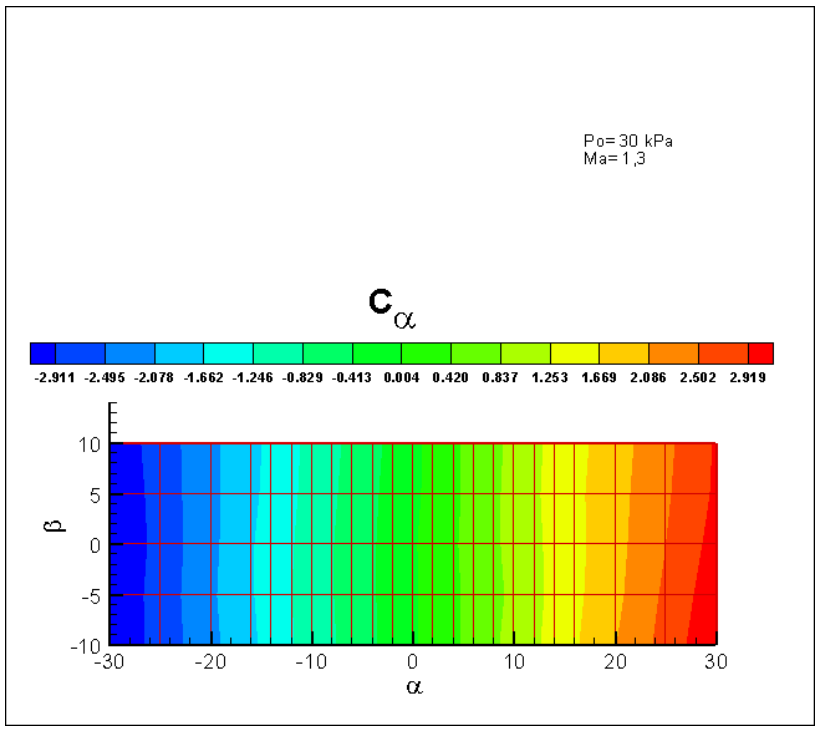

Figure 59: Evolution of C_α against α and β at Ma=1
1.15
1.3

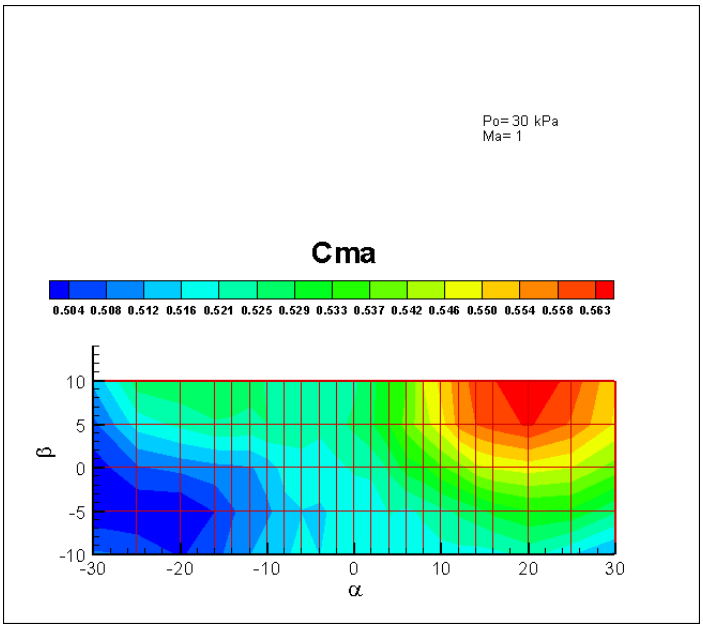

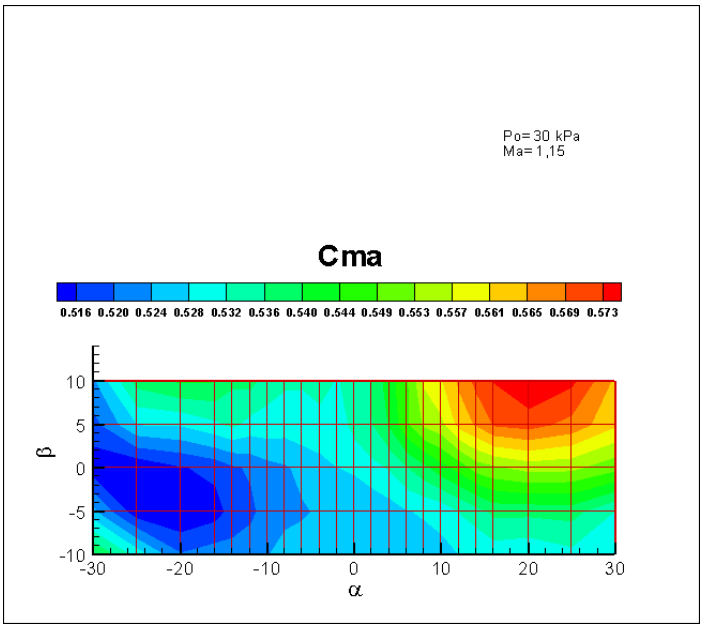

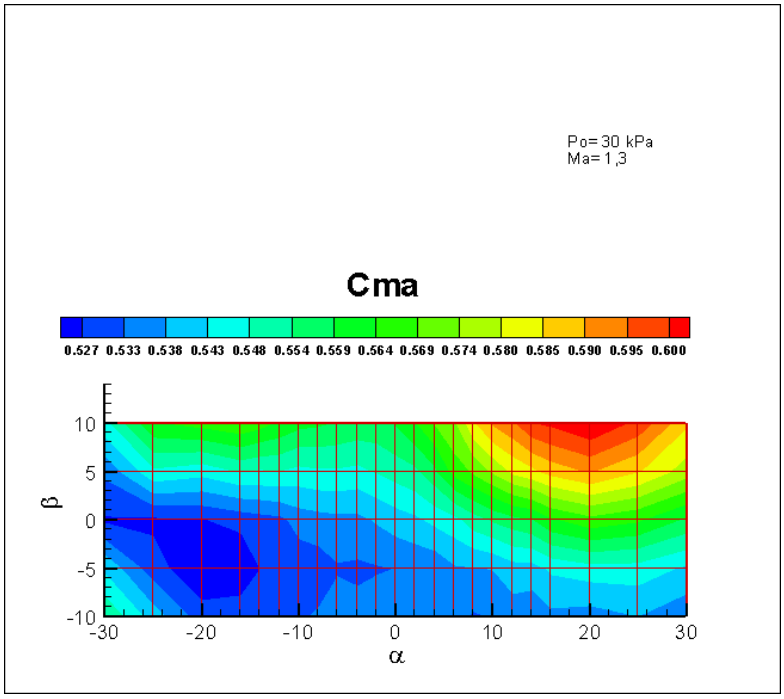

Figure 60: Evolution of C_{Ma} against α and β at Ma=1
1.15
1.3

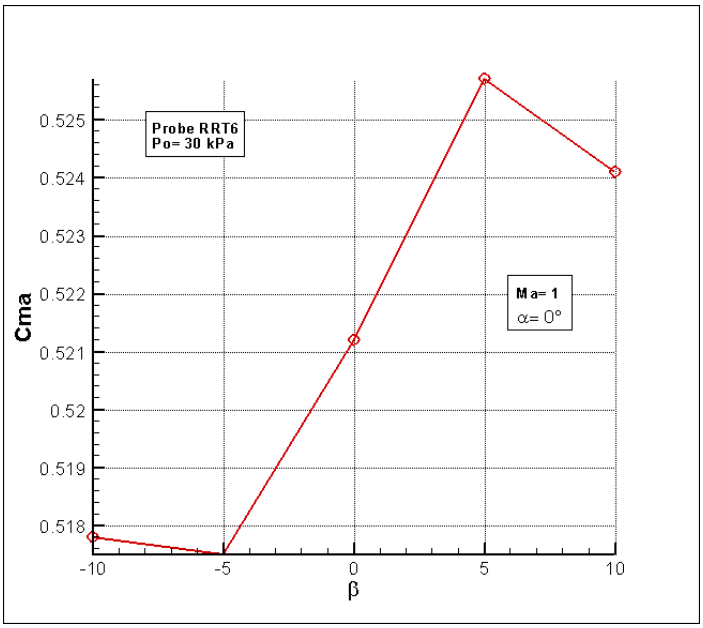

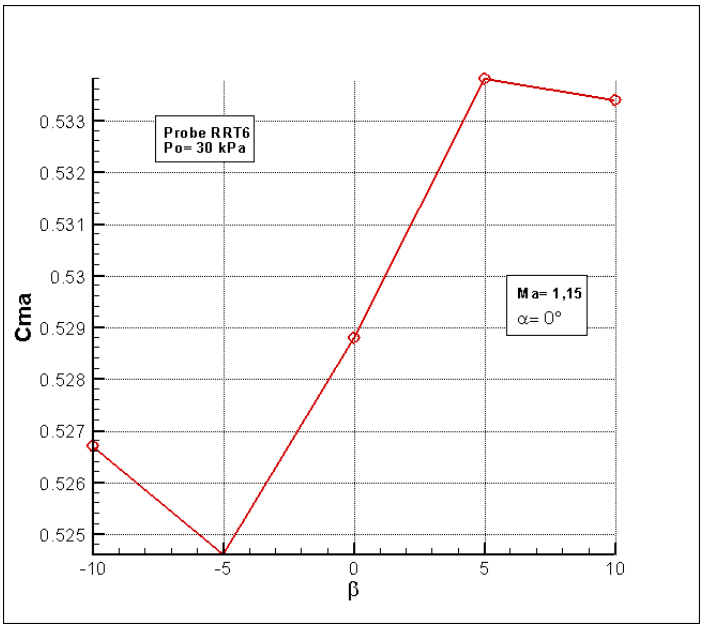

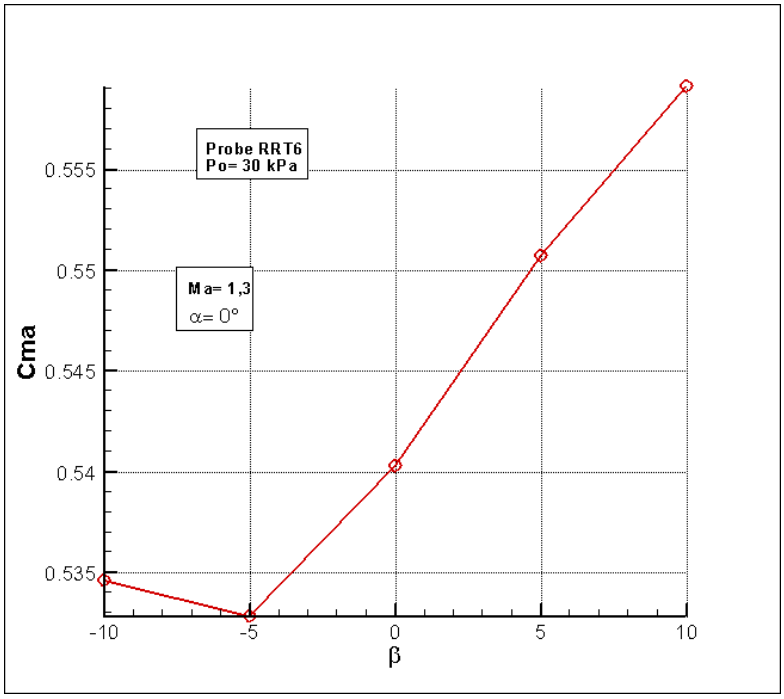

Figure 61: Evolution of C_{Ma} against β at Ma=1

1.15
1.3

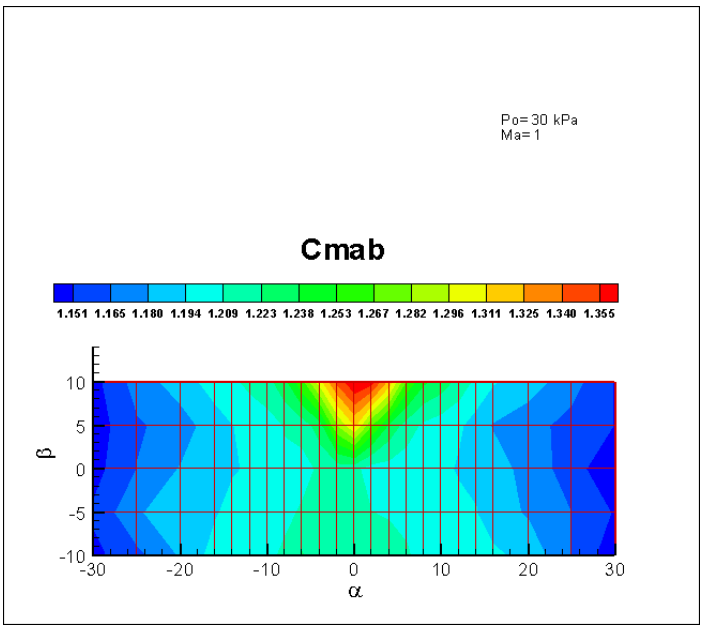

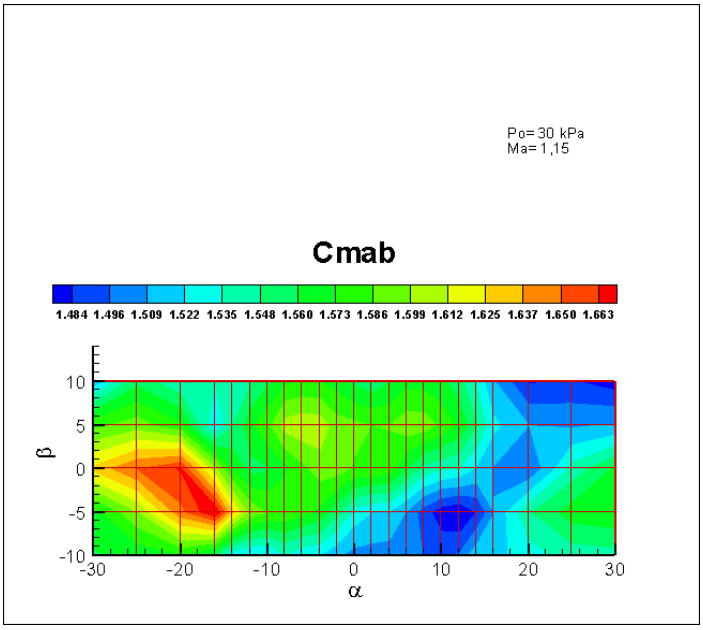

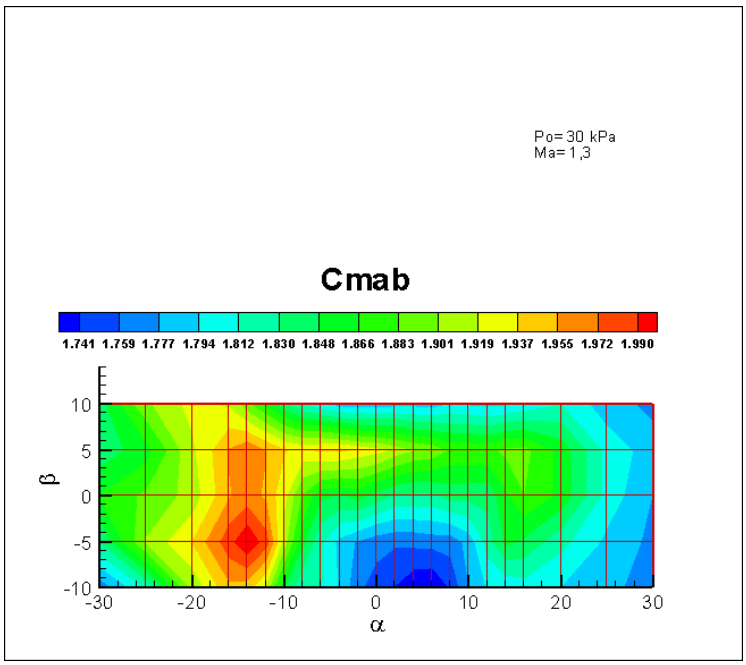

Figure 62: Evolution of C_{Mab} against α and β at Ma=1

1.15

1.3

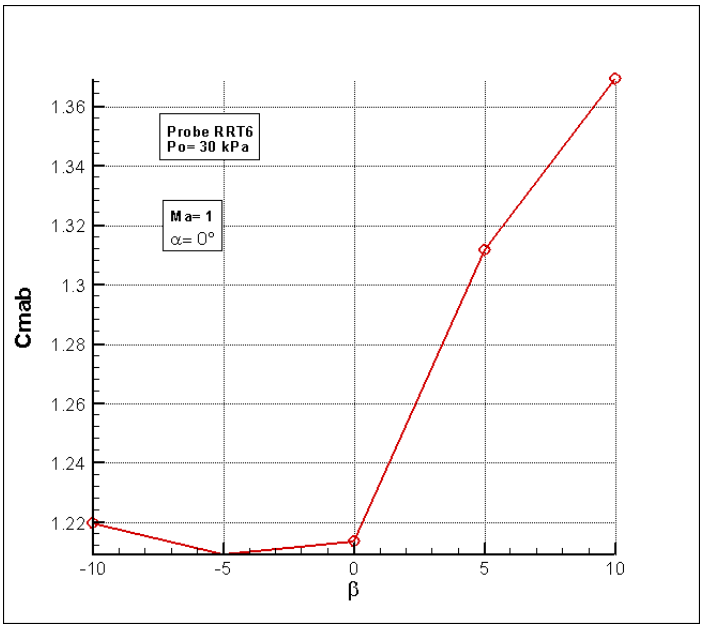

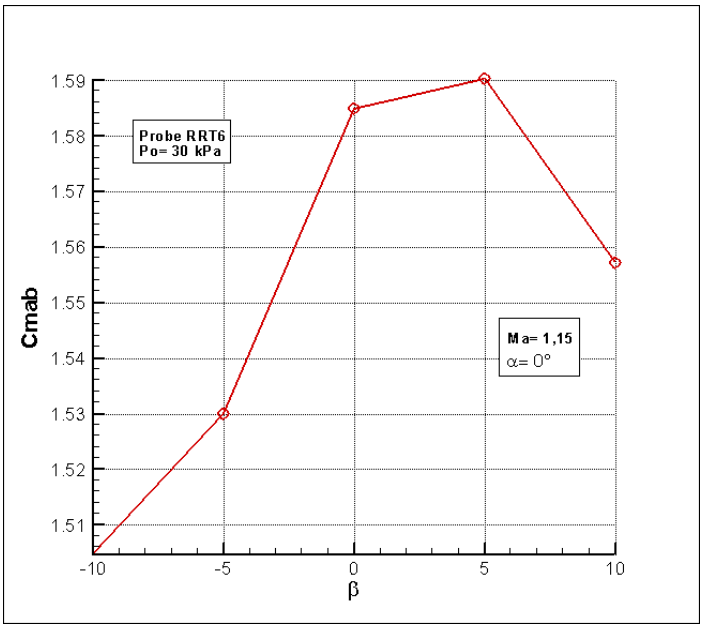

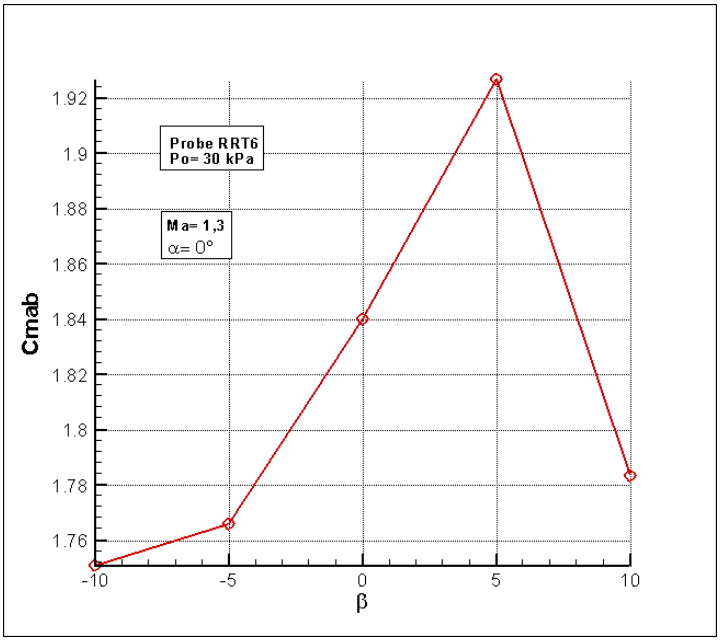

Figure 63: Evolution of C_{Mab} against β at Ma=1

1.15

1.3

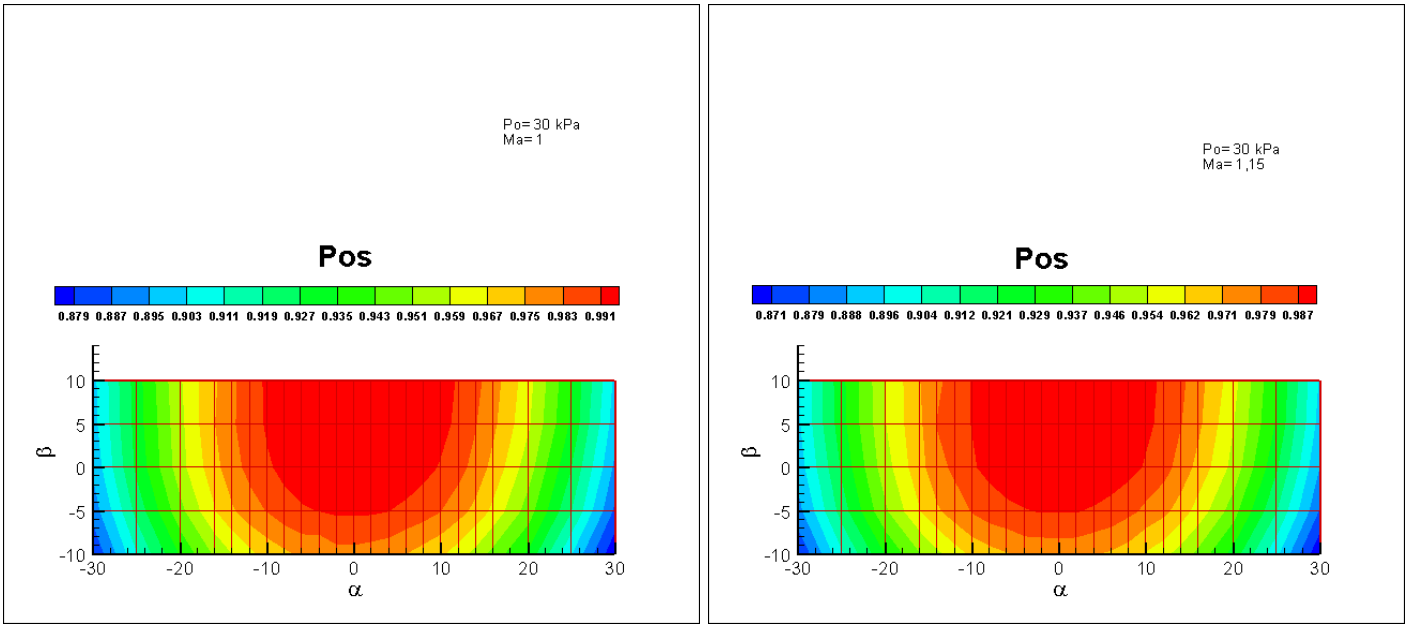

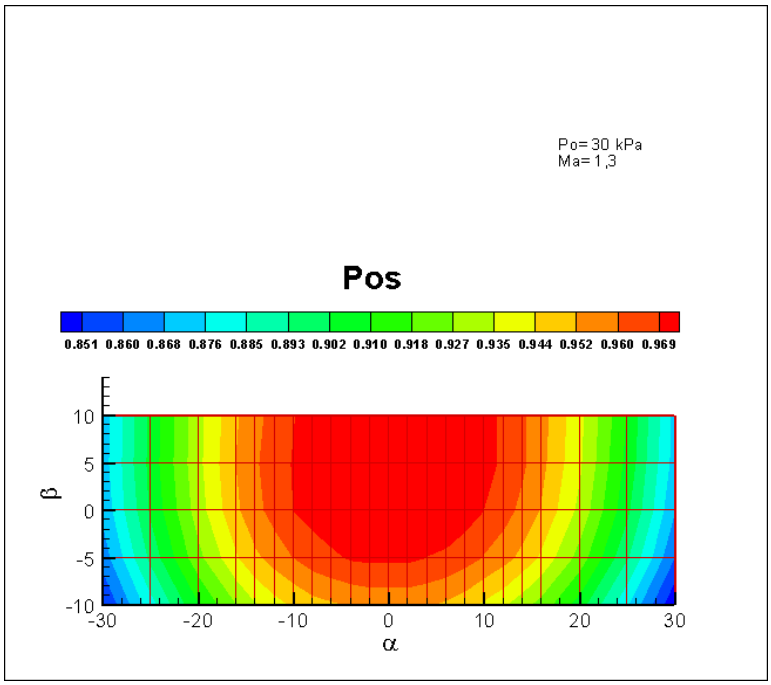

Figure 64: Evolution of p_{0s} against α and β at Ma=1
1.15
1.3

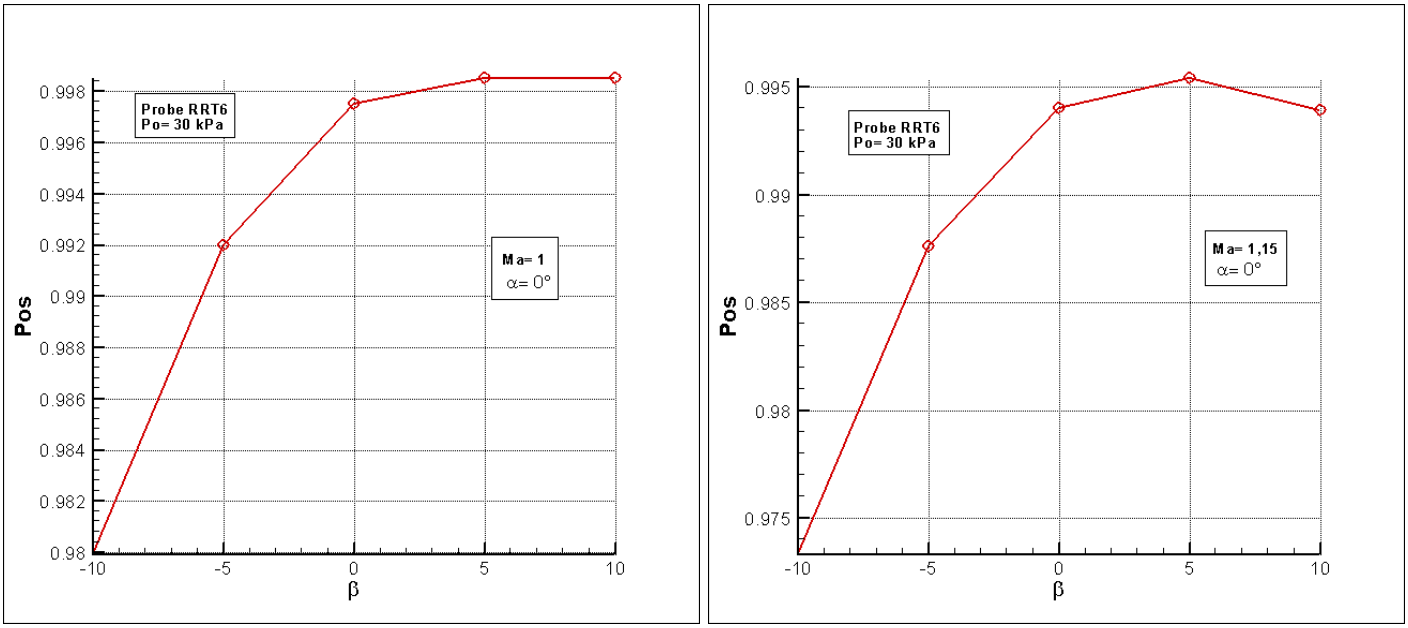

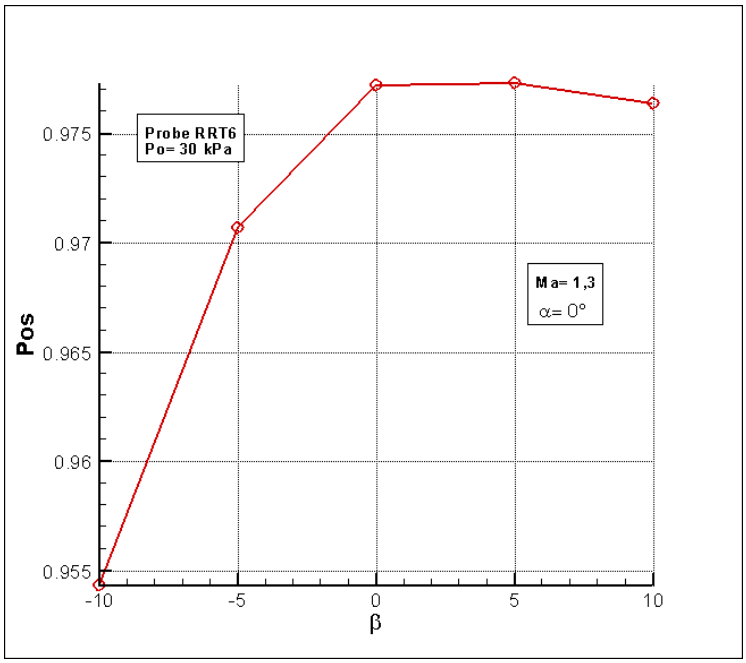

Figure 65: Evolution of p_{0s} against β at Ma=1
1.15
1.3

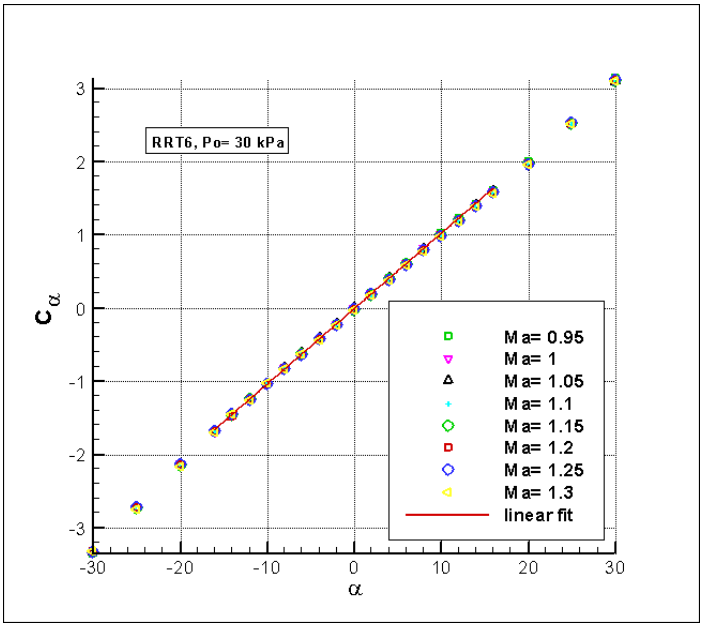

Figure 66: Evolution of C_α against α

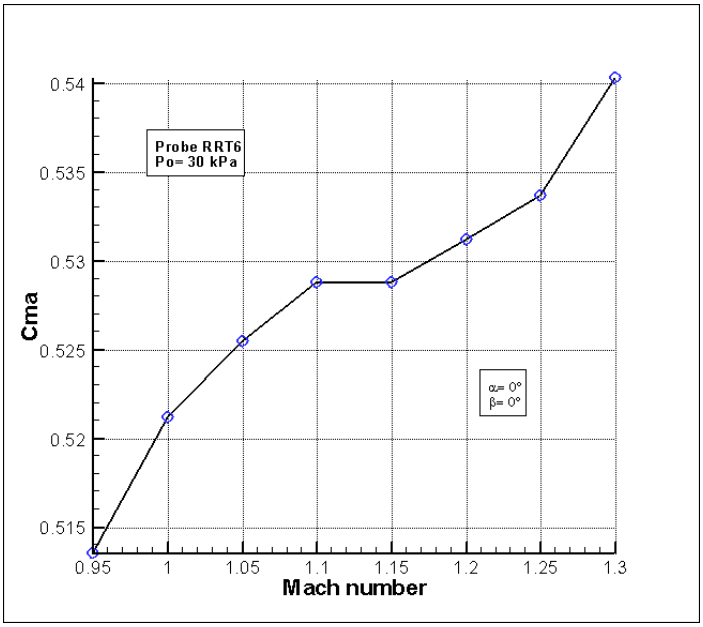

Figure 67: Evolution of C_{Ma} against Ma

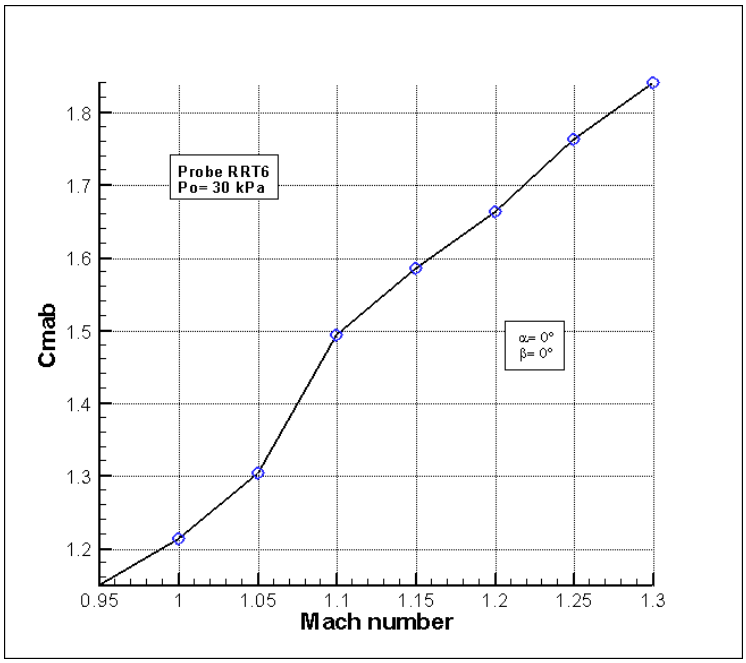

Figure 68: Evolution of C_{Mab} against Ma

Transonic, p_0= 100kPa

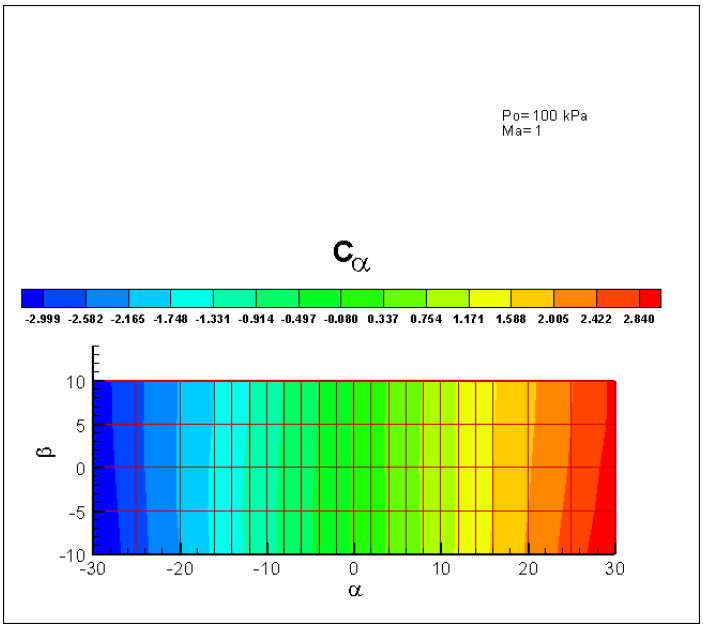

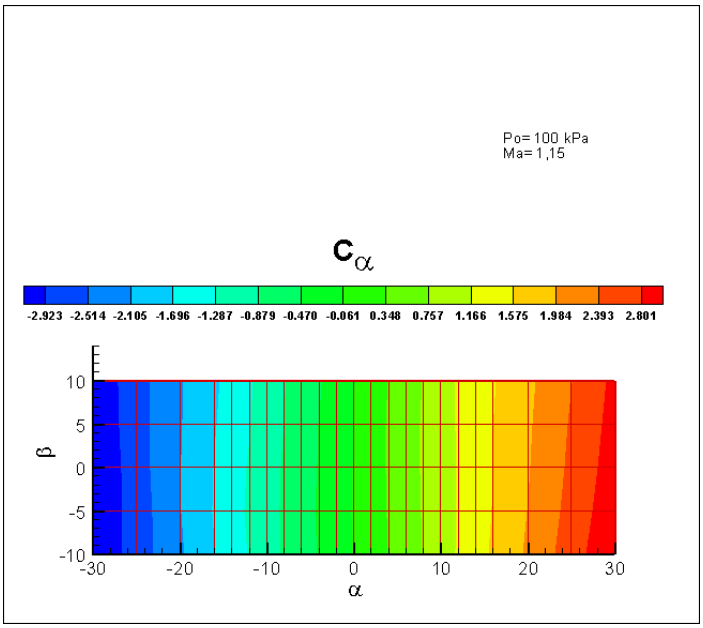

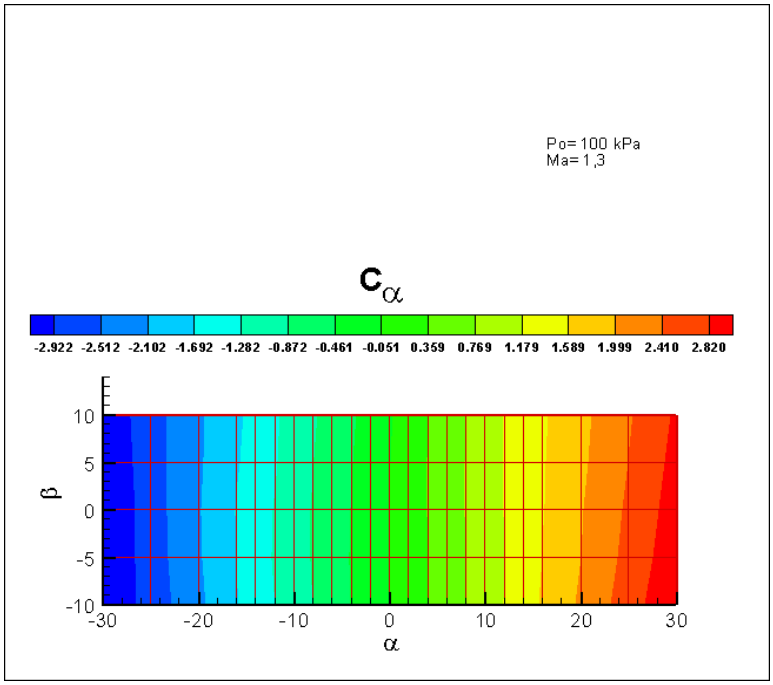

Figure 69: Evolution of C_α against α and β at Ma=1
1.15
1.3

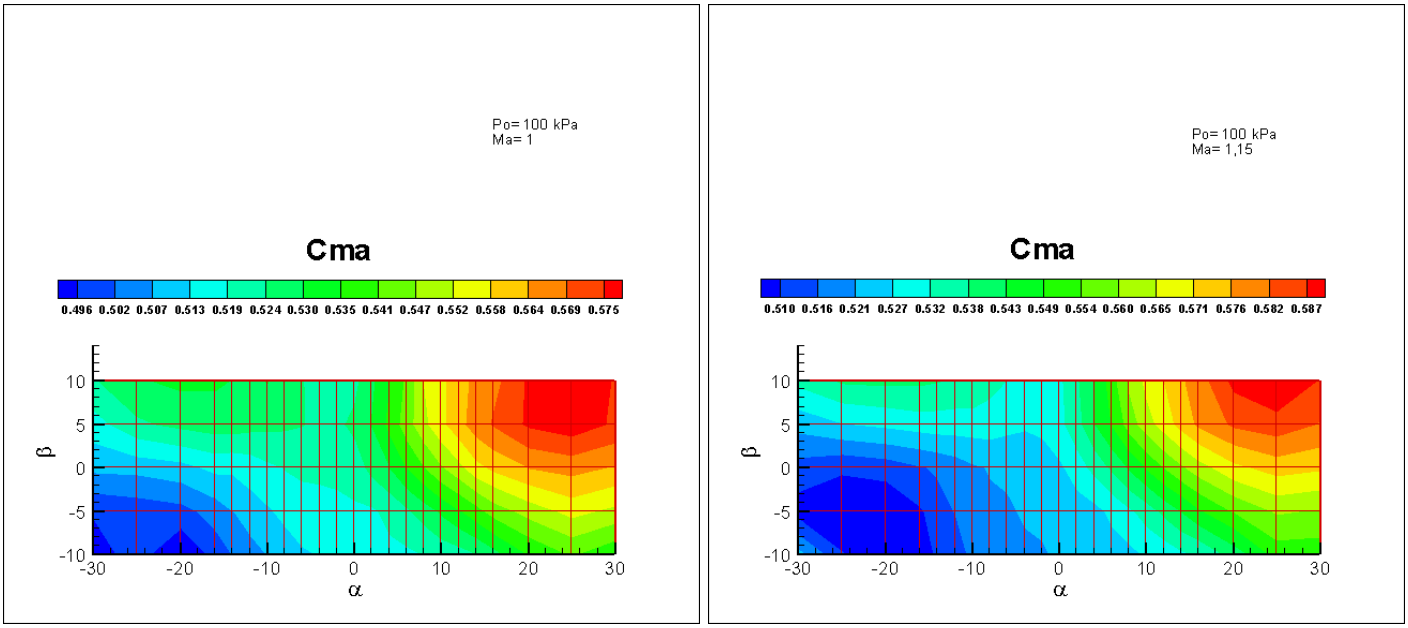

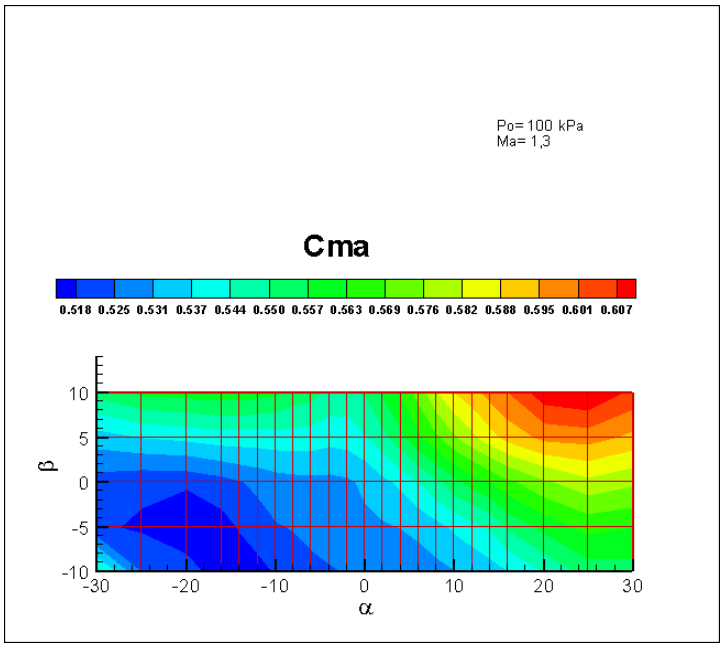

Figure 70: Evolution of C_{Ma} against α and β at Ma=1
1.15
1.3

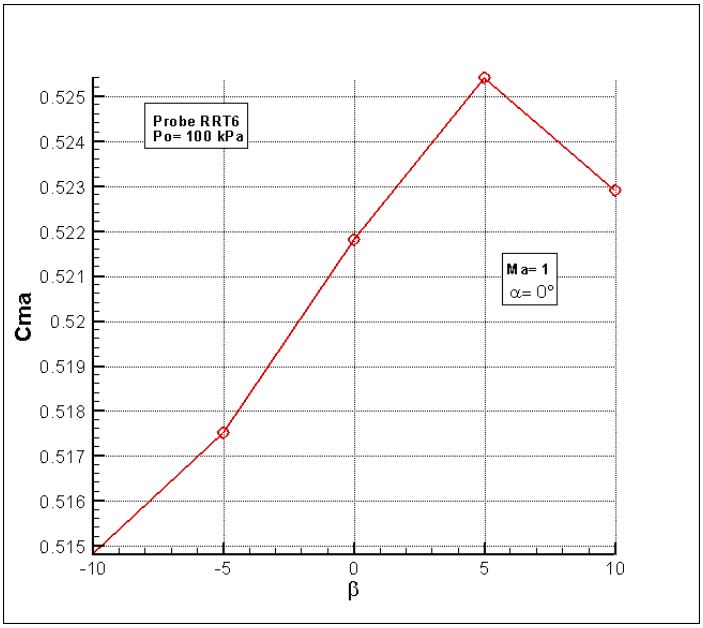

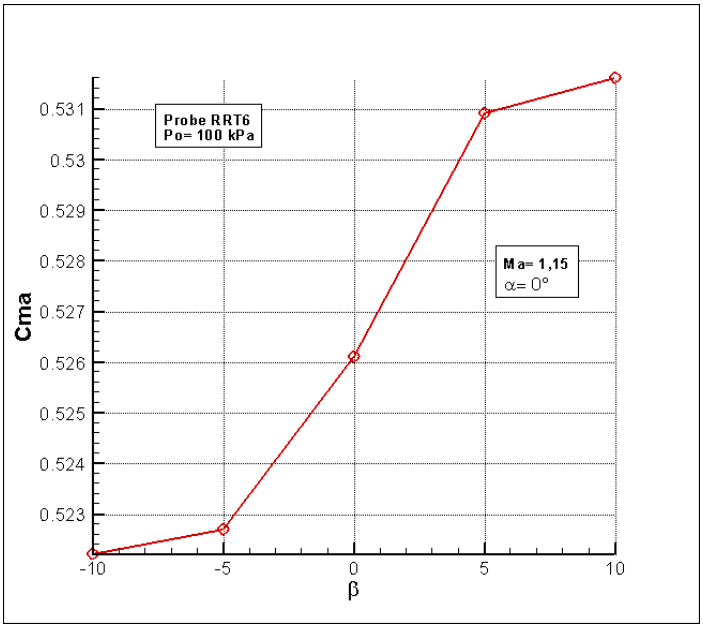

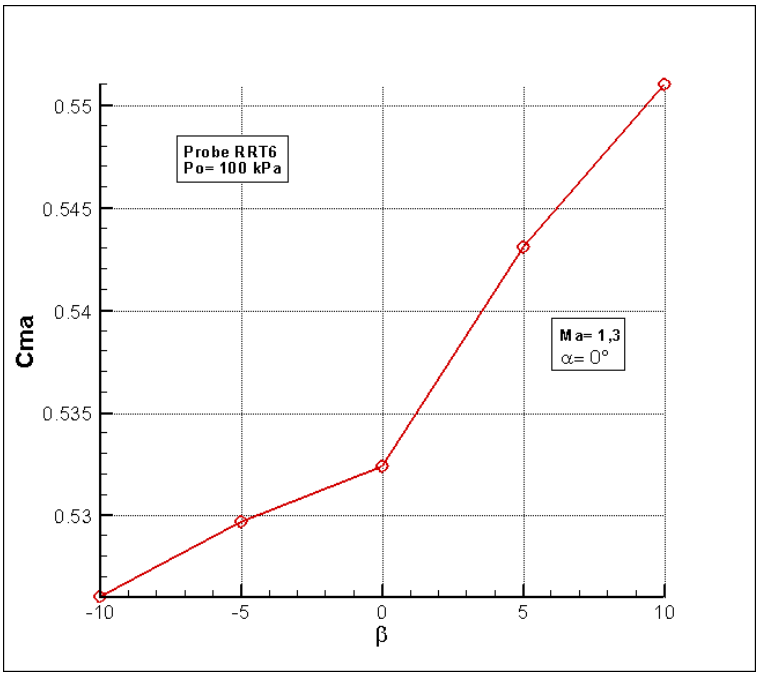

Figure 71: Evolution of C_{Ma} against β at Ma=1
1.15
1.3

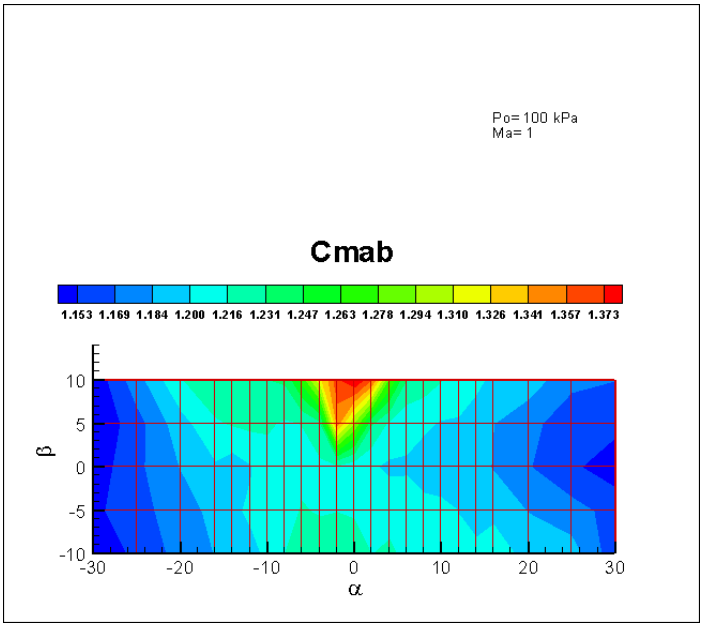

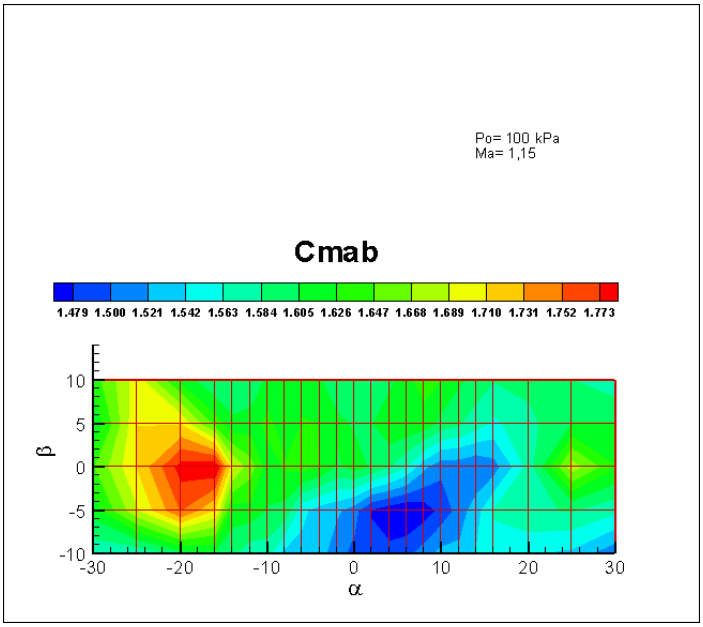

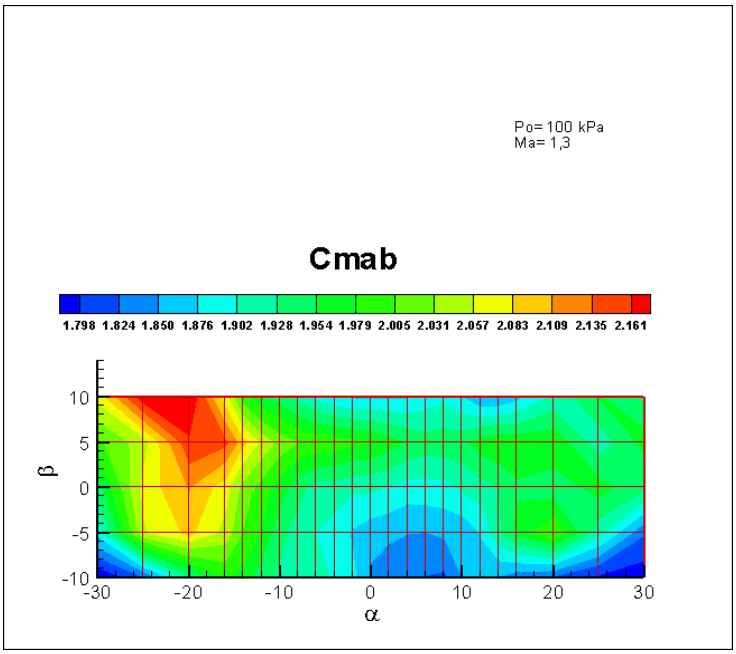

Figure 72: Evolution of C_{Mab} against α and β at Ma=1
1.15
1.3

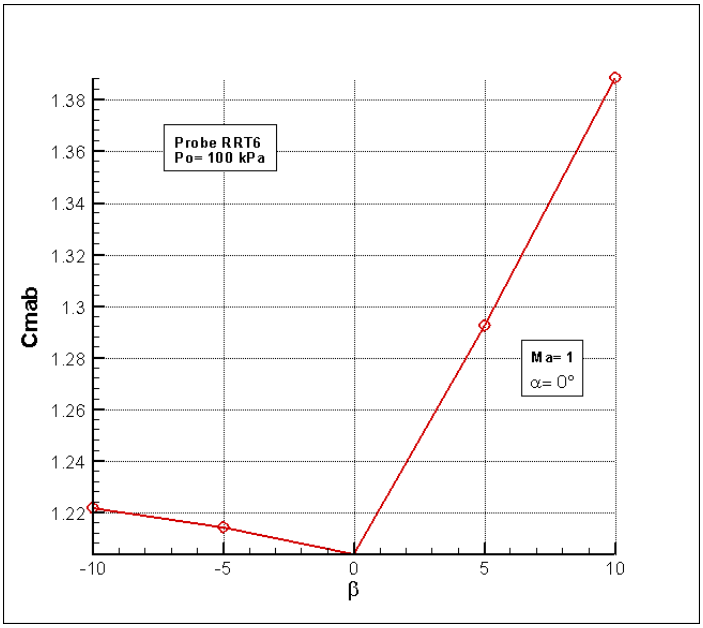

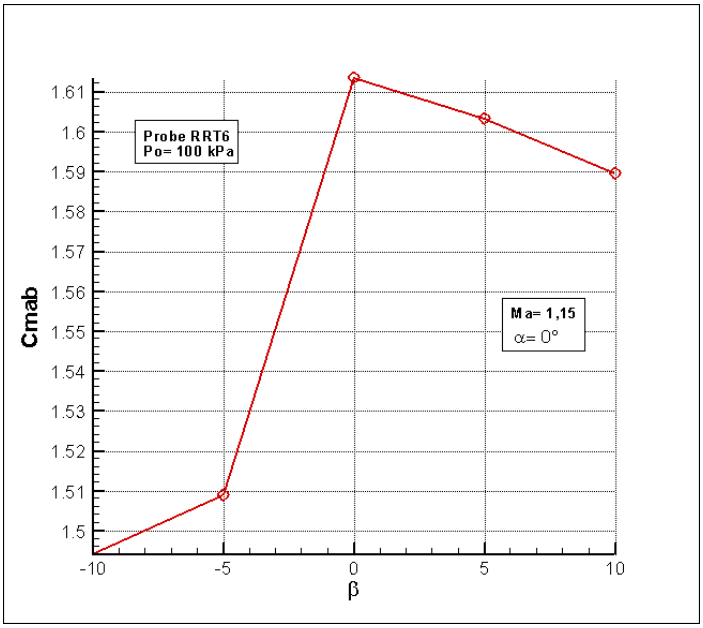

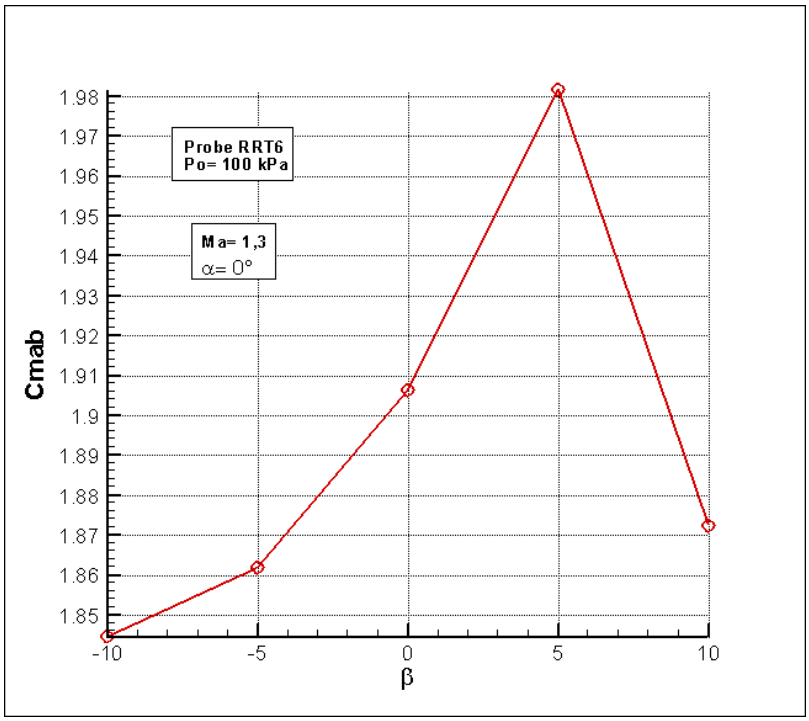

Figure 73: Evolution of C_{Mab} against β at Ma=1

1.15

1.3

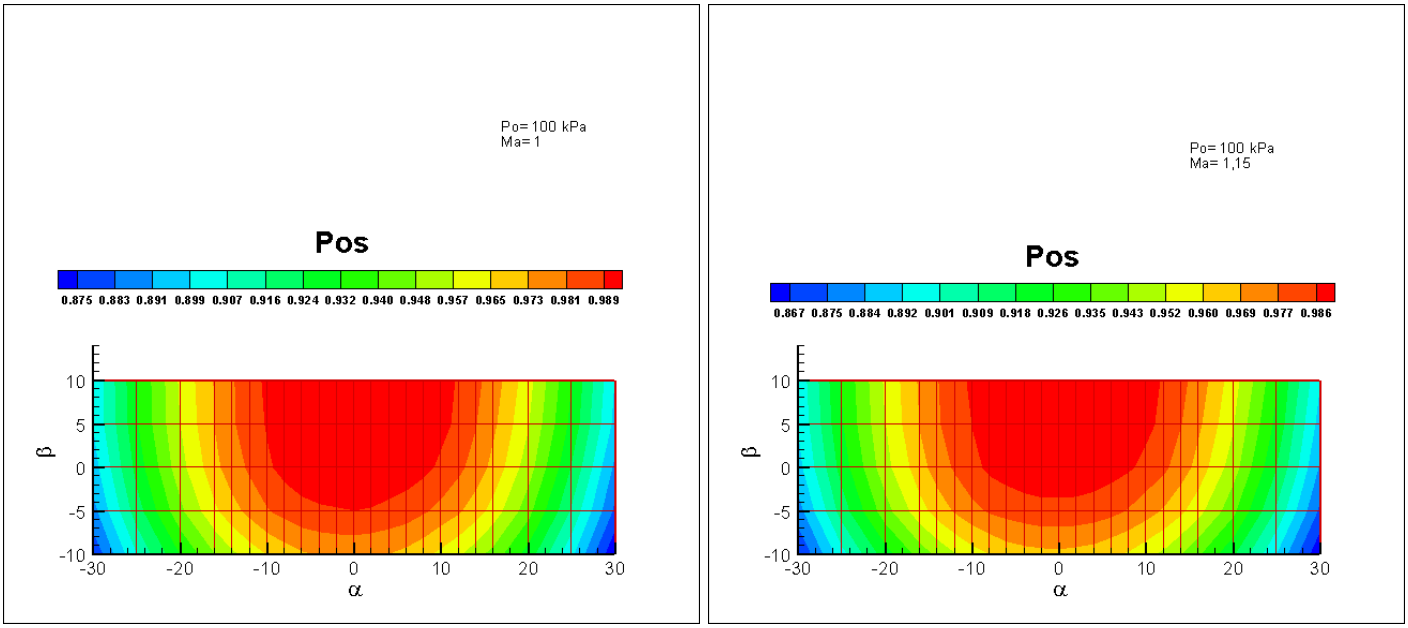

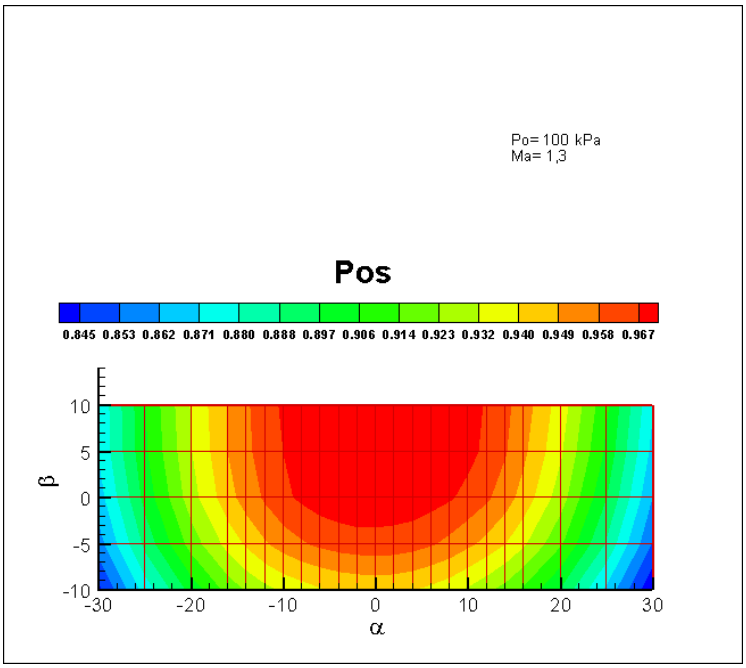

Figure 74: Evolution of p_{0s} against α and β at Ma=1
1.15
1.3

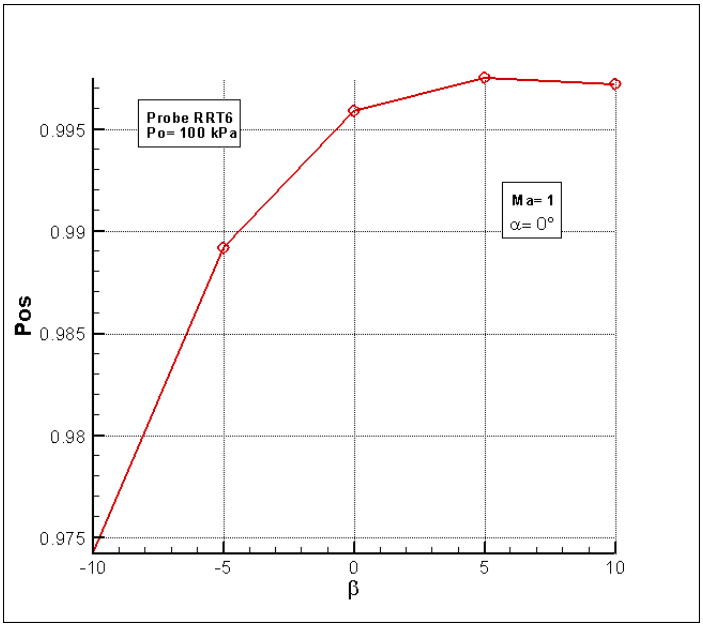

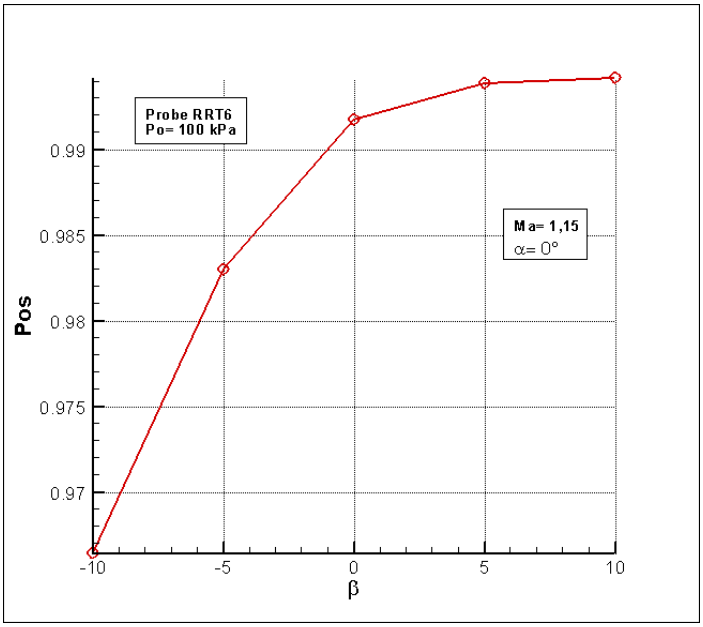

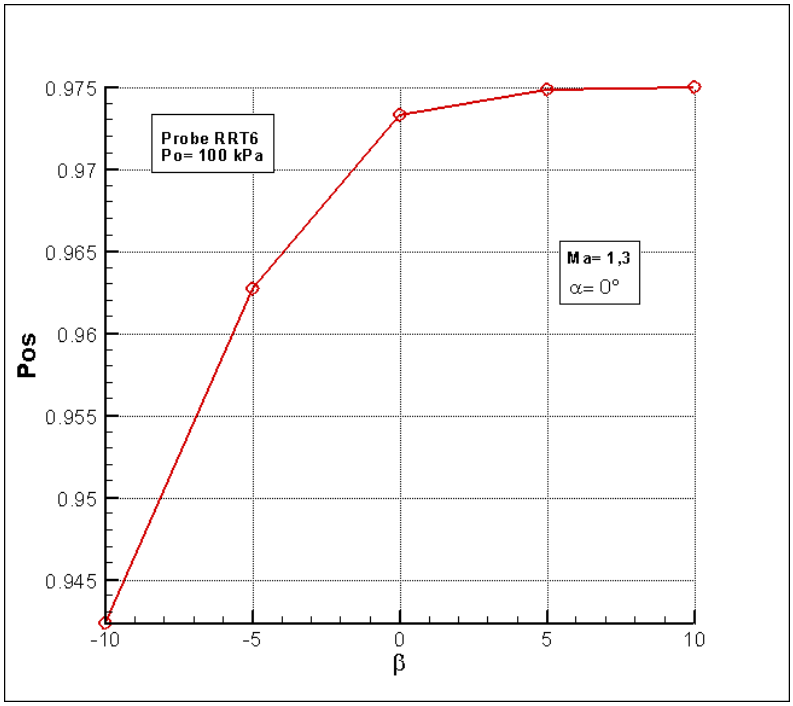

Figure 75: Evolution of p_{0s} against β at Ma=1
1.15
1.3

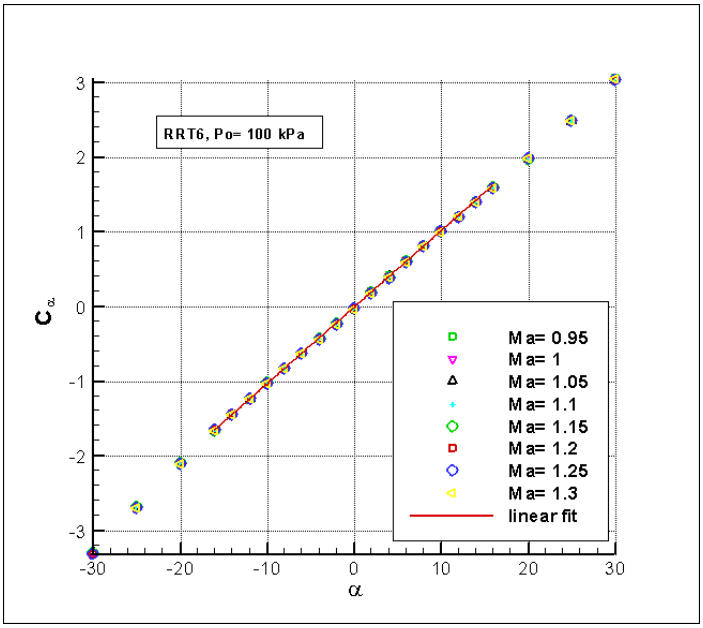

Figure 76: Evolution of C_α against α

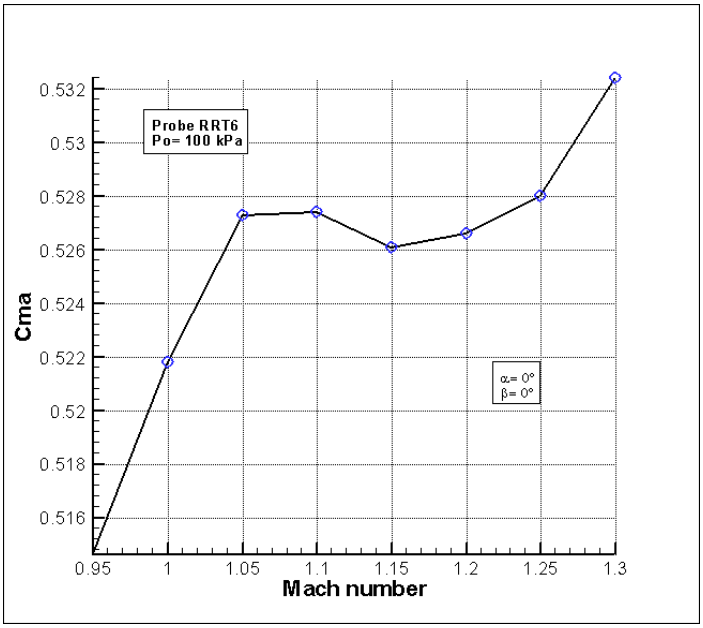

Figure 77: Evolution of C_{Ma} against Ma

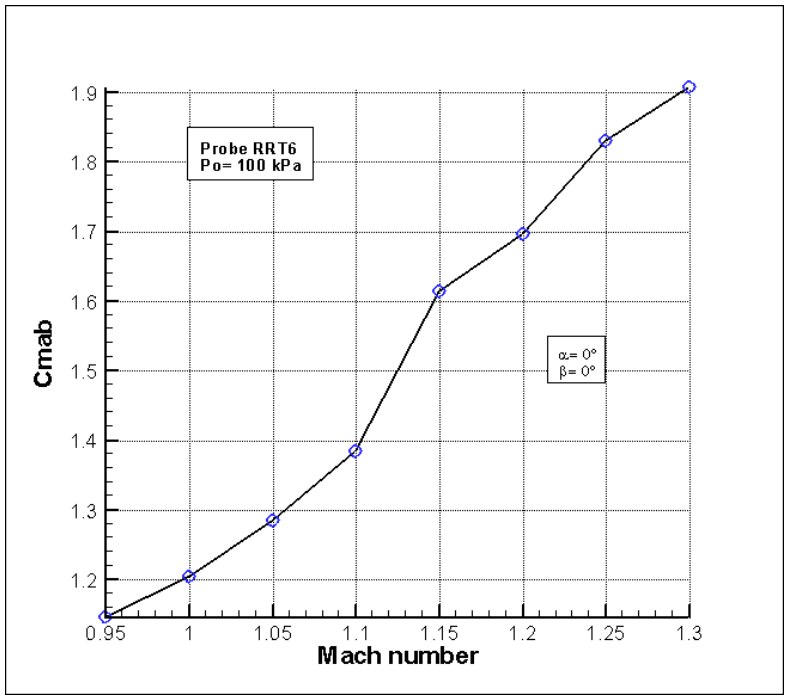

Figure 78: Evolution of C_{Mab} against Ma

Supersonic, p_0= 35kPa

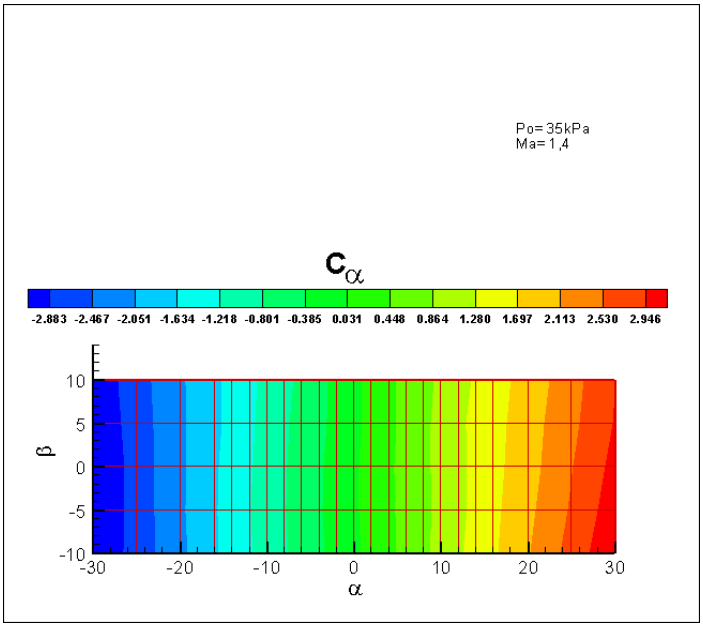

Figure 79: Evolution of C_α against α and β at Ma=1.4

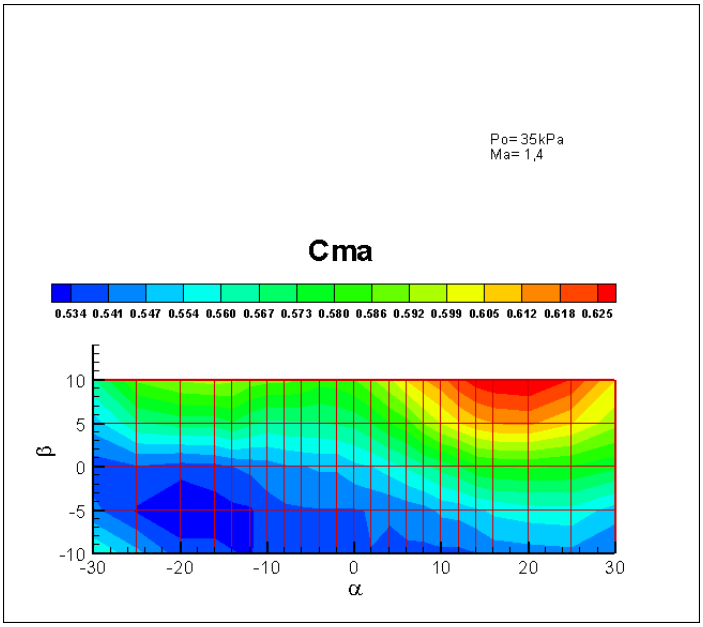

Figure 80: Evolution of C_{Ma} against α and β at Ma=1.4

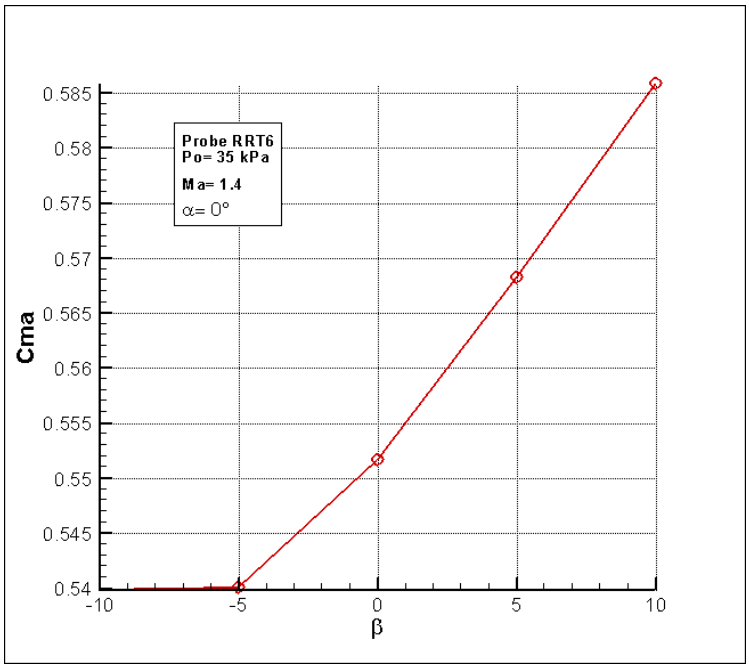

Figure 81: Evolution of C_{Ma} against β at Ma=1.4

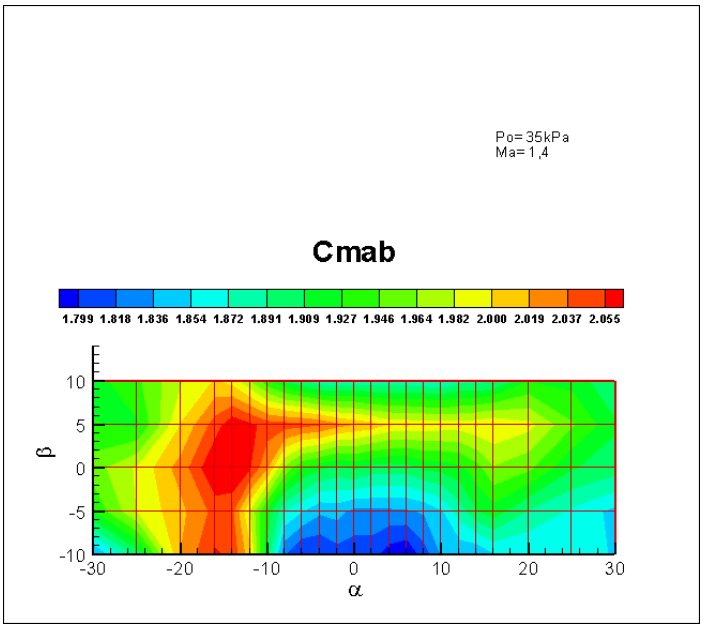

Figure 82: Evolution of C_{Mab} against α and β at Ma=1.4

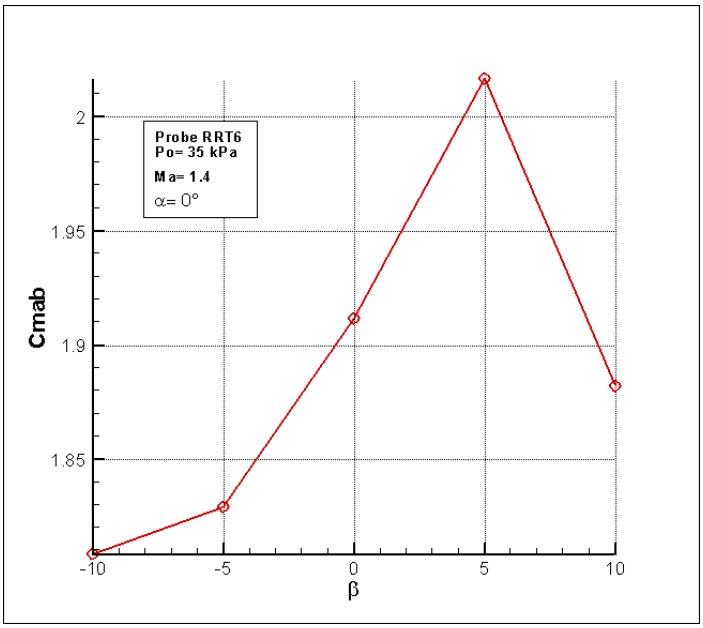

Figure 83: Evolution of C_{Mab} against β at Ma=1.4

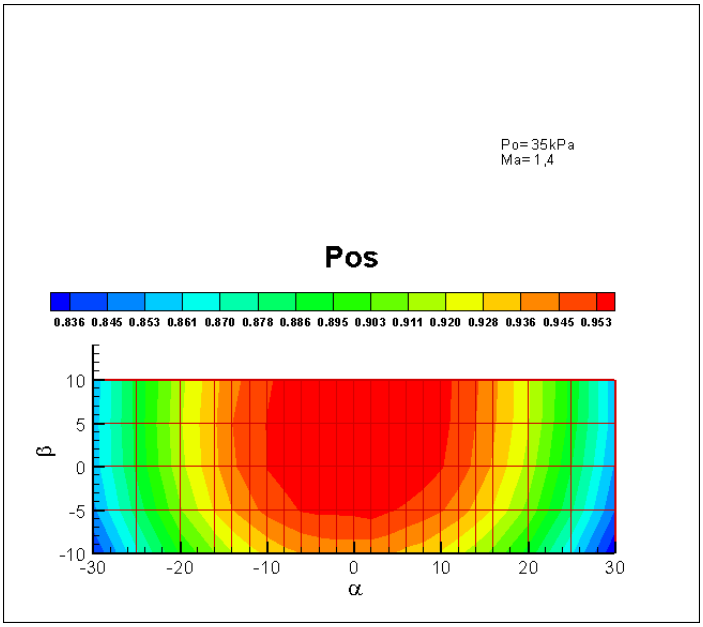

Figure 84: Evolution of p_{0s} against α and β at Ma=1.4

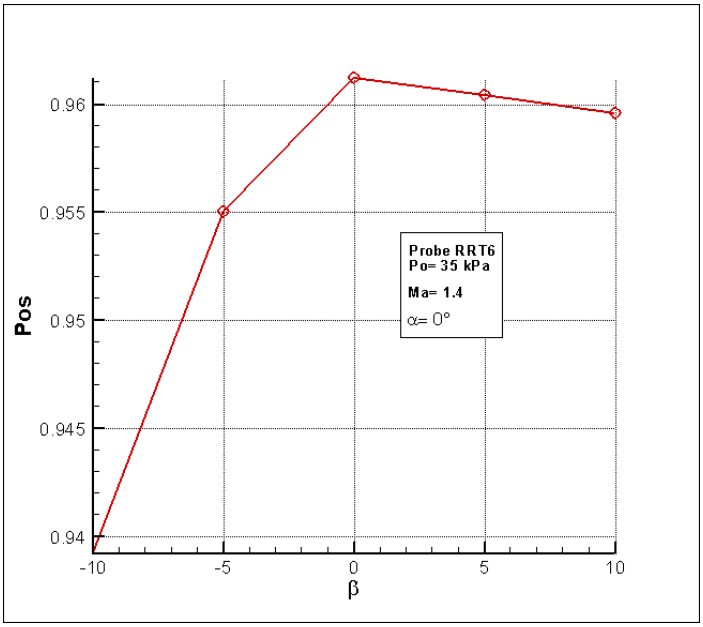

Figure 85: Evolution of p_{0s} against β at Ma=1.4

Supersonic, p_0= 40kPa

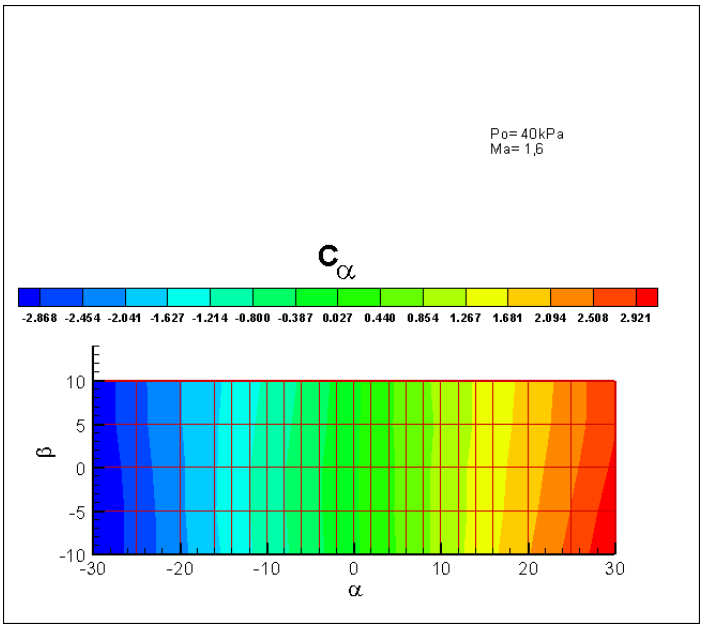

Figure 86: Evolution of C_α against α and β at Ma=1.6

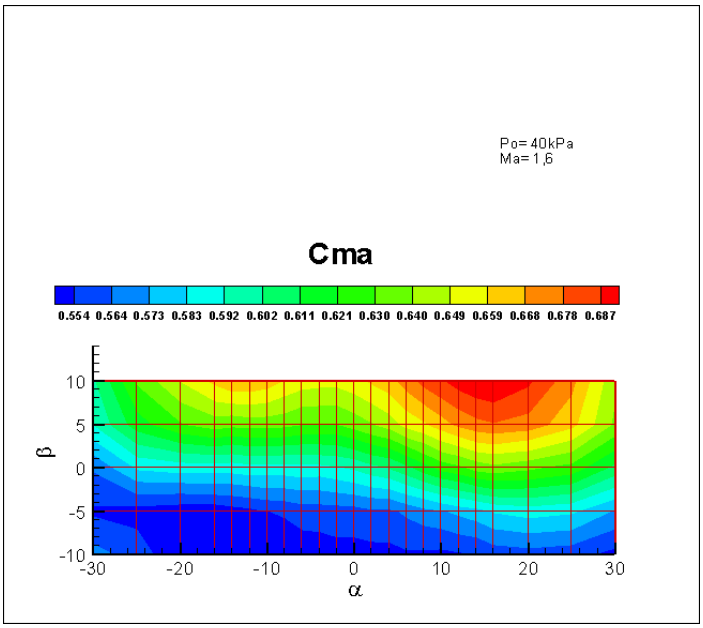

Figure 87: Evolution of C_{Ma} against α and β at Ma=1.6

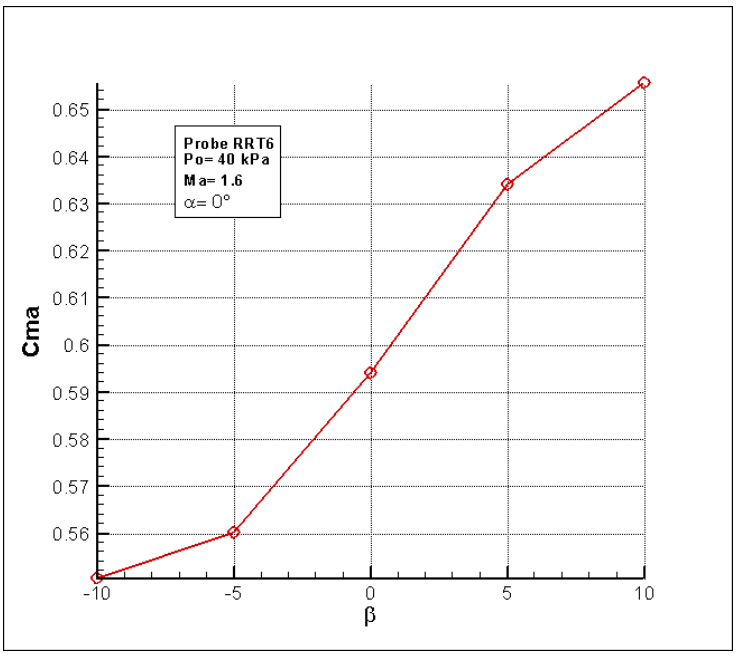

Figure 88: Evolution of C_{Ma} against β at Ma=1.6

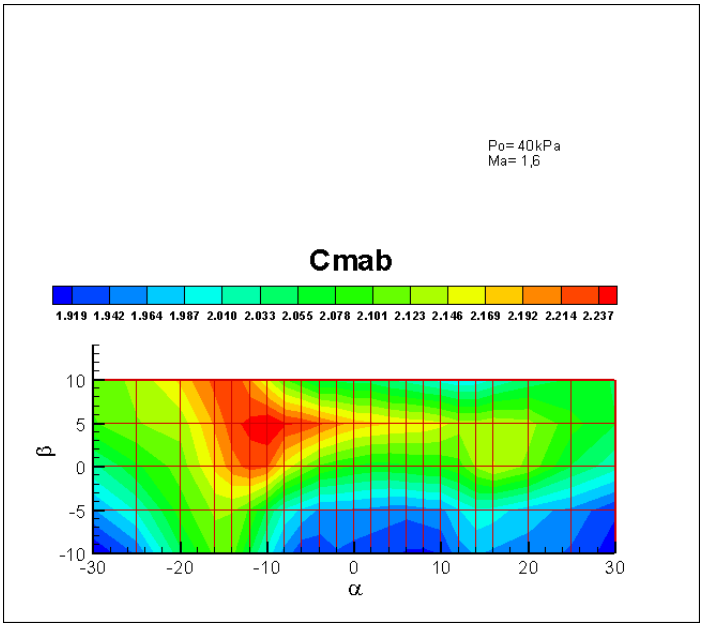

Figure 89: Evolution of C_{Mab} against α and β at Ma=1.6

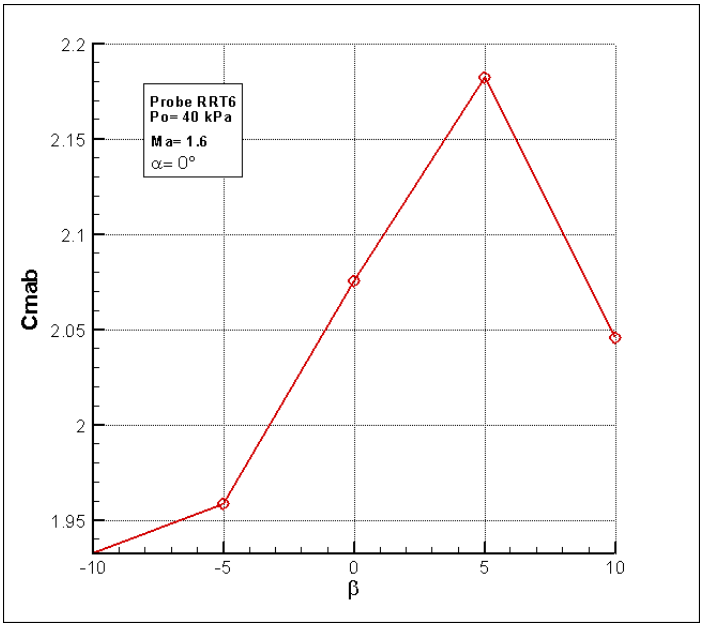

Figure 90: Evolution of C_{Mab} against β at Ma=1.6

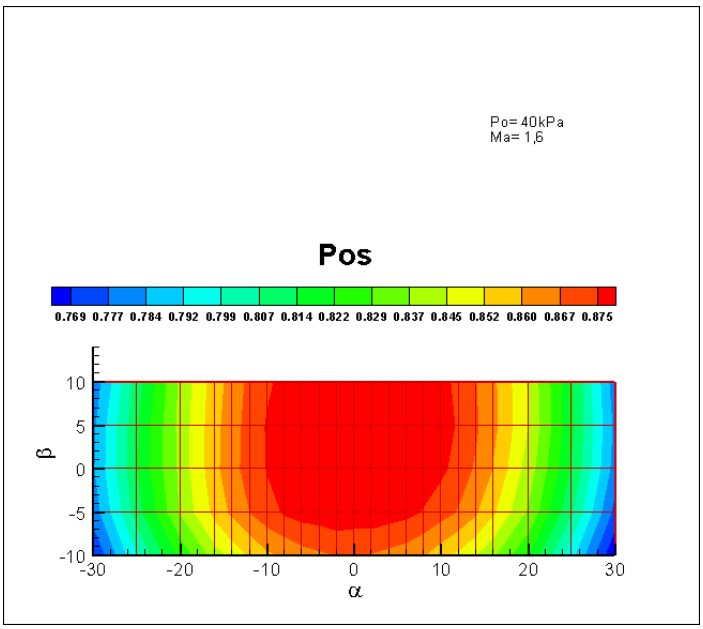

Figure 91: Evolution of p_{0s} against α and β at Ma=1.6

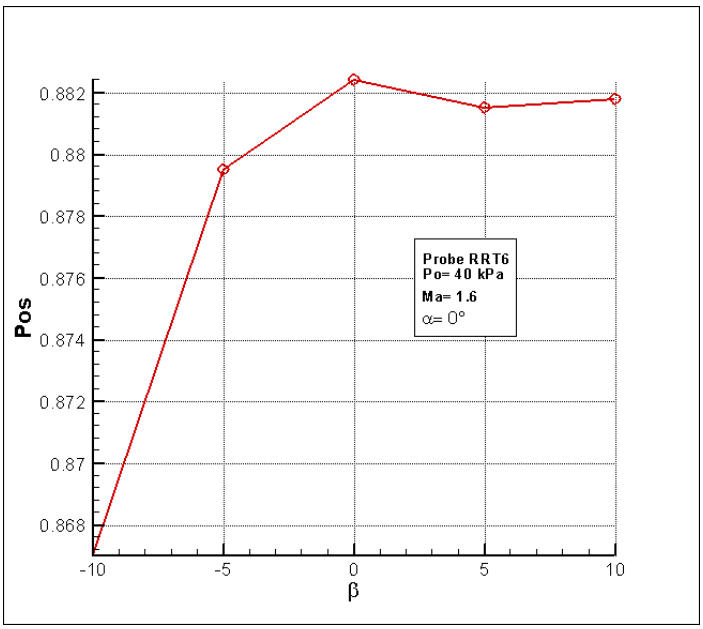

Figure 92: Evolution of p_{0s} against β at Ma=1.6

Supersonic, p_0= 51kPa

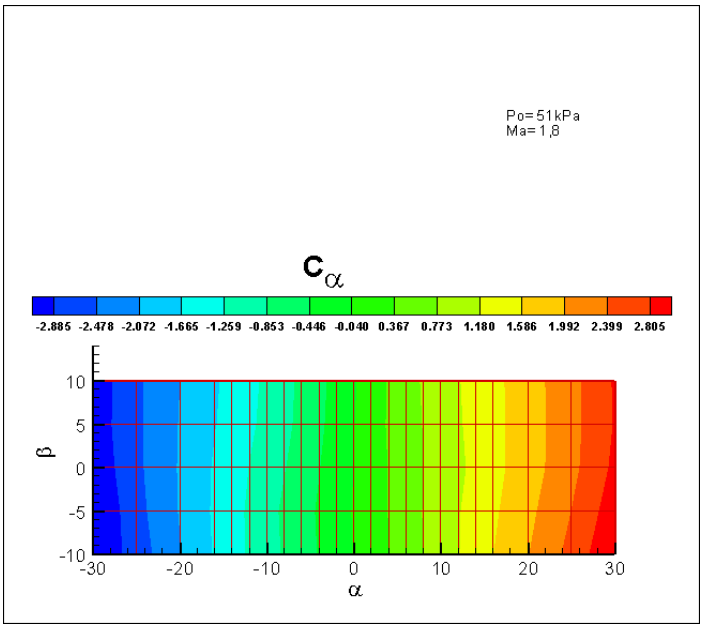

Figure 93: Evolution of C_α against α and β at Ma=1.8

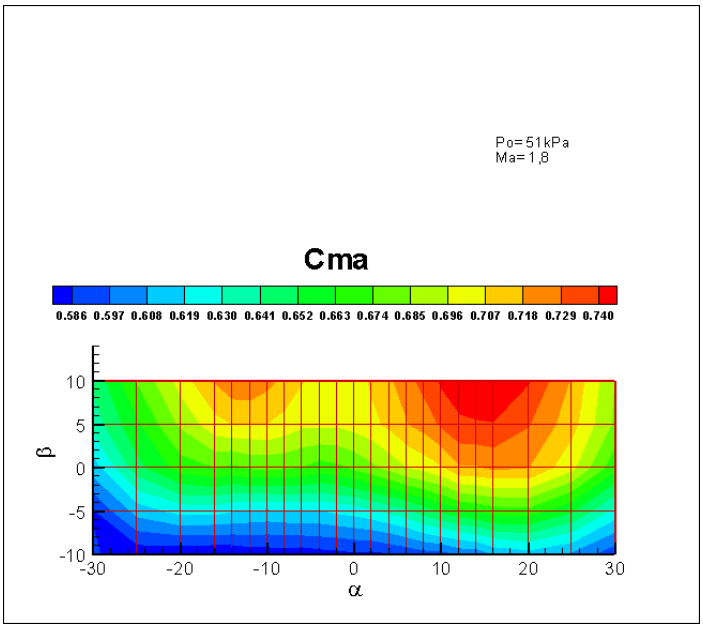

Figure 94: Evolution of C_{Ma} against α and β at Ma=1.8

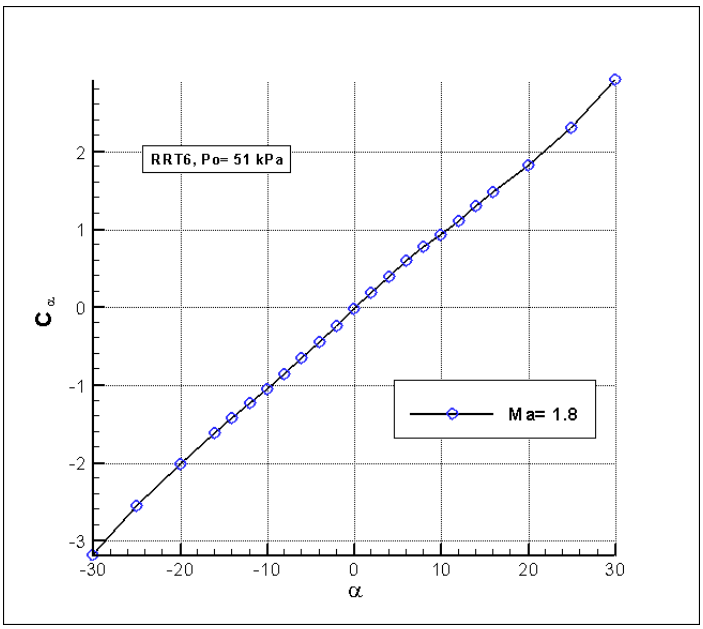

Figure 95: Evolution of C_α against α at Ma=1.8

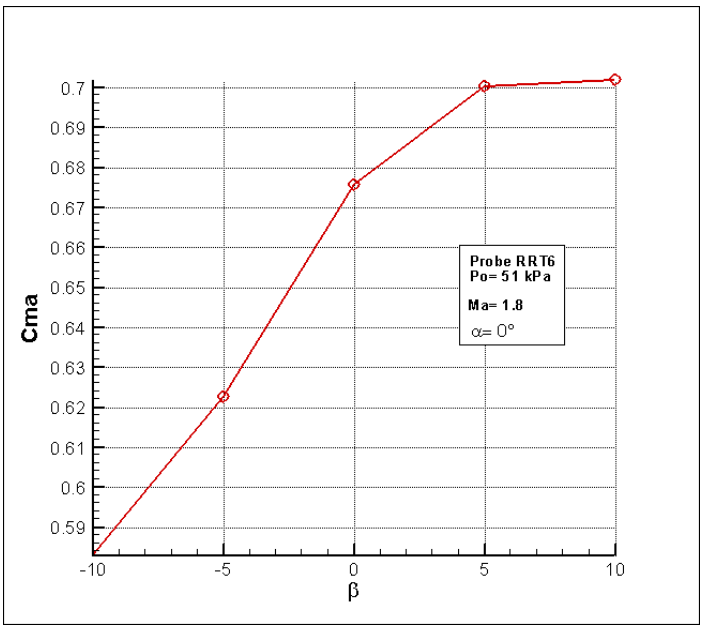

Figure 96: Evolution of C_{Ma} against β at Ma=1.8

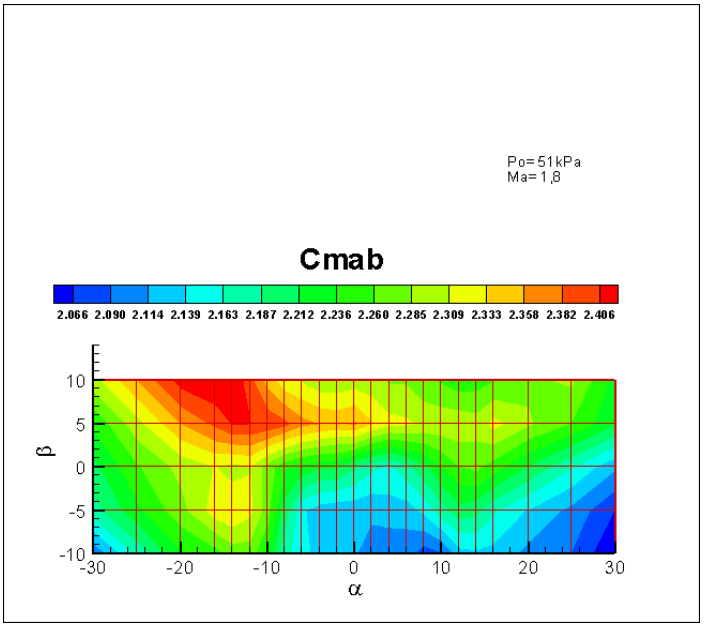

Figure 97: Evolution of C_{Mab} against α and β at Ma=1.8

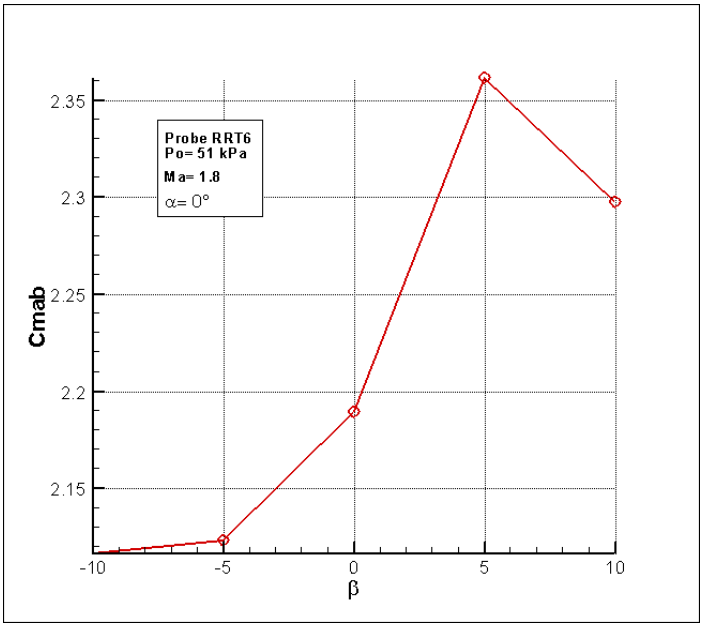

Figure 98: Evolution of C_{Mab} against β at Ma=1.8

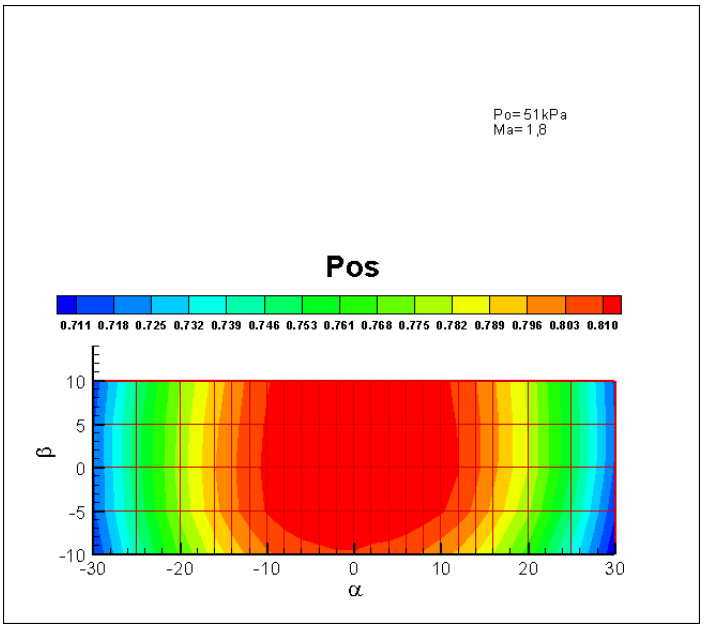

Figure 99: Evolution of p_{0s} against α and β at Ma=1.8

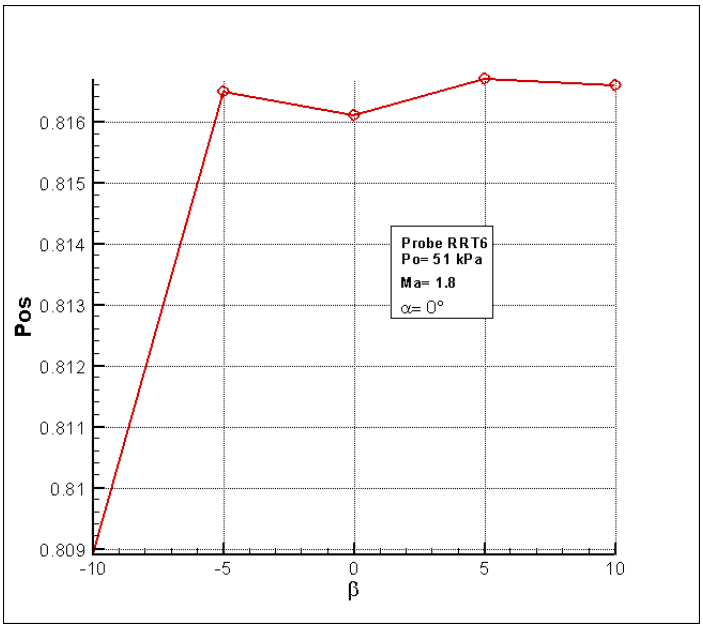

Figure 100: Evolution of p_{0s} against β at Ma=1.8

Supersonic, p_0= 100kPa

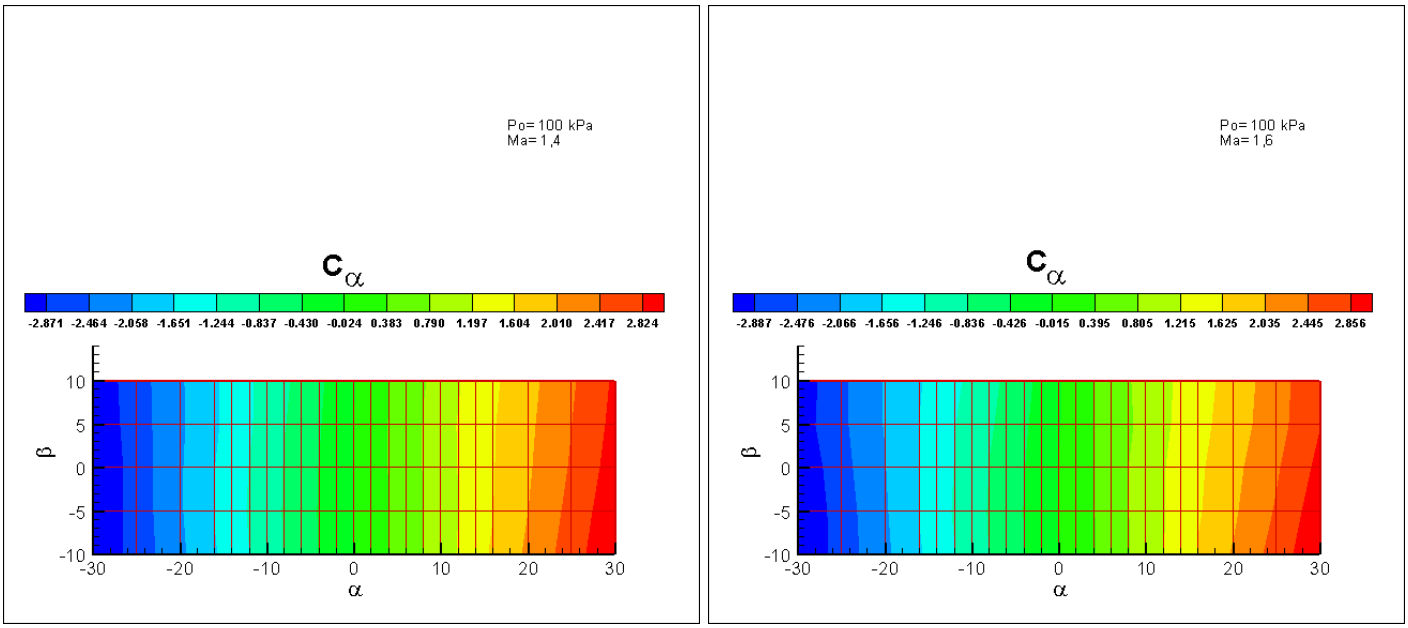

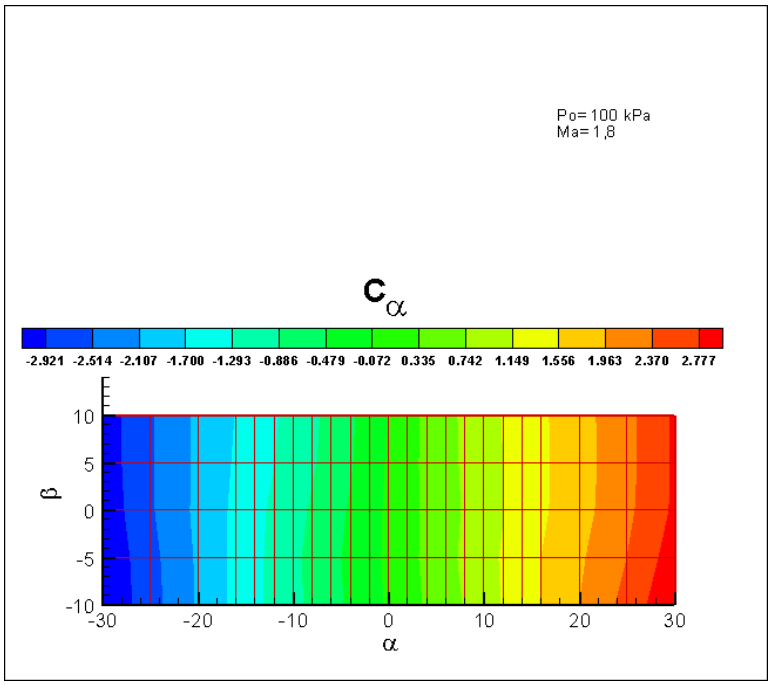

Figure 101: Evolution of C_α against α and β at Ma=1.4
1.6
1.8

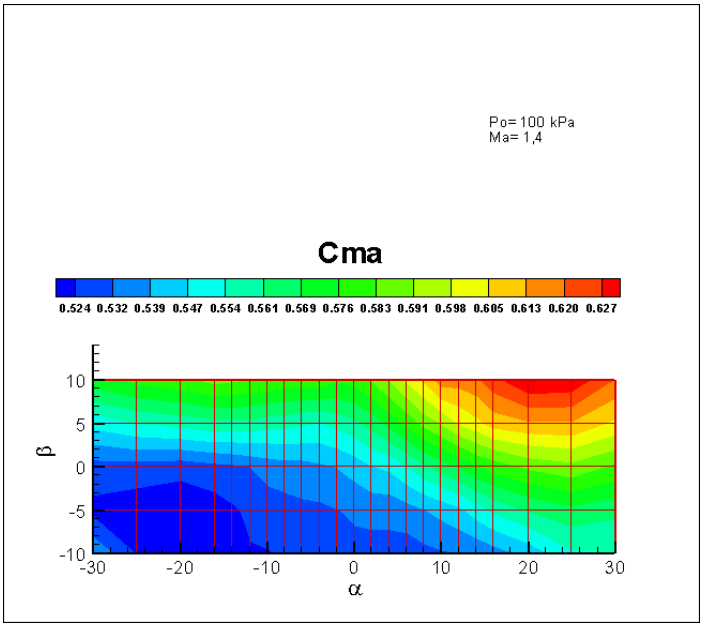

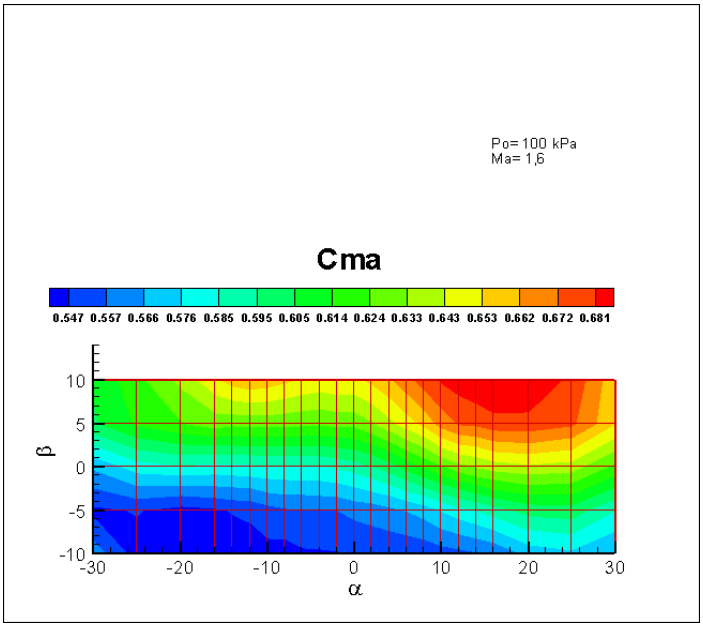

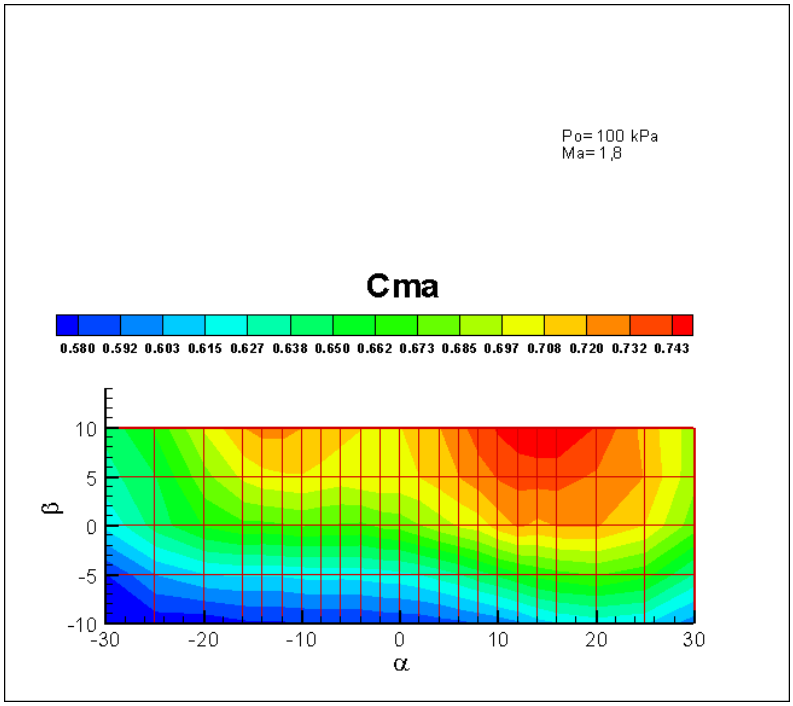

Figure 102: Evolution of C_{Ma} against α and β at Ma=1.4
1.6
1.8

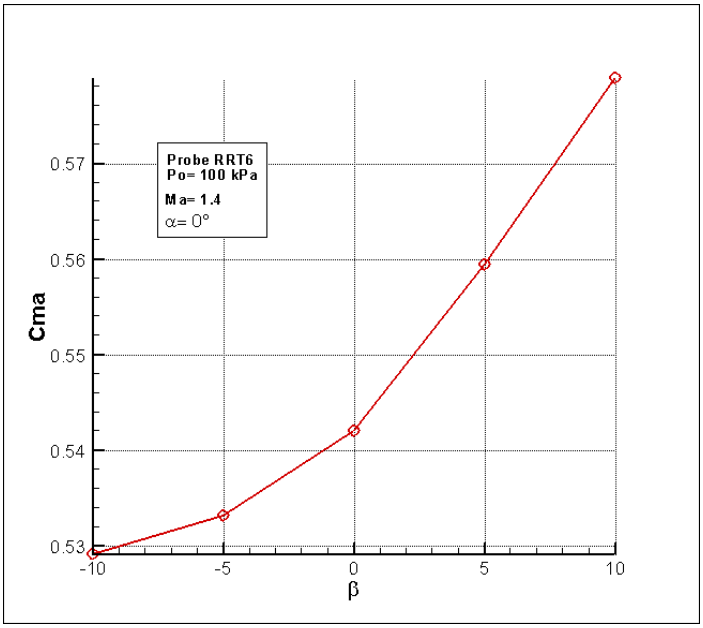

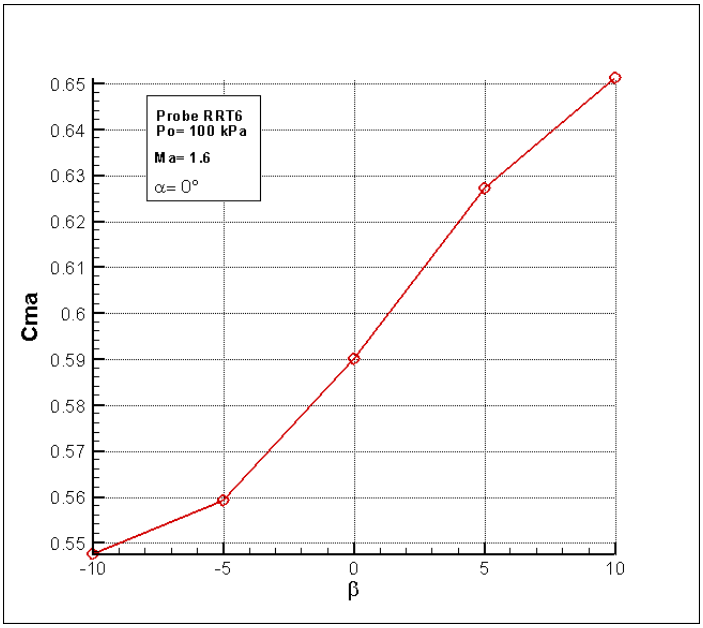

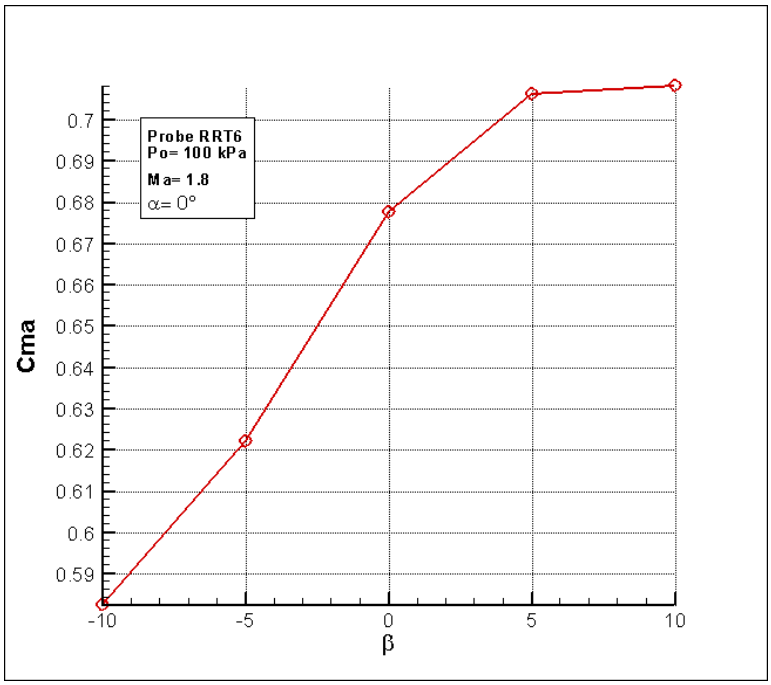

Figure 103: Evolution of C_{Ma} against β at Ma=1.4
1.6
1.8

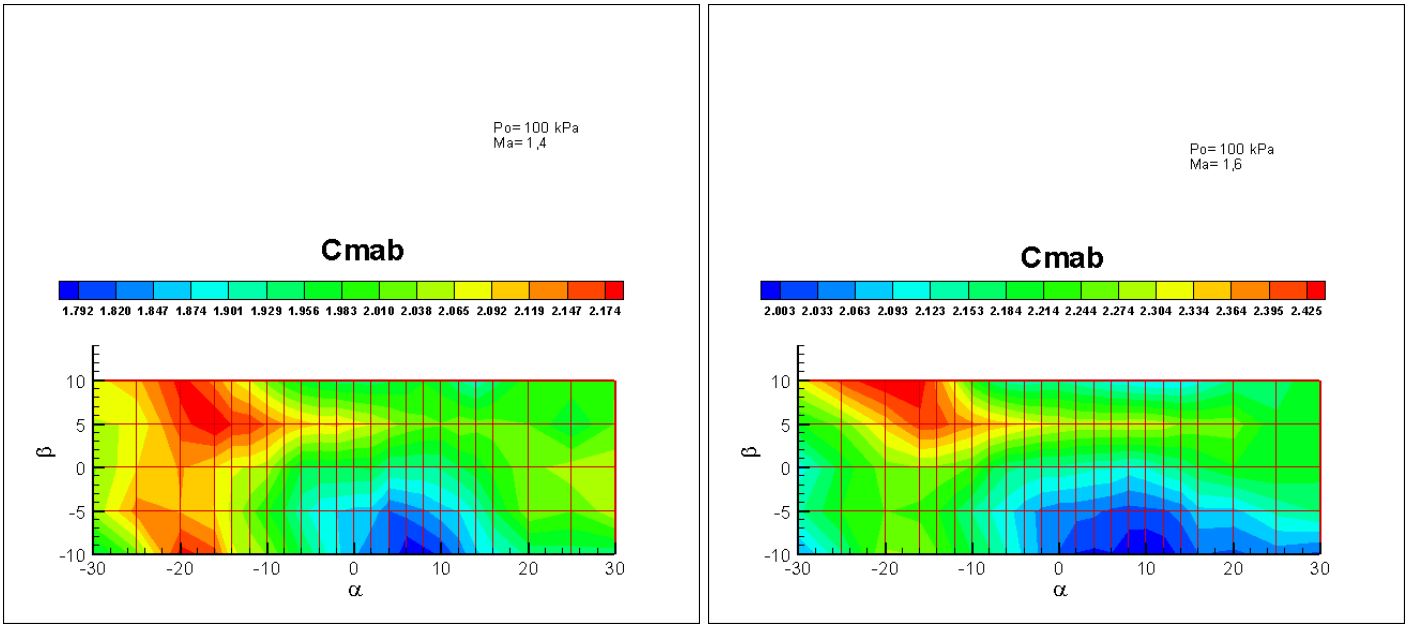

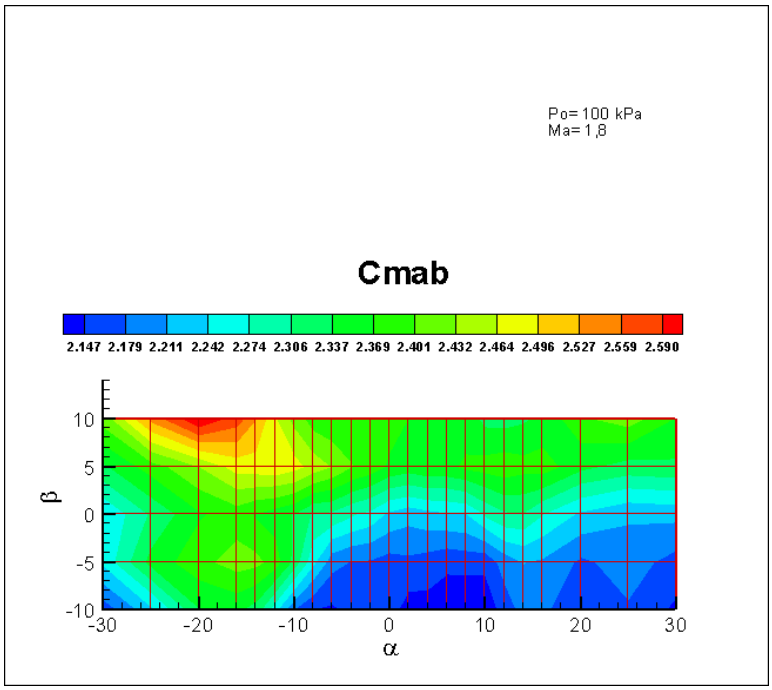

Figure 104: Evolution of C_{Mab} against α and β at Ma=1.4
1.6
1.8

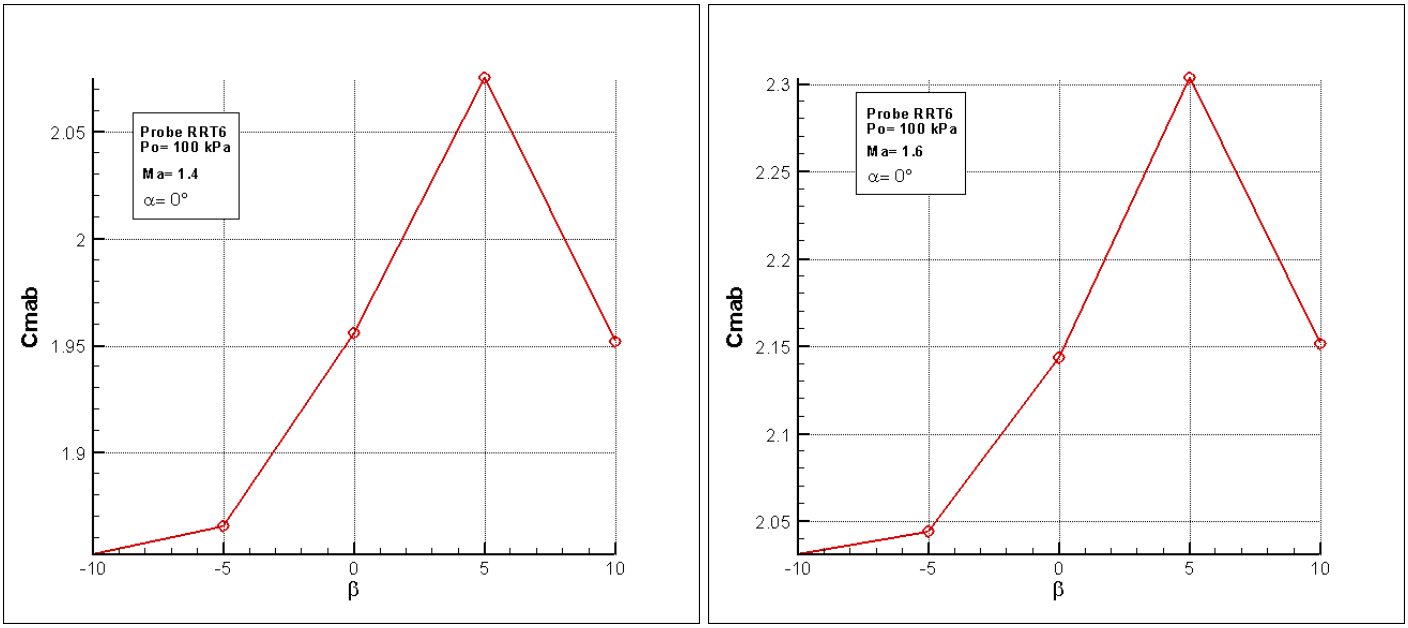

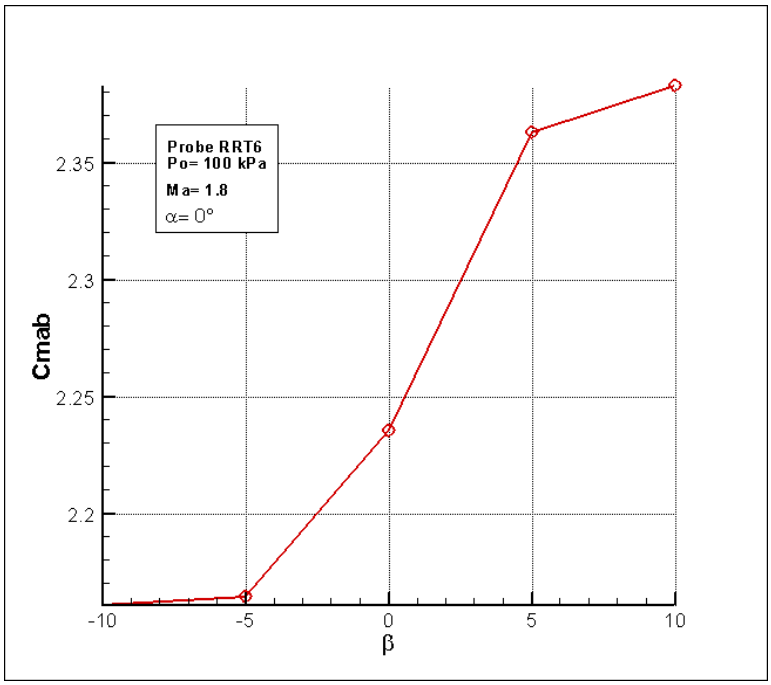

Figure 105: Evolution of C_{Mab} against β at Ma=1.4
1.6
1.8

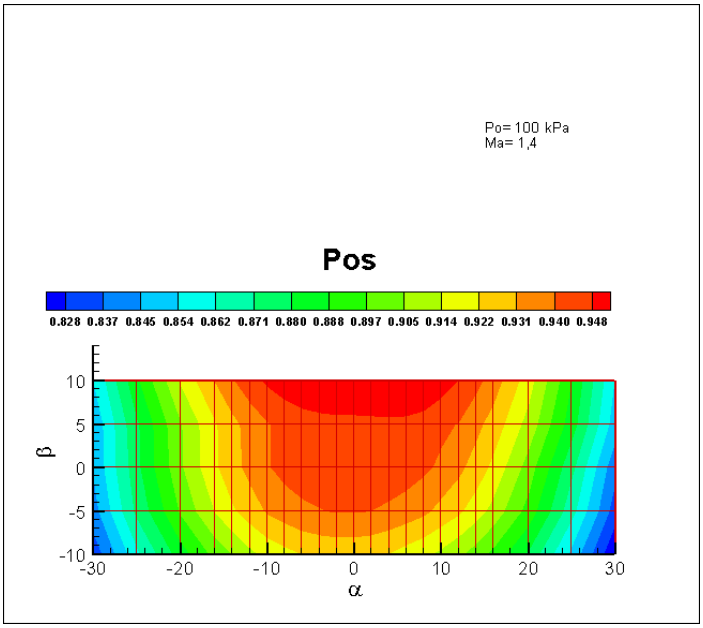

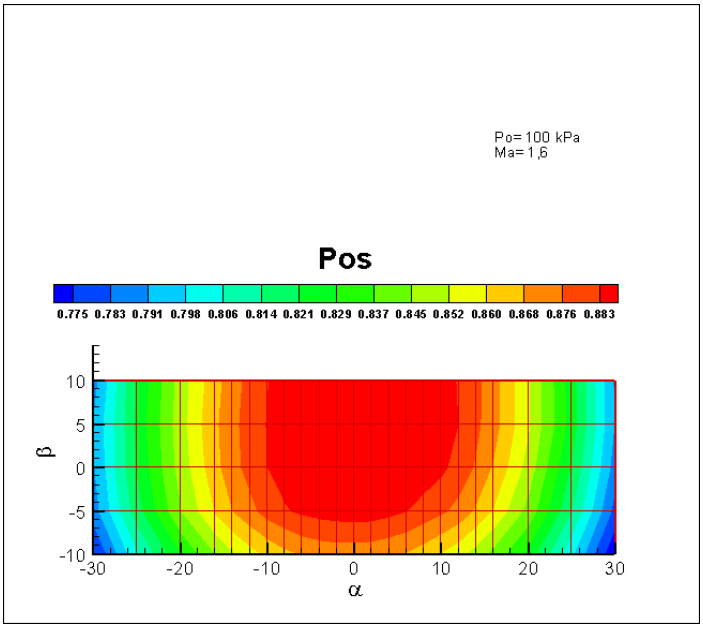

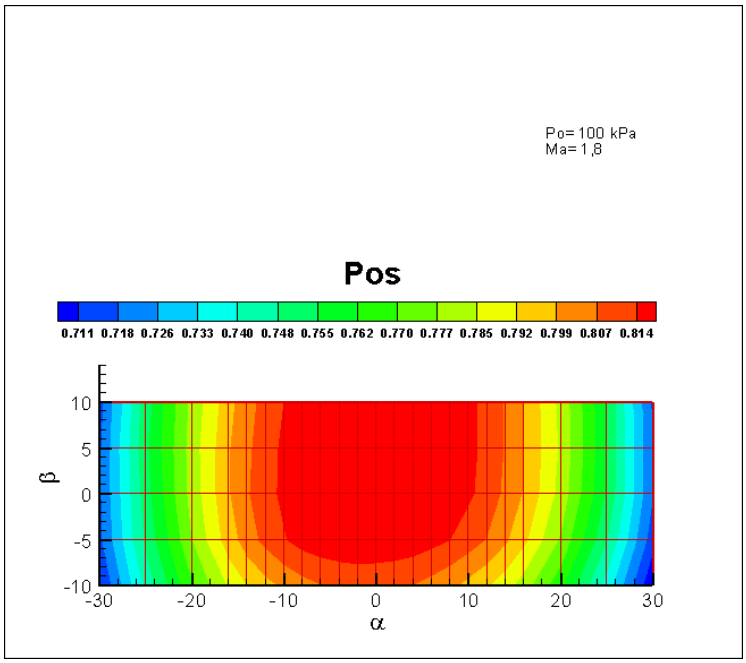

Figure 106: Evolution of p_{0s} against α and β at Ma=1.4
1.6
1.8

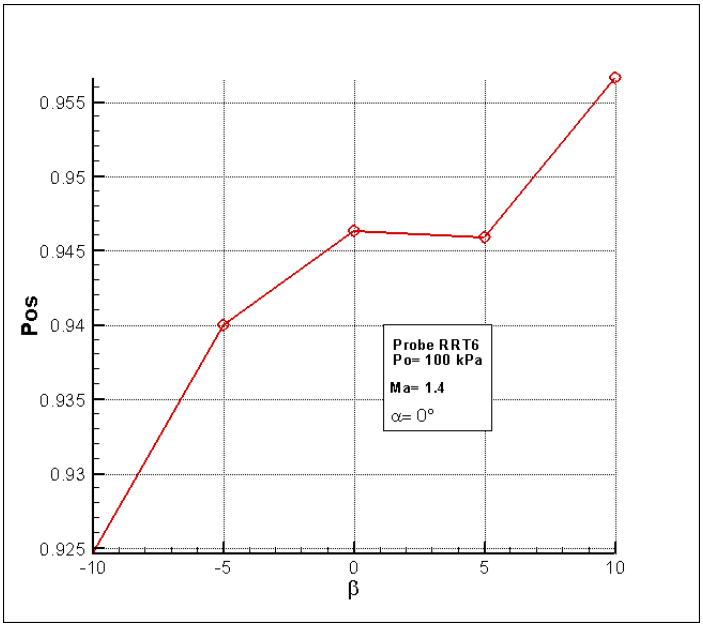

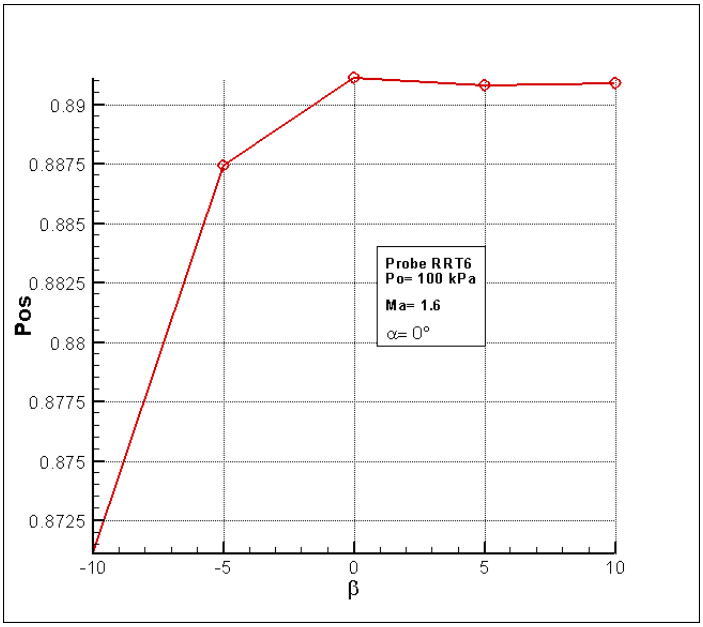

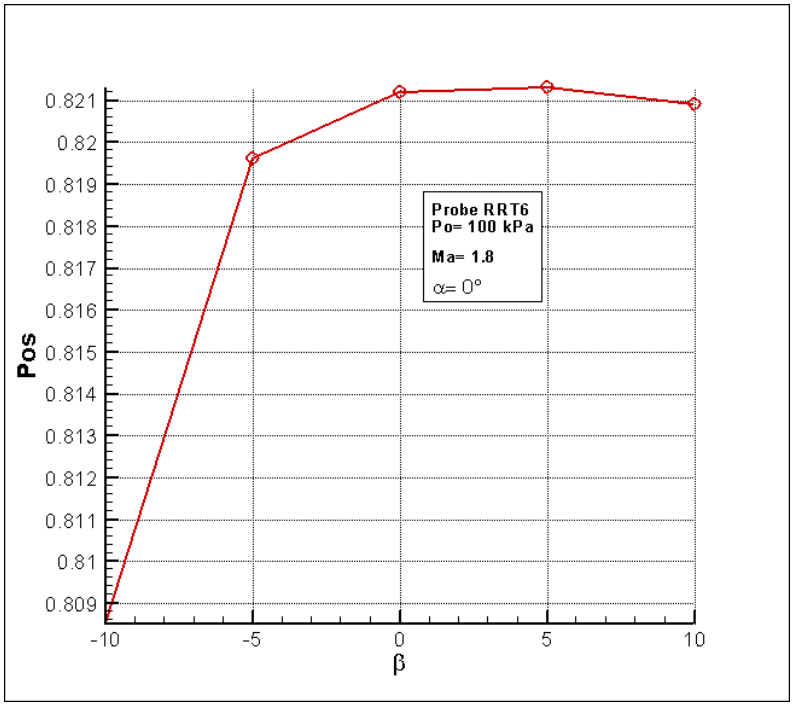

Figure 107: Evolution of p_{0s} against β at Ma=1.4
1.6
1.8

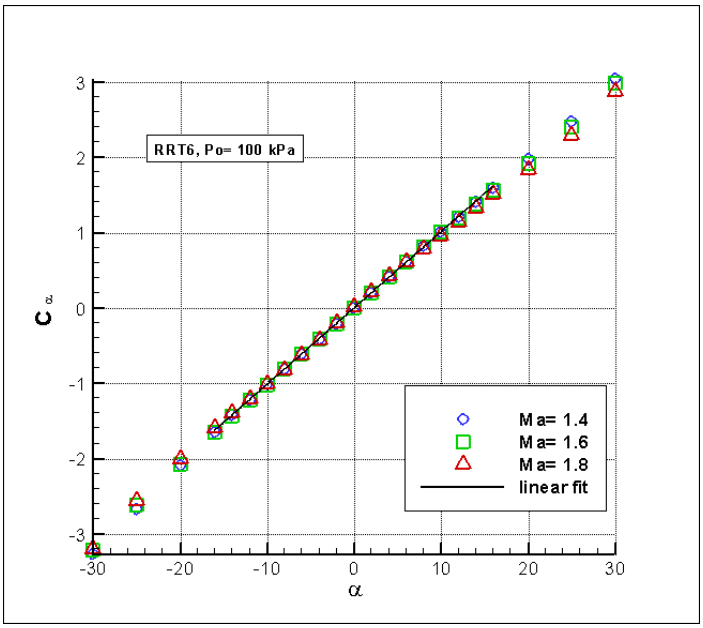

Figure 108: Evolution of C_α against α

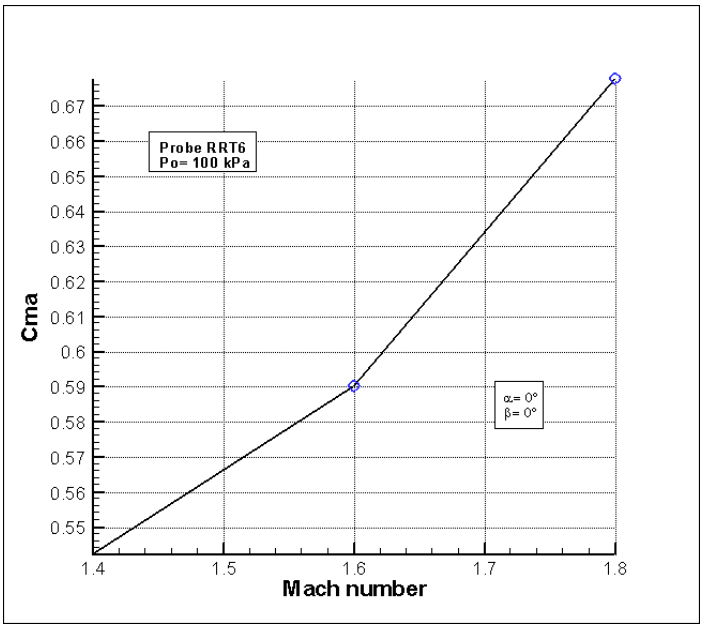

Figure 109: Evolution of C_{Ma} against Ma

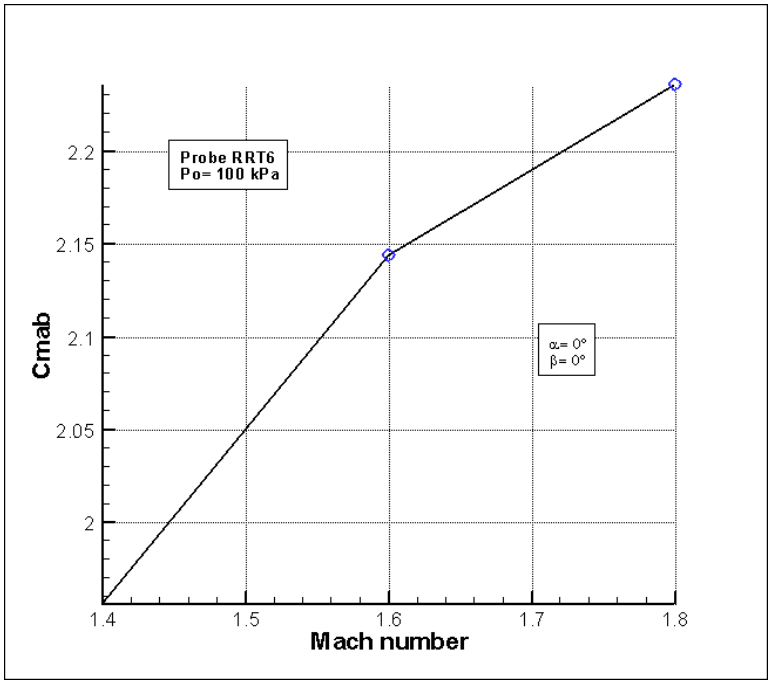

Figure 110: Evolution of C_{Mab} against Ma